Master's thesis

NTNU
Norwegian University of Science and Technology
Faculty of Natural Sciences
Department of Physics

Vilde Vraalstad

Standardising spectroscopy

A study of spectrometers and a method for characterising and comparing performance

Master's thesis in Applied Physics and Mathematics
Supervisor: Jon Andreas Støvneng
Co-supervisor: Jon Tschudi and Marion O'Farrell
June 2023

NTNU
Norwegian University of Science and Technology

SINTEF

Vilde Vraalstad

Standardising spectroscopy

A study of spectrometers and a method for characterising and comparing performance

Master's thesis in Applied Physics and Mathematics
Supervisor: Jon Andreas Støvneng
Co-supervisor: Jon Tschudi and Marion O'Farrell
June 2023

Norwegian University of Science and Technology
Faculty of Natural Sciences
Department of Physics

NTNU
Norwegian University of
Science and Technology

Abstract

Miniaturisation of spectrometers contribute to the advancement of food industry digitisation. The successful implementation for applications requiring high signal quality, such as interactance spectroscopy, relies on the compression of size while not compromising too much on performance. Crucial is a fundamental understanding of the physical limitations that govern the spectrometer operation, and the relation between spectrometer size and performance. Meanwhile, data sheets are inadequate for a proper spectrometer characterisation, and there is no standardisation or easily applicable method for comparing spectrometer performance.

This thesis is a first step towards a proper and fundamental method for performance characterisation, allowing for full understanding of the spectrometer properties and performance. For standardisation, characterisation, and comparison of spectrometers, a rough characterisation of spectrometer performance is developed, rooted in first principles and physics. The treatment is focused on diffraction grating spectrometers, which are commonly applied for near-infrared (NIR) absorbance and Raman spectroscopy.

Using the "black box"-approach, a set of performance characteristics for spectrometer operation is defined. Based on a simple, user-friendly, and reproducible setup, a corresponding set of simple and fast methods for experimentally measuring the characteristics is suggested. The performance characteristics are intended for better understanding of the data, for evaluating whether a spectrometer is suited for a given application, and for aiding comparison of different spectrometers. The characterisation is not complete, and does not cover properties such as stray light, stability and robustness, or properties relating to heterogeneous samples, such as spatial coregistration. However, the important properties relating to signal-to-noise ratio (SNR) and resolution are covered, with particularly thorough discussion of the resolution, and they are successfully determined with sufficient accuracy for three diffraction grating spectrometers.

Work still remains to translate and transfer the results to the application domain, describing the effect on multivariate models from different performance characteristics. The work will hopefully then be a useful tool for better understanding the data, spectrometer limitations, and importance of design optimisation, and aid the comparison of instruments for a given application. Additionally, it can simplify multidisciplinary work, making us better equipped for realising miniaturised interactance spectroscopy.

Sammendrag

Miniatyrisering av spektrometre bidrar til utviklingen av en digitalisert matindustri. For en vellykket implementering i anvendelser som krever høy signalkvalitet, slik som interaktans-spektroskopi, er det viktig å redusere størrelsen uten å gå for mye på bekostning av ytelsen. For å oppnå dette er det avgjørende å ha en grundig forståelse av de fysiske begrensingene til spektrometeret, samt forholdet mellom spektrometerets størrelse og ytelse. Samtidig er spektrometrenes datablad utilstrekkelige for en grundig karakterisering, og det finnes ingen standardisering eller enkel og anvendbar metode for å sammenligne ytelsen til ulike spektrometre.

Denne masteroppgaven er et første skritt mot en fullstendig og grunnleggende metode for karakterisering av spektrometre, som gir en helhetlig forståelse av egenskapene og ytelsen. Det har blitt utviklet en grov karakterisering basert på grunnleggende prinsipper og fysikk, for standardisering, karakterisering og sammenligning av spektrometre. Analysen fokuserer spesielt på diffraksjonsgitter-spektrometre, som er mye brukt for nær-infrarød (NIR) absorbans- og Raman-spektroskopi.

Et rekke ytelsesparametre for spektrometre har blitt definert ved bruk av en «black box»-tilnærming. Det har blitt foreslått en tilhørende serie med enkle og raske metoder for eksperimentell måling av disse ytelsesparametrene, basert på et enkelt, brukervennlig og reproduserbart oppsett. Hensikten er å gi økt forståelse av dataene, forenkle vurderingen av om et spektrometer er egnet for en gitt anvendelse, og forenkle sammenligning av forskjellige spektrometre. Karakteriseringen er per nå ikke komplett, og omfatter ikke egenskaper som strølys, stabilitet og robusthet, eller egenskaper knyttet til måling av heterogene prøver, slik som romlig samregistrering. Likevel dekkes viktige egenskaper knyttet til signal-støyforhold (SNR) og oppløsning, med spesielt grundig diskusjon av oppløsning, og de har blitt målt med tilstrekkelig nøyaktighet for tre diffraksjonsgitter-spektrometre.

Det gjenstår fortsatt å oversette og overføre resultatene til anvendelses-domenet, ved å beskrive effekten av ulike ytelsesparametre på multivariate modeller. Arbeidet vil forhåpentligvis da bli et nyttig verktøy for bedre forståelse av dataene, spektrometerets begrensninger og viktigheten av designoptimalisering, samt forenkle sammenligning av instrumenter for en gitt anvendelse. Dessuten kan det forenkle tverrfaglig samarbeid, og gjøre oss bedre i stand til å realisere miniatyrisert interaktans-spektroskopi.

Acknowledgements

This Master's thesis is the result from work conducted during the spring of 2023, as the final step of obtaining a Master of Science degree in Applied Physics at the *Norwegian University of Science and Technology* (NTNU). The work has been carried out in the Applied Optics group at the department of Smart Sensors and Microsystems at SINTEF Digital, under the supervision of Jon Tschudi and Marion O'Farrell. The thesis is conducted within the *Centre for Research-Based Innovation in Digital Food Quality* (SFI DigiFoods) which is funded by the Research Council of Norway. The main supervisor from the Department of Physics at NTNU, Jon Andreas Støvneng, managed the administrative process.

First and foremost, I would like to express my deepest gratitude to Jon and Marion for offering me such an exciting Master's project, and letting me join your group. The project has been highly instructive and rewarding. I am very lucky to get the chance to continue the work from this thesis in a PhD, and am genuinely thrilled to take a deep dive into the world of spectroscopy.

Words cannot express how grateful I am for Jon and Marion and their endless support, patience, and guidance throughout the work with this thesis. They have always been available and prioritised me, even during busy times, and shared generously of their exceptional knowledge.

I would also like to extend my appreciation for my colleagues at SINTEF for such a warm welcome. I could not have wished for a better last semester of my studies, and that is solely due to the incredible work environment. I am truly grateful to be allowed to stay in the group for my PhD.

A special thank you goes to Torbjørn Skauli for engaging in highly useful discussions, and for providing me insight into the current draft of the IEEE P4001 standard. Parts of the work is inspired by this standard, and we have gotten permission to share these ideas.

Furthermore, I would like to thank my colleague Kari Anne Hestnes Bakke for spending time reviewing the thesis, and offering truly valuable feedback.

Finally, I want to thank my family and friends for the unwavering support, and the student organisations *Gløshaugen Revy og Teaterlag* and *Nablarevyen* for filling my leisure time with so much joy.

Vilde Vraalstad
Oslo, Norway
June, 2023

Table of Contents

List of Figures

List of Tables

Glossary

Abbreviations

ADC Analogue-to-digital converter. An electronic device that turns the amplified photoelectron signal of a photodetector into a digital number.

CCD Charge-coupled device. A type of silicon-based photodetector array.

DN Digital numbers. The raw photodetector signal from the output of the ADC, and thus the units of the raw spectrometer signal.

LSF Line spread function. Describes the blurring, broadening, and spread of light from the spectrometer optics. See subsection 3.1.2 for further description.

FWHM Full width at half maximum.

NIR Near-infrared light.

PTC Photon transfer curve. See subsection 3.3.4 for description.

SNR Signal-to-noise ratio. The relative signal strength with respect to noise.

SRF Spectral response function. The combined effect of slit size, line spread and detector element width on the spectral response to a single wavelength. See subsection 3.1.2 for further description.

Definitions

Accuracy The maximum expected error, or deviation from the true values, associated with a measurement. Strictly speaking, this is actually a measure of its inaccuracy, and the term uncertainty can equivalently be used. See section 3.2.

Binning Combining blocks of adjacent detector elements, by summing or averaging their values. A form of resampling. See subsection 3.3.5.

"Black box"-approach Considering the overall performance of the spectrometer. The defined characteristics are directly measurable by observing the performance, without knowledge

of the internals, and can be interpreted directly without further analysis. See chapter 5.

Diffraction grating spectrometer Spectrometer that use a diffraction grating to separate the light into a spectrum. See section 3.1.

Dynamic range The ratio between the highest and lowest achievable signals in the spectrometer, i.e., the saturation level and noise floor. See subsection 5.1.2.

Error Difference between the measured and true values. Systematic and random systematic error sources are described as errors, and cannot be reduced by averaging of repeated measurements. Random error sources cause random fluctuations, are described as noise, and can be reduced by averaging of repeated measurements. See section 3.2.

Gain factor The conversion factor from photoelectrons to DN by the output amplifier and ADC. See subsection 3.3.4.

Geometrical optics Describes the propagation of light by light rays. Neglects the wave properties of light, and thus effects such as interference and diffraction.

Noise Random fluctuations that corrupt the signal, and reduce its accuracy and precision. Caused by random errors, and can be reduced by averaging of repeated measurements. See section 3.2.

Precision A measure of the lack of random errors produced by a sensor or instrument. Devices with high precision will produce repeated readings with very little spread. See section 3.2.

Resampling Using the data points in the raw spectrum, for generating a new and modified spectrum. Describes several different operations on the data, including binning and smoothing. See subsection 3.3.5.

Resolution Spectral resolution, also termed the optical resolution. Described by the SRF peak width, commonly termed the bandwidth. See subsection 5.1.2.

Saturation When the measured signal, and its noise, no longer follow the input level. The lowest of the detector full-well capacity, and maximum level of ADC linear response. See subsection 5.2.2.

Sensitivity The ability to detect low light levels.

Smoothing Signal smoothing by using a smoothing filter. A form of resampling, where the signal is convoluted with a given function, and resampled with the original sampling interval. See subsection 3.3.5.

Spectral range The range of wavelengths that are detected by the spectrometer. See subsection 5.1.2.

Spectral sampling interval The wavelength increment between the centres of adjacent detector elements. See subsection 5.1.2.

Choice of terminology

This thesis uses the term *detector element* for the spectral pixels in the detector array. As spectrometers only image in one (spectral) dimension, the term *pixel* would be equally descriptive. However, it is omitted to avoid confusion, as it in the field of hyperspectral imaging usually refers to spatial pixels. On the other hand, *detector element* explicitly describes the spectral dimension.

For describing the wavelength interval measured by a single spectral sampling, the term *band* is commonly used, particularly in the field of hyperspectral imaging. This may be used for any method of sampling, both sampling by individual detector elements, and through resampling and binning. Often, the chosen sampling method is not explicitly specified, which may cause confusion, as then the term *band*, and particularly *number of bands*, may correspond to various properties. For example, the number of bands may correspond to either the number of detector elements, or how many independent wavelengths that can be measured. To avoid confusion, the term *band* is used with caution, its meaning is explicitly specified, and when suitable, it is replaced with other terms that are equally descriptive.

As spectrometers only has a spectral dimension, the *spectral resolution* is referred to simply as the *resolution*. Most literature use the term *bandwidth* to describe the spectral response function (SRF) peak width, which determines the resolution. In this thesis, as the term band is used with caution, the term *bandwidth* is avoided and replaced with *SRF peak width* and *resolution*, as these are equally descriptive.

The term *spectral response function* (SRF) is used for describing the spectral response to a single wavelength. Also the terms *bandpass function* and *optical transfer function* are used in the literature.

The term *line spread function* (LSF) is used for describing the blurring, broadening, and spread of light from the spectrometer optics. While this definition is used in some publications, others use the term for describing the combined effect of the optics and the slit function, or synonymously with the SRF, describing the combined effect of the optics, slit function, and detector function.

Part I

Background

Chapter 1

Introduction

We live in a digital world that keeps getting increasingly more advanced. We walk around with highly advanced computers in our pockets, observe farther into the distant universe than ever before, and have realised self-driven buses. However, the food and agricultural industries are still highly manual, and have not kept up with the seemingly ever-increasing technological development. This leaves a large potential for optimisation through digitisation, with better resource use, higher food quality, reduced food loss, and increased food security. Meanwhile, the European Commission stresses the prime importance of food analysis for the public safety [1], and in 2020, Norway had a total food waste of 454 350 tons, i.e., 84.7 kg per citizen. Of this, more than 30% was from the food, agriculture, and sea food industries. The Norwegian food industry agreed in 2017 on a commitment for reducing food loss by 50% by 2030, a goal which is inspired by the United Nations sustainability goals [2]. Lots of work still remains for this goal to be reached, which is addressed by the research in the Centre for Research-Based Innovation (SFI) in Digital Food Quality, DigiFoods by short [3]. DigiFoods explores new technology for digitisation of sectors such as food processing, seafood, and agricultural industries. Central in the applied technological solutions is the use of spectroscopy.

Spectroscopy is the optical metrology related to accessing and utilising the spectral information content of light. It is realised using spectrometers, which are instruments that measure the spectrum of incoming light. Through analysing the modifications on light from samples, information about the chemical structures is acquired in a non-destructive manner. This is the basis of e.g. absorbance and Raman spectroscopy. Such retrieval of chemical properties without needing to destroy the samples represent a highly useful method for optimisation of processes such as characterising, sorting, and monitoring of raw materials and food products. Light in the near-infrared (NIR) region is particularly useful for such applications. NIR spectroscopy is successfully realised by large instruments for inline applications, measuring the quality of food moving on conveyor belts, such as for sorting potatoes based on their dry matter content [4], or for estimation of fatty acid content in salmon fillets [5]. The inclusion of smaller spectrometers for inline food monitoring is a next step in the process of food industry digitisation, allowing for mobile and handheld measurement solutions. The combination of portability and direct onsite application with high throughput and a noninvasive way of analysis is a decisive advantage, and will address new ways of sorting food, earlier in the value chain, before reaching the factory floor.

NIR interactance spectroscopy measures the sample outside the field of illumination, and collects light that has reached deeper into the sample than reflectance spectroscopy, in which the field of view equals the field of illumination. This obtains more information about the interior of the sample, which is required for a variety of applications where the sample surface is not representative of the interior, such as for determining sugar content of strawberries or meat content in king crabs. In the latter case, the current state-of-the-art is manual squeezing and bending of the product to literally get a feel for the quality, since this is not obvious from looking at the surface [6]. This illustrates the potential of interactance spectroscopy to revolutionise such industries. However, due to the increased path length of the light through the sample, the intensity of the light is correspondingly reduced. Interactance spectroscopy thus require spectrometers with particularly high sensitivity for obtaining sufficient signal-to-noise ratio (SNR). In general, smaller spectrometers will have lower sensitivity, and the realisation of small and compact measurement solutions for interactace spectroscopy is particularly challenging. Enabling this technology will be an important contribution to the modernised food industry.

The instrumental development of miniaturised NIR spectrometers is rapid, and almost every year new concepts and products are introduced to the market [1]. There is now a new generation of small, affordable, and easy-to-use spectrometers that employ diverse technological solutions [7, 8]. However, the progressing of miniaturisation unavoidably has influenced performance characteristics such as sensitivity and SNR compared to the larger benchtop instruments [1]. Some of the extremely compact and cost-effective NIR spectrometers have been engineered by accepting a somewhat limited general applicability and performance in general use [8]. This may be sufficient for applications with lower sensitivity requirements, such as reflectance spectroscopy, but is not sufficient when higher sensitivity is required. The realisation of more compact spectrometers for interactance spectroscopy relies on the compression of size while not compromising too much on performance.

The need for high sensitivity of the miniaturised spectrometers seem to be somewhat underestimated. For example, [9] states that the main challenges of downsizing is to maintain spectral resolution, and to select a useful spectral range, and does not mention the sensitivity requirement. The trend of very small and cheap spectrometers, without focus on design optimisation for improved data quality and sustaining sufficient performance, may give false expectations of what is physically obtainable, and hamper the realisation of miniaturised interactance spectroscopy.

Crucial to successfully pushing the size limit and realising miniaturised interactance spectroscopy is a fundamental understanding of the physical limitations that govern the spectrometer operation. While this may be of higher priority to the spectrometer designers, there seem to be a knowledge gap to the chemometricians that analyse the resulting spectrometer data. They tend to apply spectrometers "as is" and accept the quality of the data they get. Transferring knowledge of the physics and spectrometer operation limits may be a crucial step towards a common understanding of the effect on performance by spectrometer miniaturisation, and the need for design optimisation. This will allow for multidisciplinary collaboration, making us better equipped for realising miniaturised interactance spectroscopy. The need of a multidisciplinary design team for the successful realisation is strongly emphasised in [10] and [11].

A first step towards the full understanding of the relation between spectrometer size and performance is a proper and fundamental method of performance characterisation. As was stated by [12] in 2019, the performances and differences of miniaturised spectrometers due to operational

characteristics have been poorly studied to date, and attention needs to be paid to the various factors that affect the spectrometer performance [13]. Additionally, there exist no overall superior spectrometer design suited for all applications, and the different designs have different advantages and disadvantages suited for different application requirements. Understanding on the effect from different design parameters on the performance is thus also highly useful for this evaluation. Spectrometer performance assessment is mostly performed based on an "outside-in" approach, systematically evaluating the analytical performance and applicability limits of various miniaturised spectrometers, based on their ability to produce sufficient results in a variety of applications [8]. However, an "inside-out" approach based on physics relating to the spectrometer operation seem to be scarcely explored.

Additionally, as discussed by [14], the current specifications in data sheets are insufficient for a proper assessment of the spectrometer performance. Commonly given characteristics are not really helpful for assessing actual spectrometer performance in a given application, and may give a false impression when not properly evaluated. Having a standardised and adequate set of performance characteristics would he highly useful, and aid both the users, buyers, and developers of spectrometers. [11] describes how a preliminary evaluation of the spectrometer characteristics may not be possible without carrying out several laboratory experiments, and emphasises that scientific and technical fundamentals should not be ignored for proper specifications. Additionally, as stated by [15], the terminology and methods for characterising, reporting, and understanding spectrometers vary, which complicates the comparison of instruments for application specific needs. The lack of a proper specification is even acknowledged by spectrometer manufacturers, e.g., by stating on their websites that it is challenging to judge the performance of a spectrometer based on the data sheet.

The situation is similar for hyperspectral imaging. Taking on the task of developing a common standard for specification of hyperspectral cameras is the IEEE P4001 working group, which was formed in 2018. They aim at a standard for unifying the use of terminology, spectral camera characterisation methods, and the meta-data structures that are needed to represent spectral camera performance [15]. While much of this is directly applicable for spectrometers, some adjustments are required, which leaves room for additional standardisation work relating to spectroscopy.

This thesis takes on such an approach of spectrometer performance characterisation rooted in first principles, with focus on diffraction grating spectrometers for NIR absorption spectroscopy applications. This is a first step of knowledge transfer between the separated fields within spectroscopy. The aim is to describe the spectrometer operation, develop a method of describing the performance, and corresponding methods for experimental determination. This is intended for better understanding of the data, for evaluating whether a spectrometer is suited for a given application, and for aiding comparison of different spectrometers.

1.1 Outline

Chapter 2 presents the fundamental theory applied throughout the thesis, including general properties of light and optical instrumentation elements, and introduces spectroscopy.

Chapter 3 introduce the working principles of spectrometers, with focus on the diffraction grat-

ing spectrometer. Errors, noise, and the important quality factor SNR are discussed, and common methods concerning both data acquisition and analysis are presented.

Chapter 4 reviews the current status of the field of standardising spectroscopy, by presenting the results from literature search, and discusses the incompleteness of data sheets for a proper performance characterisation.

Chapter 5 presents the results from establishing a set of performance characteristics for a proper spectrometer specification. The characterisation is not complete, but covers the important properties of SNR and resolution, with particularly thorough discussion of the resolution definition.

Chapter 6 describes experimental methods for measuring the defined performance characteristics, using simple measurements on a simple and user-friendly measurement setup.

Chapter 7 discusses the results from the thesis work in relation to the project goal, and outlines the avenues for future work that can bring the project forward.

Appendix A gives a short summary of the presented methods, indented as an instructions manual, while appendix B contains corresponding code files for data analysis.

Chapter 2

Fundamental theory

The world is governed by physics, and a fundamental physical understanding is useful for explaining most phenomena. Spectroscopy and the operation of spectrometers is no exception, and for completeness, this chapter gives a brief review of the fundamental physics explaining relevant properties encountered later in the thesis, the operation principles of basic optical components, and the basics of spectroscopy.

2.1 Properties of light

Fundamental to our understanding of light, and to all properties governing spectroscopy, is the quantum mechanical concept of *wave-particle duality*. Light behaves as both waves and particles, and may be described as both. Different descriptions may be used for different phenomena. The electromagnetic wave description is governed by Maxwell's equations, which describes e.g. the propagation of light through the optical components of the instrument, and wave phenomena such as interference and diffraction. The particle description describes light as consisting of photons, and describes e.g. how light is detected by semiconductor detectors, and absorbed by samples. Both descriptions go hand in hand, and are required for a full description of the world, and even for explaining the operation of spectrometers.

The following sections are partly a restatement from previous work by the author [16], with some modifications.

2.1.1 Wave description

The fundamental rules governing electromagnetic phenomena are Maxwell's equations,

$$\nabla \cdot \boldsymbol{E} = \rho \tag{2.1a}$$

$$\nabla \cdot \boldsymbol{B} = 0 \tag{2.1b}$$

$$\nabla \times \boldsymbol{E} = -\frac{\partial \boldsymbol{B}}{\partial t} \tag{2.1c}$$

$$\nabla \times \boldsymbol{H} = \boldsymbol{J} + \frac{\partial \boldsymbol{D}}{\partial t} \tag{2.1d}$$

They describe how the electric and magnetic fields $\boldsymbol{E}$ and $\boldsymbol{H}$ are generated by charges, expressed by the electric charge density ρ and current density $\boldsymbol{J}$, and propagate. The effects by the electric and magnetic fields on matter are described by the electric displacement $\boldsymbol{D}$ and the magnetic flux density $\boldsymbol{B}$, and are for non-dispersive and linear media expressed by the constitutive equations,

$$\boldsymbol{B}(\boldsymbol{r}, t) = \mu_0 \boldsymbol{\mu}(\boldsymbol{r}, t) \otimes \boldsymbol{H}(\boldsymbol{r}, t) \tag{2.2a}$$

$$\boldsymbol{D}(\boldsymbol{r}, \boldsymbol{t}) = \varepsilon_0 \boldsymbol{\varepsilon}(\boldsymbol{r}, t) \otimes \boldsymbol{E}(\boldsymbol{r}, t) \tag{2.2b}$$

dependent on the material's relative electric permittivity ε and relative magnetic permeability μ. ε_0 and μ_0 are the vacuum permittivity and permeability constants, respectively. In frequency domain, the convolution simplifies to a product.

Combining Maxwell's curl equations 2.1c and 2.1d with the constitutive equations 2.2, and using that temporal and spatial derivatives commute, and the vector relation $\nabla \times (\nabla \times \boldsymbol{A}) = \nabla(\nabla \cdot \boldsymbol{A}) - \nabla^2 \boldsymbol{A}$, the homogeneous electromagnetic wave equations for linear, isotropic, and source-free media, i.e., with $\rho = 0$ and spatially constant ε and μ, can be derived as

$$\nabla^2 \boldsymbol{E} = \mu\mu_0\varepsilon\varepsilon_0 \frac{\partial^2 \boldsymbol{E}}{\partial t^2} \tag{2.3a}$$

$$\nabla^2 \boldsymbol{H} = \mu\mu_0\varepsilon\varepsilon_0 \frac{\partial^2 \boldsymbol{H}}{\partial t^2} \tag{2.3b}$$

The time-harmonic solution to Equation 2.3 yields the expression for the electric field of a general electromagnetic plane wave,

$$\boldsymbol{E}(\boldsymbol{r}, t) = \Re\left[\boldsymbol{E}_0 \exp\left(i\left(\boldsymbol{k} \cdot \boldsymbol{r} - \omega t - \delta\right)\right)\right], \tag{2.4}$$

and similarly for the magnetic field. E_0 is the amplitude of the wave, δ is the phase, ω is the angular frequency, and $k = 2\pi N/\lambda$ is the propagation constant for the wavelength λ in a medium with refractive index N. The refractive index is generally complex-valued, $N = n + i\kappa$. Inserted into Equation 2.4, this yields

$$\boldsymbol{E}(\boldsymbol{r}, t) = \Re\left[\boldsymbol{E}_0 \exp\left(-\frac{2\pi\kappa}{\lambda}\hat{\boldsymbol{k}} \cdot \boldsymbol{r}\right) \exp\left(i\left(\frac{2\pi n}{\lambda}\hat{\boldsymbol{k}} \cdot \boldsymbol{r} - \omega t - \delta\right)\right)\right], \tag{2.5}$$

the expression for a plane wave propagating in a material with velocity dependent on the real refractive index n, and exponentially decreasing amplitude in the propagation direction according to the extinction efficient κ. $\hat{\boldsymbol{k}}$ indicates the unit vector in the propagation direction.

2.1.1.1 Light-matter interaction

As stated through Equation 2.4, the propagation of electromagnetic waves in matter is dependent on the propagation constant $k = 2\pi N/\lambda$, and thus the material-dependent refractive index $N = n + i\kappa$. N specifies the interaction between the wave and the material, and relates the material phase velocity

$$v = \frac{1}{\sqrt{\mu\mu_0\varepsilon\varepsilon_0}}, \tag{2.6}$$

to the speed of light in vacuum,

$$c = \frac{1}{\sqrt{\mu_0\varepsilon_0}} = 2.998 \cdot 10^8 \,\mathrm{m\,s^{-1}}, \tag{2.7}$$

through the relation

$$N = \frac{c}{v} = \sqrt{\varepsilon\mu}. \tag{2.8}$$

For non-magnetic materials with $\mu = 1$, N is related to the dielectric function $\varepsilon = \varepsilon_1 + i\varepsilon_2$, which specifies the electromagnetic response of the material, as

$$N = \sqrt{\varepsilon}. \tag{2.9}$$

When a light wave propagates through an interface between two media, it will either be *reflected* or *transmitted*, with the probability of reflection given by the reflection coefficient. The reflected light remains within the plane of incidence, and the angle of reflection θ_r equals the angle of incidence θ_i. When transmitted into the new medium, the light is refracted according to Snell's law, $n_0 \sin\theta_0 = n_1 \sin\theta_1$, where n_0 and n_1 are the refractive indices of the two media.

When a wavefront of light is passing an obstacle, or through an aperture, with width in the order of the wavelength, it will be spread out, a phenomenon known as *diffraction*. According to Huygens' principle, every unobstructed point on the wavefront acts as a source of secondary spherical waves, and the actual field at any point beyond the wavefront is a superposition of all these wavelets [17, p. 268]. Hence, when only a small part of the wavefront passes through the aperture, the interfering waves will produce a diffraction pattern with bright and dark fringes. Diffraction is wavelength dependent, due to the dependence in the relative size of the obstacle or aperture. In addition, as only light of equal wavelength can interfere, the diffraction patterns are unaffected by the other wavelengths present. Hence, through diffraction, light of different wavelengths will be spread into different angles, and separated into a band of colours at each diffraction maxima.

Optical properties, and especially the refractive index, are generally *dispersive*, meaning that they are wavelength dependent. In dispersive media, different wavelengths of light meet different refractive indices, and thus experience different propagation velocities. Important consequences are different refraction angles when passing through interfaces between two media, causing effects such as optical *aberrations*, e.g., from lenses that focus different wavelengths differently.

2.1.2 Particle description

Light consist of photons, which are quanta of the electromagnetic field with energy E described by the Planck-Einstein relation,

$$E = \frac{hc}{\lambda}, \tag{2.10}$$

where λ is the wavelength of the corresponding electromagnetic wave, $c = 2.998 \cdot 10^8\,\mathrm{m\,s^{-1}}$ the speed of light in vacuum, and $h = 6.626 \cdot 10^{-34}\,\mathrm{J\,s}$ Planck's constant.

Photons incident on a material will have a probability of being absorbed and exciting electrons in the material. This is the *photoelectric effect*, and the excited electrons are termed *photoelectrons*. The probability depends on the material properties and photon energy, as only photons with energy larger than the binding energy of electrons in the material will be absorbed and excite photoelectrons. Single photons are fully absorbed and excite photoelectrons, and multiple photons with lower energies than the binding energy cannot add to excite a photoelectron. Hence, the probability of the single photon for exciting a photoelectron is independent of the light intensity and duration of exposure, while the expected total number of excited photoelectrons is the sum of the individual probabilities of all photons.

Generally, visible and NIR light has sufficient energy to generate photoelectrons in metals, while insulators require higher photon energies. In semiconductors, electrons can be excited to higher energy levels, from the valence band to conduction band, by photons with energy higher than the energy separation between these bands, i.e., the *band gap*. For example, the band gap of silicon is 1.14 eV, and photoelectrons can be generated by photons with wavelengths up to approximately 1100 nm.

Similarly as for metals and semiconductors, also atoms and molecules have electrons in defined energy levels that can absorb photons and be excited to higher energy levels. Different chemical substances thus absorb light of different energies corresponding to different transitions.

2.1.3 Light spectra and monochromaticity

While a single electromagnetic wave exhibits a single wavelength λ, a light beam consists of the superposition of multiple electromagnetic waves. These can all exhibit the same wavelength, giving monochromatic light of a single colour, or multiple wavelengths, either discrete or in a continuum. White light generally consists of a spectrum of different wavelengths in the visible range. The distribution of wavelengths among the waves is called the spectrum of the light beam, and is given by the power of the light as a function of wavelength.

The degree of monochromaticity of a light beam is determined by its bandwidth, i.e., the width of the wavelength spectrum of the light. Due to the principles of operation, laser light generally has discrete wavelengths with very narrow bandwidth, in most cases sufficiently narrow to be considered monochromatic. Spectral emission lines from a gas are also narrow and considered monochromatic. On the other hand, the radiation from a blackbody, which emits a continuous spectrum dependent on its temperature T, is very broadband. The spectral radiance L_λ from the blackbody, i.e., the emitted power per unit area, solid angle, and wavelength interval, is given

by Planck's law, and expressed in the wavelength domain as

$$L_\lambda(T) = \frac{2hc^2}{\lambda^5} \frac{1}{\exp(hc/\lambda k_B T) - 1}. \tag{2.11}$$

Here λ is the wavelength, $c = 2.998{\cdot}10^8\,\mathrm{m\,s^{-1}}$ is the speed of light in vacuum, $h = 6.626{\cdot}10^{-34}\,\mathrm{J\,s}$ is Planck's constant, and $k_B = 1.381 \cdot 10^{-23}\,\mathrm{J\,K^{-1}}$ is Boltzmann's constant. It can be converted to the spectral photon radiance $L_{q,\lambda}$, where the subscript q indicates photon units, through dividing by the photon energy hc/λ,

$$L_{q,\lambda}(T) = \frac{2c}{\lambda^4} \frac{1}{\exp(hc/\lambda k_B T) - 1}. \tag{2.12}$$

2.2 Optical instrumentation elements

This section introduces optical components and instrumentation elements that are used in spectrometers. It is partly a restatement from previous work by the author [16], with some modifications.

2.2.1 Optical components

Lenses are transmittive devices that utilise refraction to focus or disperse a light beam. The combination of shape and material refractive index determine its focal length f and refracting power $P = 1/f$, and hence how strongly the beam is refracted. Collimated incoming light will be focused in the focal point at a distance f from the lens, and similarly, when turned around, light from the focal point will be collimated.

Apertures are holes or openings placed in the beam trajectory, used to block the part of a beam that is not passed through. They are used to control the intensity of a light beam, shield from undesirable light, and block specific rays to limit the field of view. *Pinholes* are small, circular apertures. *Slits* are rectangular, narrow apertures that e.g. can be used at input or output planes of optical systems to transmit a specific quantity of light.

Optical filters allow only certain wavelengths of light to pass through, while blocking or attenuating others. They are commonly based on absorption of specific wavelengths, or interference effects in dichroic materials. Common types of filters are long pass and short pass filters, where only wavelengths longer and shorter than the cut-off wavelength are transmitted, respectively, bandpass and notch filters, where only certain bands of wavelengths are transmitted or rejected, respectively, and neutral density filters, where all wavelengths are attenuated evenly. Filters can for instance be applied to remove overlapping higher diffraction orders from the output of a diffraction grating, and to filter out a desired wavelength range from white light.

Diffusers make the light more diffuse, i.e., more homogeneous and uniformly distributed. They usually operate through scattering, where the light rays that constitute a beam are scattered in different directions, either in the transmitted or reflected direction. A common design, the ground glass diffuser, has a diffuse surface of the glass created through polishing with particles, or grits, of a given size.

Integrating spheres are optical components producing very diffuse and homogeneous light. They consist of a hollow spherical cavity covered with a diffuse reflective coating, causing multiple diffuse reflections and scatterings of the input light over the entire sphere surface, as illustrated in Figure 2.1. The output is then uniformly distributed and *Lambertian*, meaning that the radiance is independent of the observation direction. Photodetectors and spectrometers can be mounted in the output ports of the sphere, and will then receive a known portion of the total light. To ensure properly uniformly distributed light, the output ports should be located so that they only receive light that has been reflected many times. Integrating spheres are commonly used for optical power measurements, as they preserve power while making it homogeneous and spatially uniform, and in spectral radiance source standards, as they provide uniform illumination with constant light level across a relatively large area.

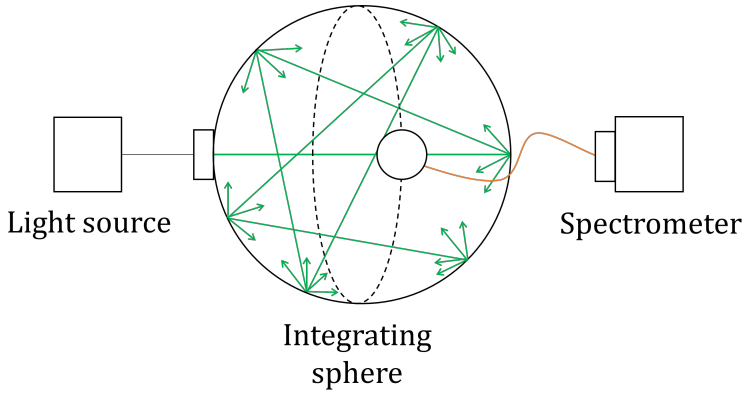

Figure 2.1: Illustration of the working principle of an integrating sphere. The input light undergoes multiple diffuse reflections and scatterings over the entire sphere surface, giving highly diffuse light at the output, where e.g. a spectrometer can be connected.

Light sources, such as light bulbs and light-emitting diodes (LED), emit spectra. Their bandwidth and degrees of continuity depend on the principles of operation. Halogen light bulbs work similarly as an incandescent lamp, with a heated wire filament of tungsten, with the exception that it additionally is filled with halogen gas, which reacts chemically with evaporated tungsten from the filament, and thus prevents blackening of the lamp. It is based on thermal radiation, and considered a greybody, approximating blackbody radiation with a very broadband spectrum.

Optical fibres are waveguiding cables that transmit light along the axis through repeated total internal reflections. They are used to transmit light over a distance, e.g., between two instruments, or over long distances for fibre-optics communications, and can also be used to collect light from a scene. In spectrometer measurement systems, they are commonly used both for collecting light from the sample, and delivering the light to the spectrometer. Optical fibres generally consist of a core where the light propagates, surrounded by a cladding layer with lower refractive index. This causes total internal reflections of the light incident on the cladding layer interface, as shown in Figure 2.2. The acceptance angle θ_{max} is defined by the numerical aperture

$$NA = n \sin \theta_{\text{max}} = \sqrt{n_{\text{core}}^2 - n_{\text{clad}}^2}, \tag{2.13}$$

where n, n_{core} and n_{clad} are the refractive indices of the surroundings, fibre core, and cladding layer, respectively. The light collection properties of the fibre is then described by the étendue,

which is the product of the maximum projected solid angle, $\Omega = \pi n^2 \sin^2 \theta_{\max} = \pi\, NA^2$, and the acceptance area, i.e., the cross section of the core with diameter d, as

$$A\Omega = \pi \left(\frac{d}{2}\right)^2 \pi\, NA^2 = \frac{\pi^2}{4} d^2\, NA^2. \tag{2.14}$$

Fibres used for spectrometers often have $NA = 0.22$, corresponding to an acceptance angle of approximately 0.22 radians in air, and a diameter of a few hundred micrometers, e.g., 550 µm.

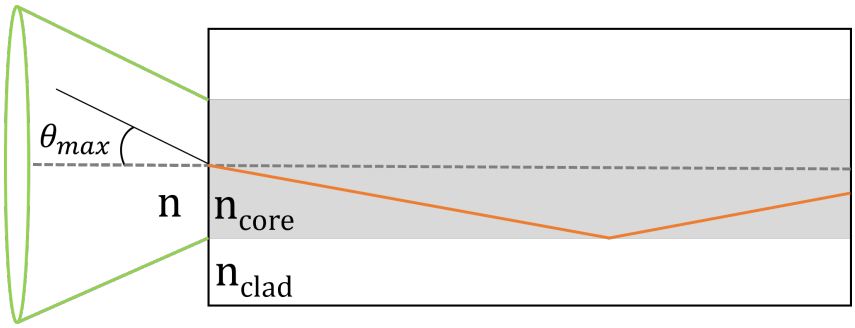

Figure 2.2: Illustration of an optical fibre, consisting of a core of refractive index n_{core} where the light propagates, surrounded by a cladding layer of refractive index n_{clad}. The light undergoes total internal reflections when incident on the cladding layer interface. The fibre collects light within the acceptance angle $\theta_{\max}$. The figure is not to scale, as the acceptance angle usually is much lower, commonly approximately 0.22 radians.

2.2.2 Photodetectors

Photodetectors are sensors of light, and convert the incident light into an electric signal. Different types exist, such as photographic films, photoconductive sensors, photon multiplier tubes, and photodiodes, e.g., CCD, CMOS and InGaAs detectors, which usually are applied in spectrometers. These usually have much higher quantum efficiency compared to other detector types.

Charge-coupled device (CCD) detectors are silicon-based photodetector arrays with high efficiency and good noise performance. They utilise the photoelectric effect, as incoming photons generate photoelectrons in the semiconductor material. The initial electronic signal is then a count of photoelectrons n_e. Most detectors measure the total charge as an analogue value and digitise into the raw detected signal. The detector contain arrays of coupled capacitors, and the generated photoelectrons during the exposure time of a measurement, known as the *integration time*, are collected and stored by the nearest capacitor. Hence, each capacitor, corresponding to an individual detector element, or spectral pixel, measures the light reaching a given position during the integration time. The signal is then read out, as the capacitors are emptied sequentially, and the charge converted to a voltage, giving a signal proportional to the intensity. The signal is amplified, and turned into a digital value by an analogue-to-digital converter (ADC). The raw spectrum is then given in digital numbers (DN).

The capacitors in the detector arrays can be visualised as buckets, or wells, that collect photoelectrons. Each capacitor has a limited capacity for holding photoelectrons, described by the full well capacity n_{sat}, at which the detector element is said to be in *saturation*. At saturation, the

detected intensity gets a cut-off, and the excess electrons flow into adjacent detector elements, causing an apparent widening of the spectrum.

The probability of an incident photon to generate a photoelectron in the semiconductor is described by the *quantum efficiency* (QE). It is defined as the product of the number of excited photoelectrons per interacting photon, termed the *quantum yield gain*, and the probability of an incoming photon to interact with the electron. For the wavelengths under consideration, corresponding to visible and NIR light, the quantum yield is unity, as the generated photoelectron does not have sufficient energy to further excite another photoelectron. Hence, the quantum efficiency describes the interaction probability of the incoming photon and electrons in the material. Its level depends on the optical active thickness and band gap properties of the detector material, and it may vary considerably across the spectrum. As the band gap of silicon, which is used in CCDs, is 1.14 eV, light with wavelengths up to approximately 1100 nm can interact and generate photoelectrons, and the quantum efficiency drops to zero for longer wavelengths. A typical CCD detector quantum efficiency is shown in Figure 2.3.

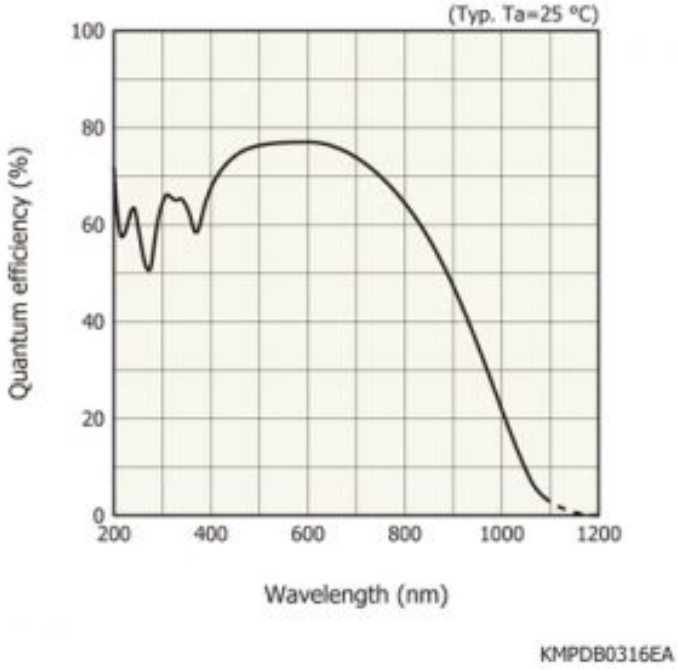

Figure 2.3: The quantum efficiency for a typical silicon CCD detector, the S11156 from Hamamatsu. The figure is borrowed from the detector data sheet [18].

Photodetectors tend to have a dark current that is always present, even when no outside radiation enter the detector. It is caused by random generation of electrons and holes within the detector material, and adds to the signal in the same way as the generated photoelectrons. The dark current is given by i_d, usually in units of electrons per second, and depends on the device and conditions such as temperature. Its contribution to the signal builds up over the integration time t, to a total number of electrons per detector element $n_d = i_d \cdot t$. It is generally considered constant over the detector elements, but may vary slightly, giving a fixed pattern addition to the signal. Its contribution is easily is corrected for through dark correction, by measuring and subtracting the dark signal. However, the dark current also generates shot noise which is added to the final signal, and the dark correction introduces even more noise, as will be discussed in subsubsection 3.2.2.2.

2.2.3 Diffraction gratings

Diffraction gratings are devices with periodic structures, such as grooves or slits, that diffract light into multiple diffraction orders at specific angles. Light of different wavelengths is diffracted at different angles, and spread into spectra of colours at each diffraction order. This is the most efficient way to separate colours, and the basis of diffraction grating spectrometers.

The working principle of a diffraction grating with periodic grooves is shown in Figure 2.4. The diffraction angles for a given wavelength λ into the diffraction order m is described by the grating equation

$$\sin\theta_{\text{out}} = \sin\theta_{\text{in}} - m\frac{\lambda}{d}, \tag{2.15}$$

where $\sin\theta_{\text{out}}$ is the diffraction angle, $\sin\theta_{\text{in}}$ is the incidence angle and d is the distance between the grooves in the grating. Hence, shorter wavelengths will be diffracted at lower angles. The spread of wavelengths is generally not linear, except for small angles, where $\sin\theta \approx \theta$. Larger groove density $g = 1/d$, defined as the number of grooves per mm, give larger dispersion, and the wavelengths are then spread over a larger area, reaching larger angles.

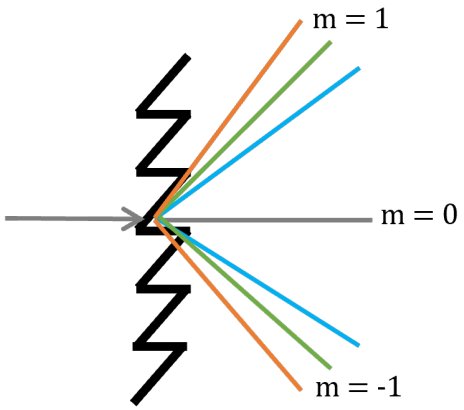

Figure 2.4: Illustration of the working principle of a transmission diffraction grating. The incoming broadband light is transmitted into the 0th order, and the wavelengths are separated into spectra at the higher orders. Here only the first orders are shown.

The light spectra at different diffraction orders may overlap, as the angle of one order at one wavelength may equal the angle of a higher or lower order of another wavelength. Hence, at a given angle, multiple diffraction orders of different wavelengths may be present. For light that is normally incident on a transmission diffraction grating, a given diffraction order is present in the transmitted light when $\sin\theta_{\text{out}} < \pi/2$, i.e., $m\lambda/d < 1$.

Similarly as the quantum efficiency for photodetectors, also diffraction gratings have a limited and wavelength dependent diffraction efficiency. Different orders have different efficiency, and the amount of light in each order can be estimated using full field simulations. A suitable grating has high diffraction efficiency for the design wavelength into the desired order, and minimal diffraction into other orders.

2.3 Spectroscopy

Spectroscopy is a characterisation technique based on the analysis of the electromagnetic spectrum of the light from an object. The light may be emitted from the object, such as through fluorescence, or for radiant objects like black bodies, the earth, and distant stars. Otherwise, the spectroscopic measurement methods involve sending the light onto a sample, and analysing the modified outgoing light, such as Raman scattering, or for acquiring absorption spectra.

A wide range of sub-disciplines constitutes the field of spectroscopy. This involves exploration of different types of electromagnetic radiation, such as ultraviolet, visible, near-infrared (NIR), and infrared (IR) light, and X-rays, for analysis of different types of material such as gas, solids, and biological tissue. It yields information such as composition, physical structure, and electronic structure at the atomic, molecular, and macro scale. Spectroscopy is explored in a large variety of fields, ranging from astronomy and physics, to biology, chemistry, food science, agriculture, pharmaceutical science, and materials science, with applications such as analysis of the constituents of distant stars, climate gas observation, detection of cancer, drug analysis, frequency dependence of optical components, and food quality analysis.

Spectroscopy is performed using *spectrometers*, which are instruments that measure the spectrum of incoming light. Many different instrument designs exist, which are customised for different applications involving light of different origins and wavelengths, with different performance requirements. For example, measuring the spectra from distant stars require completely different instruments than measuring the water content of a material.

This thesis considers diffraction grating spectrometers measuring light in the NIR region, which commonly are used for NIR absorption spectroscopy and Raman spectroscopy. In both applications, information is extracted from sending light onto the sample and inducing molecular excitations. Raman shifts are analysed through illumination with lasers, correspond to fundamental transitions, and give very narrow spectral features, while NIR absorption spectra are obtained from illumination with broadband NIR light, and involve numerous extensively overlapping bands from overtones and combination transitions, leading to broad line shapes [8]. The applications have quite different requirements of the spectrometer, e.g., in terms of resolution.

Multiple measurement geometries, i.e., relationships between field of view and field of illumination, are applied for NIR absorbance spectroscopy. *Transmission* spectroscopy measures the light that is transmitted through the sample, *reflectance* spectroscopy measures the light that is directly reflected from the sample surface where the light source hits, and *interactance* spectroscopy is a variant of reflectance, measuring the light that has propagated through the sample, by placing the field of view outside the field of illumination. The different methods generate different information of the sample, as interactance measure more of the inside, while reflectance mainly detect the sample surface. The signal properties are also different, as interactance generally involve weaker signals, and thus require higher spectrometer sensitivity.

The study and analysis of absorption spectra, for extracting the information from e.g. molecular fingerprints, is usually performed through *multivariate analysis*. The spectral features may be broad and overlapping, and still give valuable information to the analysis. Different methods such as partial least squares regression (PLS) and principal component analysis (PCA) are commonly applied to separate the contribution from different components, and to build calibration models for quantifying e.g. the content of a given substance in the sample.

Chapter 3

Spectrometer operation

Spectrometers measure the spectrum of incoming light. A range of spectrometer designs exists, employing various principles of operation, intended for a wide range of applications with different performance requirements, spanning multiple ranges of electromagnetic radiation wavelengths. For example, dispersive spectrometers separate broadband light into a spectrum, where scanning grating spectrometers scan trough the spectrum and measure monochromatic wavelengths separately, while fixed grating spectrometers measure the whole spectrum at once using detector arrays. Fourier-transform infra-red (FT-IR) spectrometers use interferometers and obtain the spectrum from the Fourier transform of the resulting interferogram, and energy-dispersive X-ray spectroscopy (EDS) measure the energy of emitted characteristic X-rays, e.g. from interaction with the electron beam in electron microscopes.

This thesis considers diffraction grating spectrometers with detector arrays that measure near-infrared (NIR) light. Such instruments are commonly used for both NIR absorption spectroscopy and Raman spectroscopy.

A full spectrometer system consist also of components such as a light source, shutters, and order sorting filters, and input optics, such as imaging devices, collection devices, such as integrating spheres or diffuser heads, and optical fibres, to collect and/or deliver the light to the spectrometers [19]. In this thesis, for simplicity and for comparison purposes, only the spectrometers, consisting of an input slit, spectrometer optics, and a detector array, are considered.

3.1 Diffraction grating spectrometer

A diffraction grating spectrometer is an optical system consisting of two lenses or mirrors that produce an image of the input slit on the detector array. In between the lenses or mirrors, a diffraction grating is placed, which diffracts wavelengths to different angles. This causes different wavelengths of light entering the input slit to be imaged to different positions on the detector array. The Czerny-Turner spectrometer has two mirrors and a reflection grating, while the transmission grating based spectrometer consists of two lenses and a transmission diffraction grating, as shown in Figure 3.1. In this section, the latter is considered and further analysed, while the remaining analysis of this thesis applies to both designs.

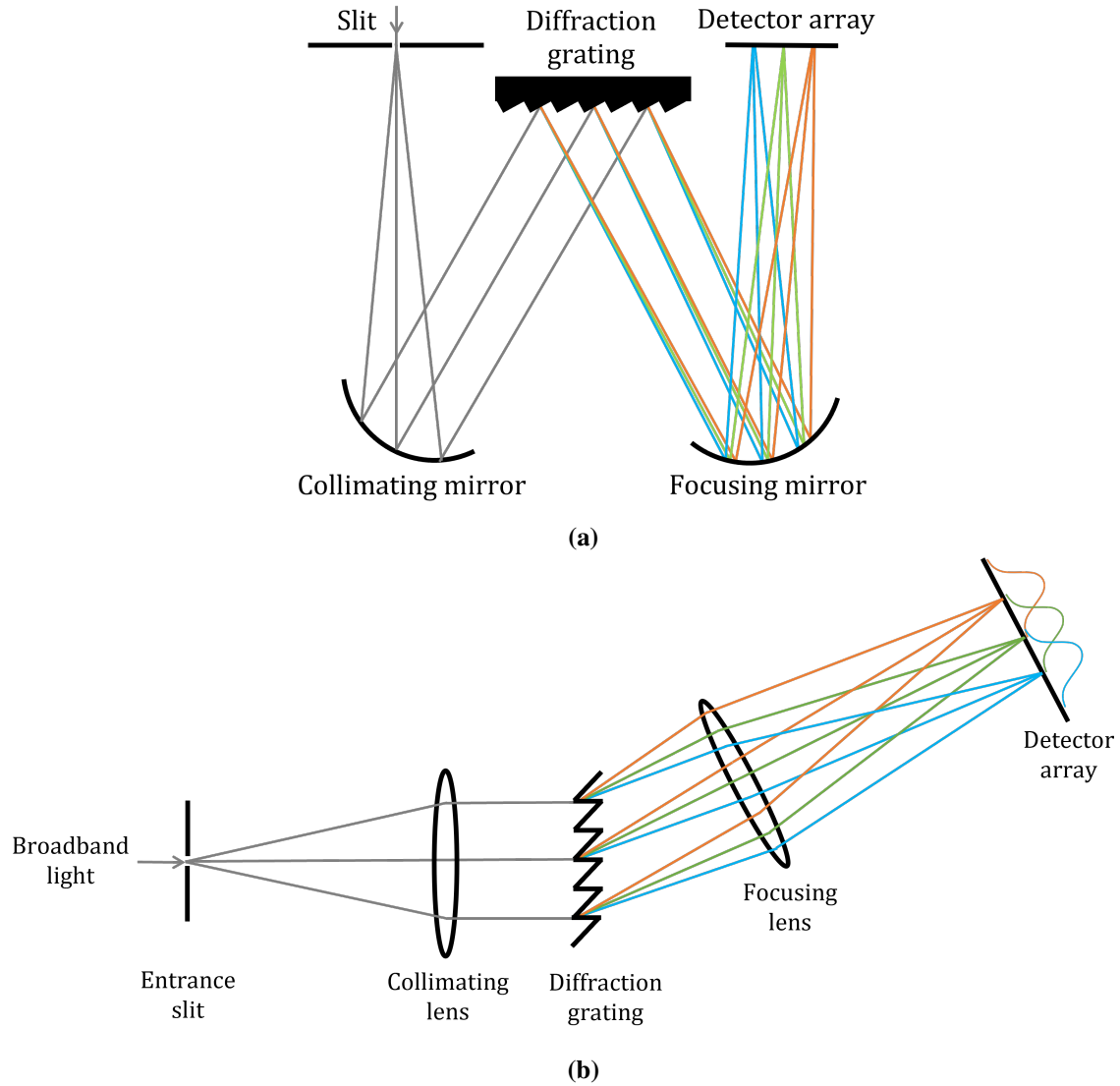

Figure 3.1: a) The Czerny-Turner diffraction grating spectrometer, consisting of two mirrors and a reflection diffraction grating, and **b)** the transmission diffraction grating spectrometer, consisting of two lenses and a transmission diffraction grating. Both designs image the different wavelengths of light entering the slit onto different positions on the detector array.

In the transmission diffraction grating spectrometer, the focusing lens and detector array are generally placed at an angle. The angle depends on properties such as the diffraction grating groove density, and whether the grating is slanted with respect to the centre ray. As seen from the grating equation, i.e., Equation 2.15, the spread of wavelengths is not linear over the detector array, and the wavelength scale on the detector array must be found through calibration.

The spectrometer is optimised for one diffraction order, usually the first order. However, also higher diffraction orders may receive some light, causing light with wavelengths $\lambda/2$, $\lambda/3$ etc. to be present on the detector array together with the first order wavelength λ. The detector signal is a measure of the number of generated photoelectrons, which is independent of wavelength, except for the differences in quantum efficiency. Hence, also the other wavelengths contribute to the detected signal. They are commonly removed in mass produced spectrometers by placing order sorting filters that absorb the unwanted light over the detector array.

The wavelength scale is commonly calibrated by using atomic emission sources, e.g., Hg, Ne, A, Kr, etc., and their combinations [19], and also the accuracy of the calibration, can be measured this way. Alternatively, optical filters with sharp spectral features can provide such a wavelength accuracy check when using a measurement setup with a broadband light source, as e.g. suggested by [20]. For example, the ThorLabs FGB67M coloured filter that operates as a bandpass filter in the range 900 nm to 1375 nm can be used, as it has such sharp features in the wavelength range up to 900 nm.

3.1.1 Geometrical slit imaging

Figure 3.2 shows a simplified illustration, with geometrical optics considerations, of the imaging of the spectrometer slit on the detector array, for the wavelength that the spectrometer is optimised for. The light is collimated by a lens, redirected by the diffraction grating, and focused to an image on the detector array a the focusing lens. The spread of the light from different incidence angles by the diffraction grating is neglected, which, as seen from Equation 2.15, holds only for small angles $\sin\theta \approx \theta$, as then the diffracted angle is approximately linear to the incidence angle. Other wavelengths are diffracted to different angles, and reach the focusing lens with other incident angles. As will be explained in subsection 3.1.2, the image of the slit is blurred due to aberrations and other effects in the optics. The image is thus not a perfect rectangular function, but rather blurred out, as indicated in the figure.

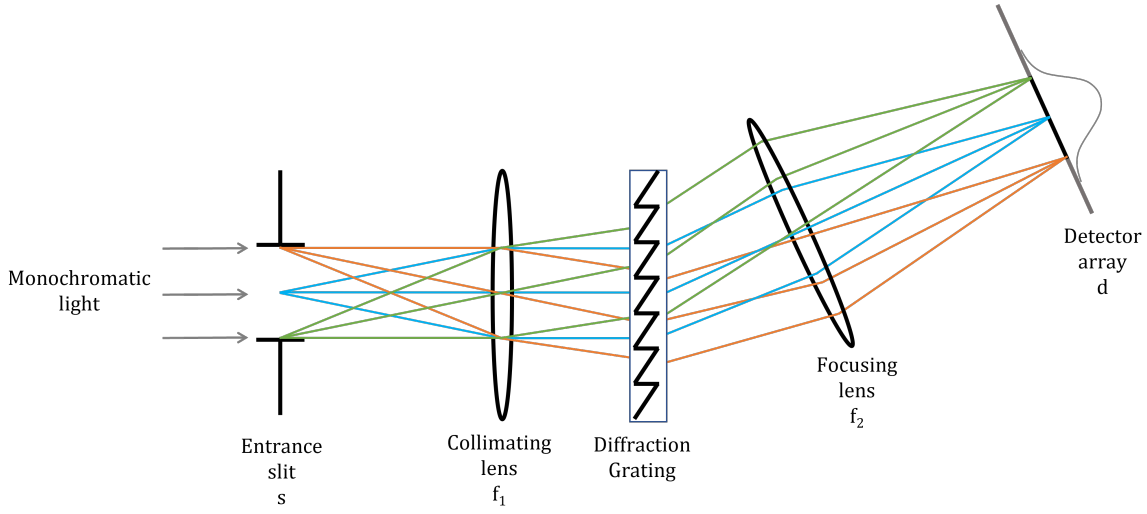

Figure 3.2: Simplified illustration of the geometrical imaging of the spectrometer slit on the detector array, for the wavelength that the spectrometer is optimised for. The spread of the light from different incidence angles by the diffraction grating is neglected.

The magnification of the slit image on the detector array, d/s, is estimated using simple geometrical optics, neglecting other effects by the diffraction grating than a simple constant redirection of the light. For a thin lens, the magnification is given by

$$M = \frac{i}{o}, \tag{3.1}$$

where o and i are the object and image distances, respectively. The combined effect from two

lenses is found by simply multiplying the individual magnifications,

$$M_{\text{tot}} = \left(-\frac{i_1}{o_1}\right) \cdot \left(-\frac{i_2}{o_2}\right) = \frac{i_2}{o_1} \cdot \frac{i_1}{o_2}. \tag{3.2}$$

As given by the thin lens formula for a collimating lens, focusing the light at infinity, $i = \infty$,

$$\frac{1}{f} = \frac{1}{o} + \frac{1}{i} = \frac{1}{o}, \tag{3.3}$$

the object distance equals the focal length f. Combining the two collimating lenses in Figure 3.2 of focal lengths f_1 and f_2, with $i_1 = o_2 = \infty$, $o_1 = f_1$ and $i_2 = f_2$, the final magnification of the image is then given by

$$\frac{d}{s} = M_{\text{tot}} = \frac{f_2}{f_1}. \tag{3.4}$$

For larger diffraction angles, this simple relation does not hold. However, the geometrical considerations give an indication of the effect of the lens focal lengths, and is useful for understanding what affects the detector image size.

Each wavelength in broadband light is individually imaged as the monochromatic light. The wavelengths are diffracted at different angles and separated by the diffraction grating, with the angle of separation dependent on the groove density of the grating, as given by Equation 2.15.

Due to the extent of the slit, the images of adjacent wavelengths partly overlap, as indicated in Figure 3.1b. A larger slit will give more light into the system, and thus a stronger signal, but also larger broadening if the images of the slits. The signal from a single wavelength in one detector element is not increased when the slit size is increased, but the total signal from all wavelengths is increased proportionally to the slit size increase.

The spectrometer does not necessarily use the whole detector array. The groove density of the diffraction grating and the focal length of the focusing lens determine how many detector elements receive light that is within the spectral range and can be detected. Using more of the detector array, e.g., by a larger groove density or larger focal length, cause less light on each detector element, which gives a larger dynamic range, i.e., more light can be analysed without reaching saturation of the detector, but, as will be discussed in subsubsection 3.2.2.2, reduces the SNR.

3.1.2 Spectral response function

Ideally, if each wavelength was represented by a thin line on the detector array, as would be the case for an ideal spectrometer with an infinitely narrow slit, each position on the detector array would correspond to a single wavelength, and all wavelengths within the detector element would contribute with equal weights to the output signal. However, as the slits have spatial extension, and the spectrometer optics tend to broaden the light, the light of a single wavelength is generally spread over the detector array, and detected by multiple detector elements. Each detector element has an extent, and measures a signal corresponding to the sum of light over its extent. This broadening of monochromatic light and its response, including the effect of both slit size, detector element size, and imperfections in the optics, is described by the *spectral response function* (SRF). It is defined as the distribution of responsivity in the spectral dimension for a

spectral line, i.e., an infinitely thin line of monochromatic light. The response to any measured spectrum by a detector element is then the convolution of the input spectrum with its SRF. As will be discussed in subsection 5.1.4, the resolution is described by the width of the SRF. In the literature, the SRF is also termed the bandpass function [19] and the optical transfer function [21].

The spectrometer can be divided into modules such as the optical imaging module and detecting module, where each module is described by a function that characterise the influence it has on the final output spectrum and the SRF. The effect of the slit is described by the slit function, a rectangular function with width corresponding to the size of the slit image on the detector array. The detector sensitivity along the detector array is described by the detector function, a rectangular function corresponding to the width of each detector element. The slit image may be distorted by effects such as aberrations and diffraction in the optics, including nonlinear spread of the light at different incidence angles on the diffraction grating, that cause blurring, broadening, and spread of the light. This is contained in the optical *line spread function* (LSF), which have rounded edges, and generally can be approximated by a Gaussian.

Caution should be made, as different publications use different definitions of the term LSF. In some publications, e.g., [22], the term is used synonymously with the SRF, thus including also the effect of the slit and detector functions. Others, e.g., [23], use it for describing the combined effect of the optics and the slit function. Some even use it differently throughout the same publication, e.g., [21] and [19], for describing both the optics alone, the combined effect of the optics and the slit functions, and the total SRF including also the detector. Here, LSF is defined as describing only the blurring from the optics.

As seen in Figure 3.3, the ideal thin SRF is obtained only for an infinitely narrow slit function. Generally, the slit function is much wider than the detector elements, which broadens the SRF, and spreads the light over the detector array. For an ideal spectrometer, with no blurring from the optics, i.e., an infinitely thin LSF, the SRF is well approximated by a rectangular function, while for real spectrometers with non-negligible blurring from the optics, the SRF has rounded edges, and approximately resembles e.g. a Gaussian function.

As stated by [24] and [25], most SRFs can be reasonably well approximated by Gaussian functions. Also other functions, such as trapezoids, can be reasonably accurate, but the Gaussian is the most widely used.

The shape of the SRF may vary across the spectral range, but is assumed varying smoothly and slowly, with negligible variation for the wavelengths that are present within a detector element. Assuming also that light of different wavelengths is spread evenly over neighbouring detector elements, the distribution of wavelengths within one detector element has the same shape as the SRF, as then the signal of the centre wavelength of a given detector element in the neighbouring detector element correspond to the signal of the centre wavelength of the neighbouring detector element in the given detector element. As only narrow areas are considered, these assumptions are generally considered valid, and hence, the distribution of wavelengths within one detector element, i.e., the corresponding band, is generally considered described by the SRF. Thus, the SRF describes both the spread of one single wavelength over the detector elements, and the distribution of wavelengths within one detector element or band, as illustrated in Figure 3.4.

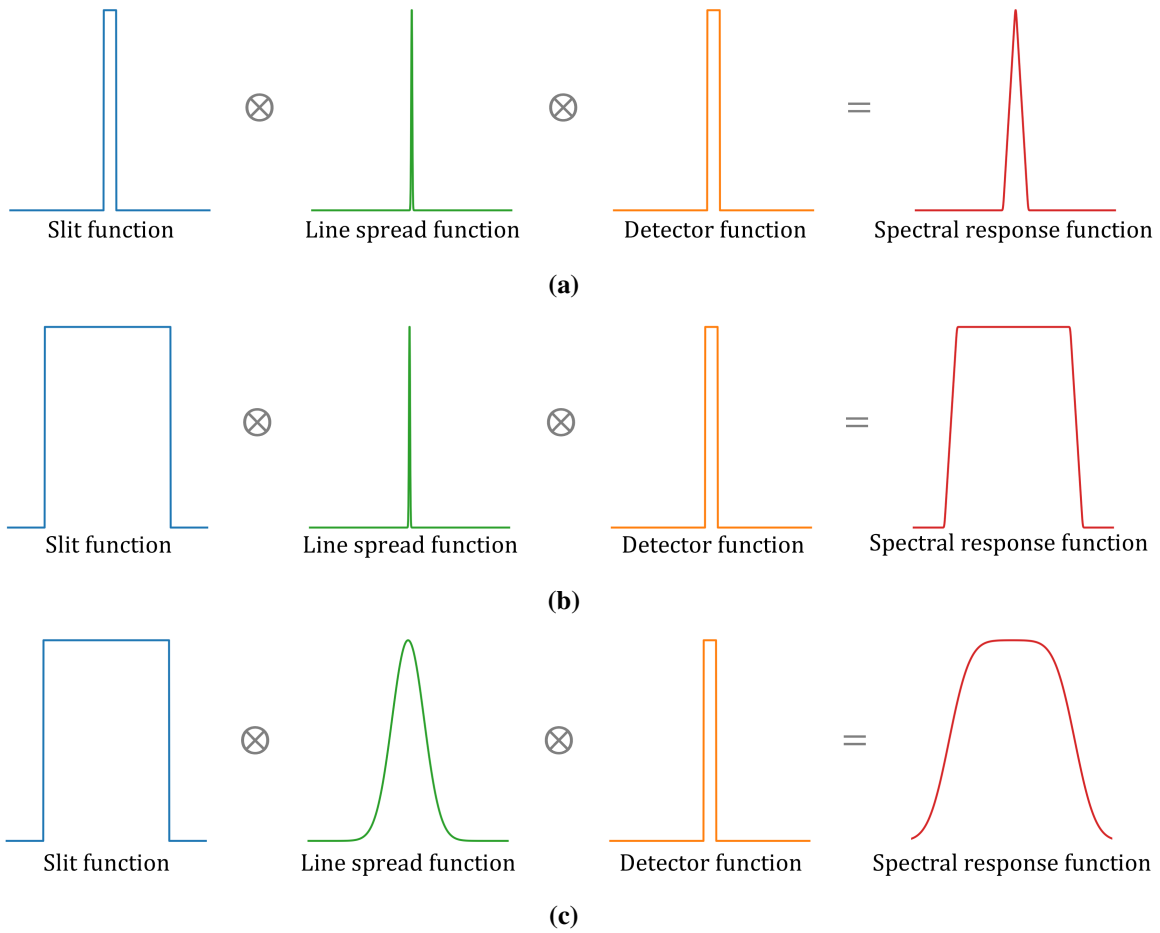

Figure 3.3: The spectral response function (SRF) for ideal and real spectrometers. The blue is the slit function, the green is the line spread function (LSF), the orange is the detector function, and the red is the total SRF. **a)** Ideal spectrometer with a narrow slit function and ideal optics, producing a narrow SRF. **b)** Ideal spectrometer with a wide slit function, producing a SRF that is well approximated by a rectangular function. **c)** Real spectrometer, including blurring from the optics that cause rounded edges of the SRF. The slit function is generally much wider compared to the detector function than what is indicated by the illustration.

The SRF is determined by measuring the response to monochromatic light. This is ideally performed by using a tunable laser or scanning monochromator [25], and measuring different wavelengths over the spectral range. It is however time-consuming, and requires expensive equipment. In addition, the wavelength accuracy measurement then relies on a well-calibrated wavelength source. A simple and fast method for obtaining the SRF at selected positions over the spectral range is by using calibration sources with gas producing spectral emission lines, as performed by e.g. [25]. One single measurement then measures the SRFs over the whole wavelength range. Compared to the tunable lasers or scanning monochromator, these calibration sources are much smaller and less expensive, and they require no wavelength calibration. However, the peaks are overlapping in the spectrum, and the method thus requires more data analysis and a defined cut-off criterion for delimiting the individual peaks. The SRF is not found for all wavelengths, but in most cases, the SRFs corresponding to the spectral lines are adequate to estimate the SRF and its variation also for the wavelengths that are not measured.

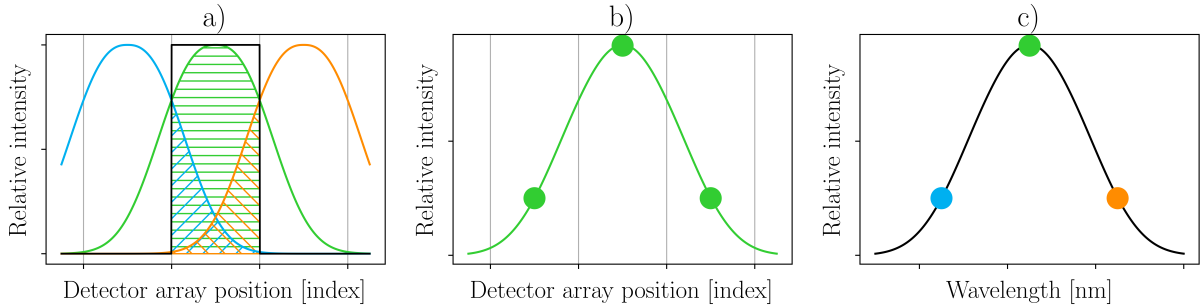

Figure 3.4: a) The slit images, i.e., the convolution of the slit function and line spread function (LSF), of different wavelengths at the detector array. Only a few wavelengths of a continuous spectrum are shown. Each wavelength gives a signal proportional to the area within each detector element, described by the convolution with the detector function. **b)** The spectral response to one wavelength by the detector array, i.e., spectral response function (SRF), which equals the convolution of the slit function, LSF, and detector function. Each plotted point corresponds to the area of the slit function within the detector element, which equals the sampling of the convolution at the detector element centre. **c)** The distribution of wavelengths within one detector element, which has the same shape as the SRF. The plotted points correspond to the area of the indicated wavelength slit functions within the detector element.

3.1.3 Signal model

This section is primarily based on [14] and [26], which considers the signal of hyperspectral cameras, and adapted to spectrometers, by considering one single spatial pixel.

A spectrometer signal is a measure of the recorded light. The initial signal on the photodetector is a count of photoelectrons n_e in each detector element, which is amplified, and turned into a digital value, given in digital numbers (DN). This final stage of amplification and digitisation is not included in the signal model, which conveniently is described in units of photoelectrons, as the photoelectron units are more intuitive and easier to interpret than the digital signal. As will be described in subsection 3.3.4, the photoelectron count can be estimated from the raw digital signal through photon transfer analysis, and thus gives a complete description.

The output signal of the spectrometer is the result of a long chain of different elements and factors of the measurement procedure, with many possible influences. Their combined effect make up the final signal.

The incoming light is described by the spectral photon radiance $L_{q,\lambda}$, in units of photons per second, unit area, solid angle, and wavelength interval. It is assumed constant in time, and the total amount of collected light is thus found from multiplying with the integration time t_{int}.

The spectrometer receives light through the slit with area A, over a field of view described by the solid angle $\Omega = \pi\, NA^2$, where NA is the numerical aperture. The light collection properties are described by their product, the étendue $A\Omega$. If using an optical fibre for collecting light, the étendue is the combined effect of the fibre and spectrometer. For simplicity, we assume homogeneous samples, so that the incoming spectral radiance is uniformly distributed over the field of view, and across the slit area. The integration of the spectral radiance over all angles of arrivals and over the whole slit area is thus simply a multiplication with the étendue.

A photon of a given wavelength that has entered the spectrometer will have some probability of exciting a photoelectron and contributing to the signal, in detector element j. This is the

combined effect of the spectral separation of the light by the diffraction grating, defining the probability of the photon reaching the detector element under consideration, and the probability of the incident photon generating a photoelectron. The latter is the combined effect of various properties. Losses occur when passing through the spectrometer optics, due to e.g. aberrations, scattering effects, reflection from lens surfaces, and other causes of imperfect transmission. The diffraction grating sends only a given ratio of the light into the desired diffraction order, and the remaining light is lost. Only a given ratio of the photons reaching the detector generates photoelectrons, which is described by the detector quantum efficiency. Only the combined effect of these properties can be observed, and is described by the the single quantity $\eta_j(\lambda)$.

Each detector element collects light over its extent on the detector array. The total light collected by the detector element is the sum of all light, independent of wavelength. As described in subsection 3.1.2, each wavelength is spread over the extent of the SRF. Assuming that the radiance is smoothly varying with wavelength, the light lost from a given detector element due to the spread is compensated for by the light similarly lost from the adjacent detector elements. The amount of light from a broadband source detected by a detector element is thus independent of the resolution. The sum of light collected is thus the spectral photon radiance within the detector element width in wavelength units, and the integral over wavelengths is simply a multiplication with the detector element width $\Delta\lambda_j$.

The photoelectron signal in one detector element j can then be expressed as the expectation value for the photoelectron count, defined by the combined effect of these properties,

$$n_{e,j} = t_{\text{int}}\, A\Omega\, \eta_j\left(\lambda_j\right)\, L_{q\lambda}\left(\lambda_j\right)\Delta\lambda_j = t_{\text{int}}\, A\Omega\, \eta_j\, L_{q\lambda,j}\Delta\lambda_j. \tag{3.5}$$

The contribution $n_d = i_d \cdot t_{\text{int}}$ from detector dark current i_d, given in units of photoelectrons per second, and any contribution from errors, such as stray light and offsets, in addition to noise, will be added to this photoelectron count, giving the full signal.

Only the combined effect of all the individual components that make up the final signal can be observed externally. The integration time is known, and the spectral photon radiance, can be found through calibrations. Also the widths of the detector elements are known. However, the combined effect of the light collection, defined by the étendue $A\Omega$, and the total efficiency η, cannot be studied separately without knowing anything of the spectrometer internals. Their combined effect can thus be contained in a single quantity, denoted by $A^* = A\Omega\eta$, which describes the net light collection, or effective throughput, of the spectrometer. A^* then has units of m^2sr, but is recommended given in units of μm^2, neglecting the sr. It describes the ratio of generated photoelectrons to incoming light, and thus the responsivity and sensitivity of the system. The expression for the final signal in each detector element can thus be rewritten and simplified using this parameter describing the net light collection per detector element A_j^*,

$$n_{e,j} = t_{\text{int}} A\Omega\eta_j\Delta\lambda_j L_{q\lambda,j} = t_{\text{int}} A_j^*\Delta\lambda_j L_{q\lambda,j}. \tag{3.6}$$

Rewriting this relation, the per-detector-element A_j^* is defined by the relation

$$A_j^* = \frac{n_{e,j}}{t_{\text{int}}\Delta\lambda_j L_{q\lambda,j}}. \tag{3.7}$$

It can be converted to wavelength units through dividing by the detector element width $\Delta\lambda_j$, defining the per-nm $A^*(\lambda)$ as

$$A^*(\lambda) = \frac{A_j^*}{\Delta\lambda_j} = \frac{n_{e,j}}{t_{\text{int}}\Delta\lambda_j^2 L_{q\lambda,j}}. \tag{3.8}$$

3.2 Noise and accuracy

Spectrometers, as any other measurement solution, estimate values through observation and data analysis. These estimated values may sufficiently indicate the true values, or, if affected by errors, they may be unreliable. The ability of the measurement solution to measure values that are close to the true values, and thus provide reliable data, is described by the *accuracy*. Similarly, the *precision* describes how repeatable the measured values are. The level of accuracy and precision may considerably affect what estimations and conclusions are made based on the measurement, and their correctness and reliability.

When considering a spectrometer, a proper characterisation of the sources of error, and their effect on the accuracy, is important. As the final measurement is the combined effect by all individual factors of the measurement procedure, many different factors may cause errors. Only their combined effect is observed, and only their effect on the final result is of interest. Thus, only sources that non-negligibly affect the measurement are of interest. The influence by an error source can be investigated through varying the influence quantities.

The sources of error may be categorised as random or systematic. The random errors cause variation of no specific pattern within repeated measurements, and their effect may be reduced by averaging of the repeated measurements. Systematic errors, on the other hand, affect all measurements in the same way, and change the overall accuracy of the measurements. For example, temperature drift is considered systematic, while thermal fluctuations in the electronics is considered random. However, not all types of errors fit perfectly into these categories. For example, the background light during measurements may be dependent on whether the weather is sunny or cloudy, which in principle is random, but cause systematic errors. For describing such errors, the category random systematic is suggested [10]. Their effect on single, isolated measurement series cannot be removed through averaging, however, when considering multiple measurement series acquired under the same conditions, such as yearly within the same month, the effect from the weather on the background light is expected to even out. In the scope of this thesis, such random systematic sources are treated as systematic.

Measurement systems are, to a greater or lesser extent, limited by *noise*, which is random fluctuations that corrupts the signal, and reduces its accuracy and precision. The noise limits the quality of the measurements and data, and the amount of information that is accessible. In this thesis, noise is defined as being caused by random errors, and its contribution can be reduced by averaging. Some systematic error sources are sometimes referred to as noise, such as the term *fixed pattern noise* referring to detector element sensitivity non-uniformities, which can be corrected through reference measurements, but these are not random error sources that can be reduced by averaging, and are thus not treated as noise in this thesis.

In the following, random error sources are described as noise, while systematic and random systematic sources are described as errors.

3.2.1 Errors

This thesis considers the instrument-specific sources of error that are given in Table 3.1. Also other sources of error may be present in a spectrometer measurement, but these are out of scope

Table 3.1: Examples of sources of error in a spectrometer that are considered systematic or random systematic. These cannot be reduced by averaging, and are not considered as noise.

Error source	Description
Wavelength errors	Errors in the wavelength calibration, causing deviations between the measured and true wavelengths of the detected light.
Not sufficient resolution	Relevant spectral features are not resolved and detected.
Stray light (internal)	Light from other wavelengths that is detected at a given wavelength position of the detector. May e.g. be caused by light in other diffraction orders of the diffraction grating.
Background light	Also termed external stray light. Unwanted light from the measurement surroundings that contributes to the measured spectrum. May be removed through background correction, but this introduces excess noise, as the shot noise from both the background light and the correction spectra is present in the corrected signal.
Non-linearity	The conversion of incoming light level to detected signal level is not linear.
Temperature drift	The signal, and particularly the dark current, is temperature dependent. Changes in temperature will then distort the measurement.
Fixed pattern noise	Non-uniformities in the sensitivity of detector elements causing a fixed variation of the signal. May be dependent on parameters such as temperature and exposure time. Can be corrected for by measuring the detector element responsivity, by using a light source with a known and preferably featureless spectrum, and comparing acquired and expected spectra. It is also automatically corrected for through white reference correction. The term may also describe the fixed pattern addition to the signal from dark current in the photodetector.

of this thesis. For example, factors in the measurement process, such as sample presentation, of movement of the spectrometer during the measurement, may cause errors. Other instrument-specific error sources are also possible. In addition, only measurements on homogeneous samples and reference objects are considered. Thus, also effects such as point spread and spatial coregistration, which describes errors in the collection of light from the sample in the spatial dimension, and cause errors for heterogeneous samples, are out of scope.

3.2.2 Noise and SNR

In this thesis, the noise in a spectrometer measurement is considered coming from the photodetector and readout electronics. An overview of the noise mechanisms is given in Table 3.2. These will be further defined and discussed in the following sections.

Table 3.2: The error sources in a spectrometer that are considered random, can be removed through averaging, and thus are treated as noise in this thesis.

Type of noise	Source	Description	Behaviour
Shot noise	Quantisation of photoelectrons	Follows Poisson statistics	Signal dependent
Dark current noise	Shot noise from dark current	Dependent on temperature and integration time	Builds up over the integration time
Readout noise	Electronic effects in the detector, e.g., thermal and flicker noise	Temperature dependent	Constant in each detector element

The important quantity that affects the signal quality is the relative signal strength with respect to the noise, as this describes the ability to discern the measured value from the noise, and thus the ability to access the information that is contained in the spectrum. This is defined as the *signal-to-noise ratio* (SNR). Different applications have different SNR requirements, depending on the required level of SNR to distinguish changes in the spectral features.

3.2.2.1 Signal statistics

This section is mainly based on [27, pp. 407-410], and is further used for deriving the statistical relations describing noise and SNR. The following discussion concerns variation of a process x in the temporal dimension, i.e., over time. It can thus be used to describe the statistics in a single detector element over time, and does not relate the values of different detector elements. The index i denotes a measurement in the temporal dimension.

The expected value of a process x, indicated with an E, is defined as the sample mean μ_x, i.e., the average that is obtained from all sample functions of the process,

$$\mu_x = E\{x\} = \lim_{N\to\infty} \frac{1}{N} \sum_{i=1}^{N} x_i. \tag{3.9}$$

It follows the linearity relation

$$E\{ax + by\} = aE\{x\} + bE\{x\}, \tag{3.10}$$

where a and b are constants, and x and y are variables.

The variance of x, which is the square of the standard deviation σ_x, is given by

$$\sigma_x^2 = E\left\{(x-\mu_x)^2\right\} = E\left\{x^2 - 2x\mu_x + \mu_x^2\right\} = E\left\{x^2\right\} - 2\mu_x E\{x\} + \mu_x^2 = E\left\{x^2\right\} - \mu_x^2. \tag{3.11}$$

For a finite number of samples N of the process x, the expected value is approximated as the sample average

$$E\{x\} \approx \frac{1}{N}\sum_{i=1}^{N} x_i = \bar{x}. \tag{3.12}$$

Using this sample average as an estimate of the population mean μ_x reduces the degree of freedom to from N to $N-1$, a bias that is corrected for by writing the sample variance as

$$s^2 = \frac{1}{N-1}\sum_{i=1}^{N}(x_i - \bar{x})^2. \tag{3.13}$$

The variance of a sum of two random variables x and y is given by

$$\sigma_{x+y}^2 = E\left\{(x+y)^2\right\} - \mu_{x+y}^2 = E\left\{x^2\right\} - \mu_x^2 + E\left\{y^2\right\} - \mu_y^2 + 2\left[E\{xy\} - \mu_x\mu_y\right]. \tag{3.14}$$

When x and y are independent and assumed reasonably well behaved, i.e., $E\{xy\} = \mu_x\mu_y$, this simplifies to

$$\sigma_{x+y}^2 = \sigma_x^2 + \sigma_y^2. \tag{3.15}$$

Hence, the variance of the sample average $\bar{x}$ from N independent measurements of x_i is given by

$$\sigma_{\text{average}}^2 = \sum_{i=1}^{N} \text{var}\left(\frac{1}{N}x_i\right) = \sum_{i=1}^{N}\frac{1}{N^2}\sigma_i^2. \tag{3.16}$$

When all single measurements x_i have the same variance σ_i^2, or in other terms are independent and identically distributed with average variance σ_i^2, the variance of the sample average $\bar{x}$ from N measurements is given by

$$\sigma_{\text{average}}^2 = N\frac{1}{N^2}\sigma_i^2 = \frac{1}{N}\sigma_i^2. \tag{3.17}$$

Hence, when averaging N measurements, the standard deviation of each value in the signal is reduced by a factor $1/\sqrt{N}$.

3.2.2.2 Noise in a photodetector

This section is mainly based on [28, pp. 490-513], and concerns the noise in individual detector elements.

The noise from a photodetector is commonly represented as the standard deviation σ in the temporal dimension, i.e., the RMS fluctuation, of the electron signal. It is here represented as an electron count n_e, as it then conveniently can be related to the signal photoelectrons, but it could also be represented by a DN count. The main types of noise mechanisms are the signal-dependent shot noise of the generated electrons and signal-independent detector noise, including both dark current noise and readout noise. Also other sources of noise are possible, but

only these main types are considered here. The *noise floor* is defined as the signal-independent noise, i.e., the sum of dark current noise and readout noise.

Shot noise, also known as Poisson noise or photon noise, is a fundamental source of noise due to the granular nature of the individual charge carriers that constitutes a signal. The signal, given by the number of generated photoelectrons n_e, is linearly related to the incoming number of photons n_p through the quantum efficiency QE, such that $n_e = QE \cdot n_p$. This generation of photoelectrons by the incoming photon flux is a random process that follows Poisson statistics, with standard deviation given by the square root of the expectation value, $\sigma = \sqrt{\mu}$. Hence, for a mean signal $\bar{n_e}$, neglecting other sources of noise than shot noise, both the standard deviation σ of the number of generated photoelectrons, and the SNR $= \bar{n_e}/\sigma = \sigma^2/\sigma = \sigma$, equals $\sqrt{\bar{n_e}}$. The shot noise is then given by

$$\sigma^2_{\text{shot}} = \sqrt{n_e}^2 = n_e = QE \cdot n_p, \tag{3.18}$$

and is dependent on the expectation value of the number of photons reaching the detector, independent on whether it is due to large integration time or illumination power. Ideally the noise in the signal is dominated by this fundamental shot noise, which is random by nature. The system is then considered shot noise limited, and the statistics are simplified as the other noise sources are neglected. As these noise conditions are achieved for higher signal levels, it is desirable with as high signal as possible to reduce the total noise.

As explained in subsection 2.2.2, photodetectors has a dark current i_d, given in units of photoelectrons per second. Its contribution to the final signal builds up over the integration time t, to a total number of electrons per detector element $n_d = i_d \cdot t$. This dark current signal generates shot noise, which add *dark current noise* to the final signal, given by

$$\sigma^2_{\text{dark}} = \sqrt{i_d \cdot t}^2 = i_d \cdot t = n_d. \tag{3.19}$$

Readout noise is generated from the photodetector and electronics when the signal is read out, in components such as the output amplifier and the ADC. The noise includes sources such as thermal noise, also known as Johnson noise, due to thermally induced motion of atoms, flicker noise, due to random variations in the diffusion of charge carriers within the device, and quantisation error from the digitisation of the photoelectron voltage. The readout noise is temperature dependent due to the contribution from thermal noise, and otherwise dependent on the device. For a given temperature, it is constant for all readouts, independent of signal and integration time. Hence, it sets a minimal noise floor level for a measured signal, and its relative effect is larger for weaker signal. The constituents are assumed to be independent, and their squared standard deviations can thus be summed, giving the total readout noise in units of electrons n_r as

$$\sigma^2_{\text{readout}} = \sigma^2_{\text{ADC}} + \sigma^2_{\text{amplifier}} + \ldots = n_r^2. \tag{3.20}$$

Analysing and quantifying individual sources contributing to the readout noise is out of scope of this thesis, as the total readout noise is directly measured and modelled.

Noise model

Assuming that the different noise sources are independent and reasonably well behaved, the squares of standard deviations σ from different sources can be summed, as shown in Equation 3.15. The total noise in one detector element j from the considered sources is then given

by

$$\sigma_j = \sqrt{\sigma^2_{\text{shot},j} + \sigma^2_{\text{dark}} + \sigma^2_{\text{readout}}} = \sqrt{n_{e,j} + i_d \cdot t + n_r^2}, \tag{3.21}$$

which gives an SNR of the single detector element that can be expressed as

$$\text{SNR}_j = \frac{n_{e,j}}{\sqrt{n_{e,j} + i_d \cdot t + n_r^2}}. \tag{3.22}$$

If the signal is constant over all detector elements, the SNR per detector element is given by

$$\text{SNR}_{j,\text{const}} = \frac{\bar{n_e}}{\sqrt{\bar{n_e} + i_d \cdot t + n_r^2}} = \frac{\bar{n_e}}{\bar{\sigma}}. \tag{3.23}$$

All detector elements are generally considered having the same magnitudes of dark current and readout noise. While the shot noise is random and independent between adjacent detector elements, this may not hold for readout noise, making the noise in the detector elements correlated. However, if the sensor and the electronics in the spectrometer are well designed, which generally holds for modern instruments, also the readout noise is independent between the detector elements. Assuming that this applies, and that the noise in the detector elements is uncorrelated, the sum of the noise from multiple detector elements M is found by summing the squared noises of the individual detector elements j,

$$\sigma^2_{\text{summed}} = \sum_{j=1}^{M} \left[n_{e,j} + i_d \cdot t + n_r^2 \right] = \sum_{j=1}^{M} n_{e,j} + M \left[i_d \cdot t + n_r^2 \right]. \tag{3.24}$$

Using the relation

$$\sum_{j=1}^{M} n_{e,j} = M\bar{n_e}, \tag{3.25}$$

this simplifies to

$$\sigma_{\text{summed}} = \sqrt{M\left(\bar{n_e} + i_d \cdot t + n_r^2\right)}. \tag{3.26}$$

Hence, when summing the signal $n_{e,j}$ over M detector elements, the SNR of the sum is given by

$$\text{SNR}_{\text{summed}} = \frac{M\bar{n_e}}{\sqrt{M\left(\bar{n_e} + i_d \cdot t + n_r^2\right)}} = \sqrt{M}\frac{\bar{n_e}}{\bar{\sigma}}, \tag{3.27}$$

increased by a factor $\sqrt{M}$ compared to the SNR of each individual detector element given by Equation 3.23.

3.3 Methods for spectrometer data acquisition and analysis

3.3.1 Multiple repeated measurements and averaging for noise estimation and reduction

The noise in one detector element j of a single spectrometer measurement i, represented by the standard deviation $\sigma_{i,j}$, can be estimated by taking the square root of the sample variance s_j^2 of the detector element. This can be measured by acquiring N spectra, and using Equation 3.13.

The noise can be reduced through averaging of multiple repeated measurements. As given by Equation 3.17, averaging N spectra that are obtained under the same measurement conditions reduce the noise with a factor $1/\sqrt{N}$. The noise in detector element j of the average of the N acquired spectra, $\sigma_{\mathrm{N,j}}$, is thus found by scaling the single spectrum noise $\sigma_{i,j}$ with $1/\sqrt{N}$.

If we could make an infinite number of measurements, we could, in principle, remove the noise. However, this requires stable spectra without drift, e.g., due to temperature changes. In addition, it requires longer measurement times, which is not always possible. The number of measurements N must be chosen based on the available measurement time, and on the system stability, as, when the signal remains stationary over the whole measurement series, a higher number of averaged measurements reduces the noise in the system. When measuring stable sources, such as for spectrometer performance characterisation, $N = 400$ is considered a suitable number of spectra for each measurement, as they are acquired over a sufficiently short time period for stability in the measurement set up, while reducing the noise with a factor $1/20$.

3.3.2 Dark correction

Acquired spectra has a contribution from dark current, any background light, and other signals and offsets that are present without illumination of the detector. Dark correction of the spectrum can be performed to remove this contribution, and obtain the proper measure of the signal. This is performed by subtracting a dark spectrum, acquired when blocking the illumination. However, as the dark spectrum has the same level of readout noise and dark current noise as the signal spectrum, and shot noise from any background light, this introduces excess noise. Caution must be made to reduce this noise contribution.

If the system is stable, an averaged dark spectrum can be used for the dark correction. This introduces no extra variance to the corrected spectrum, but adds noise to the final signal compared to the real spectrum. When averaging N_{signal} signal spectra and N_{dark} spectra, the total noise of the corrected spectrum is given by

$$\sigma_{\mathrm{corrected}} = \sqrt{\frac{\sigma_{\mathrm{signal}}^2}{N_{\mathrm{signal}}} + \frac{\sigma_{\mathrm{dark}}^2}{N_{\mathrm{dark}}}}. \tag{3.28}$$

Hence, the noise is reduced by averaging a sufficient number of both signal and dark spectra.

When the system is considered very stable, with negligible drift of the dark spectrum over time, a single dark spectrum can be acquired for a series of measurements. In this case, spending more time on the dark measurement by increasing the number of acquired dark spectra, even

beyond the number of acquired signal spectra, should be considered, as this minimises the total noise of the corrected spectrum.

If the system changes throughout the measurement series, e.g., due to temperature drift, or changes in the background light, but is considered stable over one measurement, the dark correction is improved, and possible drift is accounted for, by acquiring both signal and dark spectra for each measurement in the series. When acquiring a limited number of spectra $N_{\text{tot}} = N_{\text{signal}} + N_{\text{dark}}$ in each measurement, the optimal ratio between N_{signal} and N_{dark} depends on what noise mechanisms are present. When limited by readout noise, which gives equal noise to both the signal and dark measurements, the noise is minimised by using $N_{\text{signal}} = N_{\text{dark}}$, while for shot noise limited measurements, i.e., when shot noise is the dominating source of noise, the noise is minimised by using $N_{\text{signal}} > N_{\text{dark}}$. However, the noise curve is rather flat around the minimum, and the added noise from using numbers deviating slightly from the optimal values is assumed negligible. Acquiring some more signal spectra than dark spectra, e.g., the ratio $N_{\text{signal}}/N_{\text{dark}} \approx 60/40$, is generally a good choice for minimising the noise when both readout noise and shot noise is present.

If the system changes rapidly throughout one single measurement, e.g., due to temperature changes and varying background light, signal and dark spectra should be acquired as closely in time as possible. This can be performed by repeatedly acquiring sets of signal and dark spectra, e.g., by using a shutter for a periodic blocking the light, and correcting each spectrum individually. The noise of each corrected spectrum is then given by $\sigma_{\text{corrected}} = \sqrt{\sigma^2_{\text{signal}} + \sigma^2_{\text{dark}}}$. When averaging N corrected spectra, the total noise is given by $\sigma_{\text{corrected}}/\sqrt{N}$, which equals that given by Equation 3.28 for $N_{\text{signal}} = N_{\text{dark}} = N$.

3.3.3 White reference correction

As explained in subsection 2.2.2, photodetectors have a wavelength dependent quantum efficiency, and thus non-uniform response over the spectral range. Also other components in the spectrometer, such as the diffraction grating, exhibit wavelength dependency, which may alter the total spectrometer response. Besides the wavelength dependency, the responsivity of the detector elements may vary, e.g., due to variations in the amplifier and ADC, and some detector elements may appear brighter than the others. This effect is known as photo-response non-uniformity (PRNU), and causes a fixed variation of the signal, termed fixed pattern noise. It may be dependent on parameters such as temperature and exposure time, and may also cause differences in the dark currents.

When using the spectrometer for characterising a light source, both the wavelength dependent responsivity and the fixed pattern noise must be corrected for. This can be performed by measuring the total response curve of the spectrometer, by using a light source with a known and preferably featureless spectrum, and comparing acquired and expected spectra.

The correction is easier for absorption spectroscopy, as effect on the light spectrum from sample absorption is measured. The applied light source follows a given spectral distribution, e.g., a blackbody spectrum, which, together with the response of the spectrometer, affects the measured spectrum. The combination of the light source spectrum and spectrometer response must be corrected for to obtain the absorption spectrum of the sample. A simple method for performing such correction is white reference correction, by making a reference measurement of

a diffuse reflective sample, termed a white reference, and dividing all acquired spectra by the corresponding reference spectrum. As the spectrum may change with temperature and exposure time, a reference spectrum from the same exposure time should be acquired regularly through a measurement series, with frequency depending on how stable the system is.

3.3.4 Photon transfer analysis

The noise statistics can be used for quantifying the different noise sources in the spectrometer. This is the basis of *photon transfer analysis*, which is thoroughly discussed in [29] and [26]. This technique determines properties such as the readout noise, dark current, linearity, saturation level, and dynamic range of the signal. It relies on the assumption that the noise is additive and follow the noise model,

$$\sigma^2_{\text{total}} = \sigma^2_{\text{shot}} + \sigma^2_{\text{dark}} + \sigma^2_{\text{readout}} = n_e + i_d \cdot t + n_r^2, \tag{3.29}$$

where n_e is the photoelectron count, i_d is the dark current in units of photoelectrons per second, t is the integration time, and n_r is the readout noise in units of photoelectrons.

In addition, noise statistics are useful for relating the raw measurement to the corresponding detected photoelectron count. The recorded signal by a spectrometer is a count of photoelectrons excited from the incoming light in each detector element. The output signal is converted into DN by the amplifier and ADC of the detector, but usually, the photoelectron count is more interesting. It defines the noise, and is more linked to the physics of the signal, and the information about the sample. The photoelectron count is essentially proportional to the DN signal count, but scaled through amplification and digitisation. It can be estimated from the DN through photon transfer analysis.

For repeated measurements, the mean signal in DN units, S, is related to the mean photoelectron count as

$$\bar{S} = G_S \bar{n}_e, \tag{3.30}$$

where G_S is the gain factor. Obtaining this gain factor thus allows for estimating the photoelectron count from the DN signal.

G_S is simply found by measuring the output statistics of the signal without knowledge of any of the spectrometer internals. The variance of the signal is given by the noise model,

$$\sigma^2_S = G_S^2 \left[\bar{n}_e + i_d \cdot t + n_r^2\right], \tag{3.31}$$

which gives the relation

$$\frac{\sigma^2_S}{\bar{S}} = G_S \frac{\left[\bar{n}_e + i_d \cdot t + n_r^2\right]}{\bar{n}_e}. \tag{3.32}$$

Assuming a shot noise limited signal, the gain factor can be directly obtained from the relation between the signal and noise, as

$$G_S \approx \frac{\sigma^2_S}{\bar{S}}. \tag{3.33}$$

For investigation of the different noise sources in the signal, and direct estimation of the gain factor, the *photon transfer curve* (PTC) is useful. This is based on the total noise as a function

of signal, given by

$$\sigma_{\text{total}}\,(DN)^2 = G_S^2\left[n_r^2 + i_d \cdot t + n_e\right] = G_S^2\left[n_r^2 + i_d \cdot t\right] + G_S S\,(DN). \tag{3.34}$$

The intercept of a linear curve fit of the noise variance will indicate the noise floor, i.e., the sum of the readout and dark current noise of a given integration time, while the slope is the gain factor G_S. The integration time dependent dark current can be separated from the constant readout noise by performing a curve fit of the noise floor as a function of integration time t to the relation

$$\sigma_{\text{total}}\,(DN)^2 = G_S^2\left[n_r^2 + i_d \cdot t\right]. \tag{3.35}$$

The standard deviation PTC is the logarithmic plot of noise as a function of signal in DN units, and thus the square root of the linear relation. The variance PTC, which is the squared noise as a function of signal, plots the linear relation directly. Both variations of the PTCs are generated for the example in Figure 3.5.

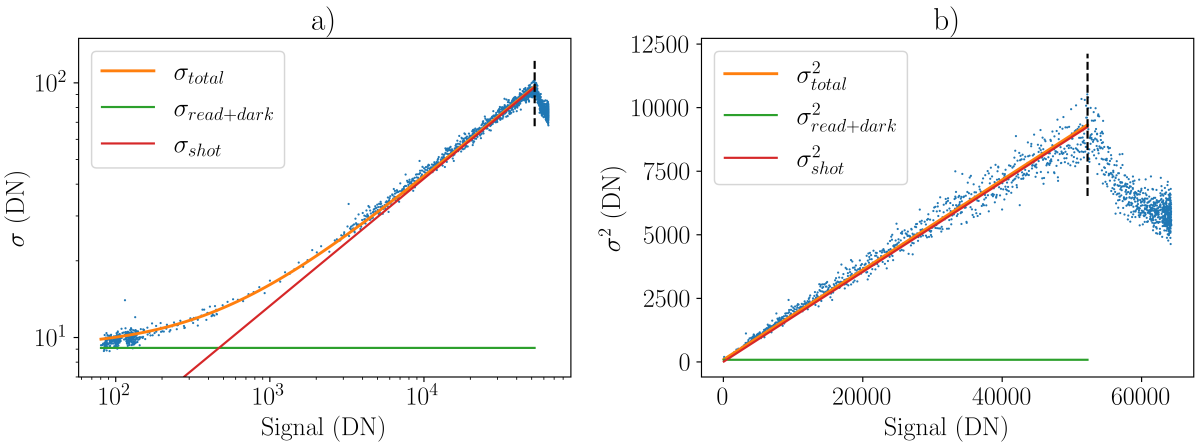

Figure 3.5: a) Standard deviation photon transfer curve (PTC) and **b)** variance PTC. The sum of readout and dark current noise is separated from the shot noise, and the slope of the shot noise is found, which is the inverse of the gain factor G_S. The signal is found to be nonlinear above approximately 52 000 counts, where the slope of the signal changes drastically.

As can be seen in the example plot, PTC is a very sensitive tool for revealing non-linearities and full-well conditions, which defines the saturation level of the spectrometer. They are revealed by any changes or deviations from the constant slope of the signal, and by a decrease in the noise as a function of signal. As both the noise floor and the saturation conditions are obtained through the analysis, their ratio, the *dynamic range*, is also directly obtained.

Photon transfer analysis assumes that the noise follows the expected noise model. Any deviation distorts the resulting estimations. Constant noise sources increase the estimated readout noise, but does not otherwise change the statistics or estimations. On the other hand, signal-dependent noise sources affect the estimated gain factor, and thus the conversion of all properties between DN and photoelectron units. Fortunately, the accuracy of the estimated gain factor can be confirmed by studying the noise statistics of the signal that is converted into photoelectron units. The shot noise should precisely follow the square root of the signal. Any deviations from this shape, such as unexpected peaks, reveals unknown sources of noise or drift of the spectrometer parameters during the measurement time.

3.3.5 Spectrum resampling

The general technique of *resampling* describes several different operations on the data, including binning, smoothing, and interpolation. It involves using the data points in the raw spectrum, for generating a new and modified spectrum. Following the derivation given in [26], the resampling operation gives a photoelectron count $n_{e,k}$ in each point k of the resampled spectrum. It involves a linear combination of the photoelectron signal $n_{e,j}$ in each detector element j, described by weights w_{jk}, such that

$$n_{e,k} = \sum_j w_{jk} n_{e,j}. \tag{3.36}$$

The weights can be described as a discrete function, or the sampled values of a continuous function in the detector elements. The resampling can then be described by convolution of the signal with a given function and resampling with a given sampling interval. The value in each resampled point k is then the weighted sum of the detector element values j, with weights defined by the function.

Assuming a linear response of the spectrometer, the total variance of each value in the resampled signal is given by

$$\sigma_k^2 = \sum_j w_{jk}^2 \sigma_j^2. \tag{3.37}$$

If each detector element contributes to more than one of the values in the resampled signal, the noise of the corresponding values are correlated. Correlations of the noise may affect the noise statistics.

3.3.5.1 Binning

Binning involves combining blocks of adjacent detector elements, by summing or averaging their values. This is simply resampling with weights equal to 1, or described by a rectangular function, and sampling interval M, where M is an integer of the original sampling interval. This creates new signal samples that are equivalent to multiples of the old sampling. It can be performed in the detector hardware before readout, denoted as *hardware binning*, or simply in the data analysis after the measurement, denoted as *software binning*. The latter is commonly denoted as "box-car averaging" [19].

As each each detector element contributes to only one single resampled value, the noise of the values in the binned signal is uncorrelated, and follow the same noise statistics as the original signal.

Binning can be used to improve the SNR of a signal. As was seen by Equation 3.27, software binning with a binning factor for M, i.e., summing or averaging M detector elements, improves the SNR with a factor $\sqrt{M}$. For hardware binning, the readout noise is additionally reduced to that of a single detector element, giving a total noise

$$\sigma_{\text{hardware binning}} = \sqrt{M\left(\bar{n_e} + i_d \cdot t\right) + n_r^2}. \tag{3.38}$$

Compared to the SNR of each individual detector element, given by Equation 3.23, this gives an increase of the SNR by a factor

$$\frac{\mathrm{SNR}_{\text{hardware binning}}}{\mathrm{SNR}_{j,\text{const}}} = \frac{M\sqrt{\bar{n}_e + i_d \cdot t + n_r^2}}{\sqrt{M\left(\bar{n}_e + i_d \cdot t\right) + n_r^2}}, \tag{3.39}$$

which simplifies to $\sqrt{M}$ for a shot noise limited system. Thus, when not shot noise limited, the hardware binning gives a larger increase of the SNR than software binning due to less relative contribution from readout noise.

Despite the reduced contribution by readout noise from hardware binning, software binning is the most common for spectroscopy. Hardware binning reduces the data size, and can thus be important for e.g. hyperspectral imaging, but spectroscopy involves only one single spectrum and moderate data sizes. Software binning is easily implemented for all signals, while hardware binning functionality must be available for the detector, which not always is the case. In addition, unlike for hardware binning, software binning can be performed without deleting any information, as a copy of the un-binned signal can be kept. These advantages are considerable compared to the increased readout noise contribution, which is only seen for very low signal levels. In this thesis, the term binning generally indicates software binning.

As will be discussed in subsubsection 3.3.5.3, the SNR is improved at the expense of reduced resolution.

3.3.5.2 Smoothing filters

Spectra can be smoothed by applying a smoothing filter. This process is a form of resampling, where the signal is convoluted with a given function, and resampled with the original sampling interval. This way, the signal is smoothed through removing noise and other high-frequency components, such as narrow peaks and spikes. Different functions have different abilities to filter out the high-frequency components, and thus give different properties of the smoothed signal. A rectangular function has a Fourier transform given by the sinc function, with long tails at high frequencies. When using this function for smoothing, as for binning, high-frequency components remain in the smoothed signal. On the other hand, for the Gaussian function, also the Fourier transform is Gaussian, and high-frequency components are removed. The Gaussian function is generally considered the most well suited at removing high-frequency components from the signal, while keeping the relevant information of the low-frequency components.

Smoothing filters may make the noise in different detector elements correlated, as the value in a single detector element may contribute to multiple values in the resampled signal. They also affect the frequency content, and may remove information from the spectrum. The method should thus be applied with caution. Photon transfer analysis must be performed before any smoothing is performed.

3.3.5.3 Relation between SNR and resolution

The resampling operation may change the SNR. For a constant signal $n_{e,j} = \bar{n}_e$ with constant standard deviation $\sigma_j = \bar{\sigma}$ over the detector elements j, the relations for signal and variance in

each point of the resampled spectrum simplify to

$$n_{e,k} = \bar{n}_e \sum_j w_{jk} \tag{3.40}$$

and

$$\sigma_k^2 = \bar{\sigma}^2 \sum_j w_{jk}^2, \tag{3.41}$$

which gives an SNR described by

$$\mathrm{SNR}_k = \frac{\bar{n}_e \sum_j w_{jk}}{\bar{\sigma}\sqrt{\sum_j w_{jk}^2}}. \tag{3.42}$$

Compared to the average SNR in a sample of the original signal, given by Equation 3.23, the resampling changes the SNR with a factor

$$\frac{\mathrm{SNR}_k}{\mathrm{SNR}_j} = \frac{\sum_j w_{jk}}{\sqrt{\sum_j w_{jk}^2}}. \tag{3.43}$$

Different smoothing filter functions give different increase in the SNR. For example, a rectangular function that spans over K detector elements will increase the SNR with a factor $\sqrt{K}$, while it has been found that the same SNR increase is obtained by a Gaussian function with a FWHM of $\sqrt{\frac{2\ln 2}{\pi}}K \approx 0.664K$, as illustrated in Figure 3.6. Hence, a Gaussian will increase the SNR with a factor $\sqrt{K} = \sqrt{FWHM/0.664}$. For a triangular function, the same SNR increase of $\sqrt{K}$ is obtained by using a FWHM of approximately $0.67K$.

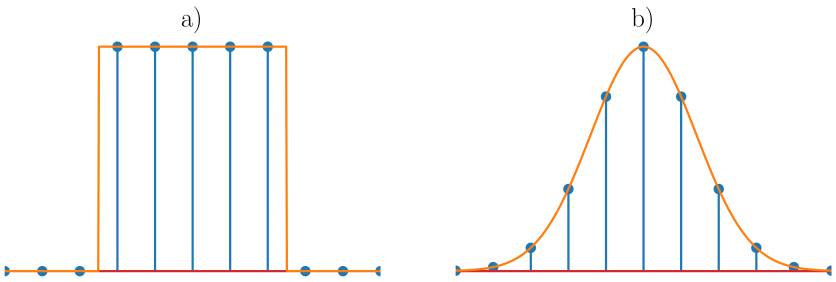

Figure 3.6: a) Rectangular function that spans over $K = 5$ detector elements and **b)** Gaussian function with FWHM corresponding to $0.664K$. They give the same increase in the SNR, with a factor $\sqrt{K}$, when used for smoothing.

The resampling may also change the resolution of the spectrum, which is described by the width of the SRF. It is essentially a change of the detector element part of the SRF, describing the sampling of the light reaching the detector array. Hence, the SNR increase is obtained at the expense of reduced resolution. The amount of smoothing should thus be chosen to increase the SNR as much as possible, while maintaining sufficient resolution for the given application. As will be discussed in subsection 5.1.4, the resolution is however not uniquely defined, and the change of the resolution from resampling is not trivial. When defining the resolution as the standard deviation of the SRF distribution, i.e., the distribution standard deviation rather than

the temporal standard deviation used for noise, the resulting resolution of the resampled signal is given by

$$\sigma_{resampled} = \sqrt{\sigma_{raw}^2 + \sigma_f^2}, \tag{3.44}$$

where σ_{raw} is the resolution of the raw signal, and σ_f is the distribution standard deviation of the resampling function. When the resolution is defined as the FWHM of the Gaussian fit of the SRF, the resulting resolution from resampling is not as trivial. For a diffraction grating spectrometer, with SRF resembling a Gaussian, it is well approximated by Equation 3.44. In any case, it would be interesting to study the relation between the resolution decrease and SNR increase for different smoothing functions. For example, for a Gaussian SRF, an increase in resolution from 2 nm to 3 nm, obtained through convolution with a Gaussian function with $FWHM = 2.23$ nm, would yield an increase in the SNR of $\sqrt{FWHM/0.664} = 1.83$. Additionally, there is generally no common optimal SRF shape, as some applications would benefit from narrow peaks and broader tails, such as a Lorentzian function, while others require more well-defined peaks, such as rectangular functions. Also taking this into account in relation to the SNR improvement, the optimal choice of smoothing functions for different applications could then be found.

3.3.6 Methods of improving the SNR

The SNR describes the signal quality, and improving the SNR is desirable. This is obtained by any changes that increase the signal or reduce the noise.

As discussed in subsection 3.3.1, the noise can be reduced through averaging of multiple repeated measurements. Averaging N spectra that are obtained under the same measurement conditions increases the SNR with a factor $\sqrt{N}$. For stable spectra, the SNR can thus be improved by increasing the measurement time and acquiring more measurements.

The signal level can be increased by increasing the slit size in the spectrometer. This requires a physical change of the instrument, but we are free to choose an optimal slit size for a given application when buying a new spectrometer. However, as discussed in subsection 3.1.2, this broadens the SRF, and, as will be defined in subsection 5.1.4, reduces the resolution.

As discussed in subsection 3.3.5, the SNR can be improved through resampling, either through hardware binning, or, more commonly, through software binning and with smoothing filters. As discussed, similarly for the increased slit size, this broadens of the SRF and reduces the resolution. It is however not broadened in the same way, and the effect of a different slit is not equal to resampling.

In total, the SNR should be increased by averaging as many measurements as possible, defined by the time available for each measurement. Further, the SNR can be improved at the expense of the resolution, through both increasing the slit size and performing resampling. A point of balance must be found, with as much increase of the SNR as possible, while retaining sufficient resolution. This is highly dependent on the application, as will be discussed in subsection 5.1.4.

Chapter 4

Current status of the field

A quick comparison of the data sheets of 5 diffraction grating spectrometers revealed variations in the given performance characteristics. While this may not be a proper representative selection of all data sheets, it serves as an illustration of the lack of a common framework for spectrometer specification. Their origin is not revealed, as this is not considered of relevance. Only dynamic range, saturation, and resolution was common to all specifications, while 4 specified spectral range, spectral sampling interval, dark current, readout noise, linearity, and SNR, 3 specified the speed, power consumption, temperature operating range, and integration time range, 2 specified stray light, and only 1 specified sensitivity. As will be discussed in chapter 5, all these mentioned properties should be specified for a proper performance characterisation. Also other characteristics, such as numerical aperture and f-number, both describing the light collection properties, slit size, gratings, and detector quantum efficiency were given for some data sheets. As discussed in subsection 3.1.3, all these affect the total sensitivity A^* of the spectrometer, and only their combined effect is of relevance. The specification is thus not suited for a simple and direct specification of the total performance. Additionally, a physics based understanding of the instruments, combined with experience, is required for comparing instrument performance using the given parameters. The specification may not display the overall performance in a fair way, and when not properly combining all characteristics that may be interdependent, such as sensitivity and resolution, false impressions can be given. In principle, through different metrics, different spectrometers can be considered the best performing, while this is not a proper specification of the full performance. In total, the given parameters of spectrometer data sheets are not considered as giving an adequate specification of the spectrometer performance.

No full and complete text book giving a sufficient introduction to the working principles of spectrometers has been found. For fully understanding the spectrometer operation and importance of various performance characteristics, various literature must be approached, in which differences in the use of terminology is present. This complicates the establishment of a common standard, for which a common terminology is required.

When setting out to explore the field of spectroscopy standardisation, surprisingly few publications with a physics based first principles approach were found. There seem to be no clear and easily applicable method for comparing spectrometers from different suppliers. When searching for "spectrometer comparison" on Google, the search results are commercial promotions of different spectrometer manufacturers, and no proper, unbiased, and sufficient method stand out,

even in the research literature. Most publications concerning NIR spectrometer performance are based on testing the quality of multivariate models in specific applications, particularly for food applications. For example, Béc et. al. have published a series of review articles on performance assessment of NIR spectrometers based on this approach [1, 8, 13].

The American Society for Testing Materials (ASTM) has published a *Standard Guide for Establishing Spectrophotometer Performance Tests*, intended for uncovering malfunctions, or other changes in instrument operation. However, it is specified that this is not intended for comparison of spectrometers of different manufacturers [30]. Also from ASTM, the *Standard Practice for Describing and Measuring Performance of Ultraviolet and Visible Spectrophotometers* describes tests for evaluating how a spectrometer performs compared to a different spectrometer that is used when developing a spectrophotometric method, in terms of photometric accuracy. This is very specific, assessing the performance related to a single method, and does not concern the requested overall performance characterisation.

The most relevant finding of the search after spectrometer standardisation literature was the *CIE 233:2019 Calibration, Characterization and Use of Array Spectroradiometers* [19]. This report seeks to educate users in the characteristics of array spectroradiometers that are important to obtaining accurate measurement results. Moreover, performance indices are proposed that will enable users to rank instruments according to the properties that affect their applications. However, it has a different scope than this thesis, relating to visible light rather than NIR, and concerning absolute radiometric measurements rather than for absorption spectroscopy applications. This affects the performance characterisation, as other properties relating to absolute radiance and colour are of importance. The suggested performance indices include spectral directional response for irradiance and radiance, spectral surrounding field effect, linearity for fixed integration time and fixed input flux, temperature dependence, polarisation response, spectral spatial response, spectral focusing distance, spectral broadening, and stray light. As will be clear in chapter 5, only some of these are concerned in this thesis, and their combination is not considered sufficient for a full description of absorbance spectroscopy performance. The report has a theoretical approach, and does not describe methods for experimental estimation.

The lack of a common standard for performance characterisation is present also in the field of hyperspectral imaging. This is approached by the IEEE P4001 working group, taking on the task of developing a common standard for specification of hyperspectral cameras. More information about the project is available on the project web-site [31]. The P4001 standard is not yet finished and available, but in relation to this thesis work, we were granted insight into the current standard draft. Parts of the work is inspired by this standard, and we have gotten permission to share the relevant ideas. The standard is intended to give a complete specification of the performance in a form which is suitable for instrument comparison. It establishes a common language, technical specification, testing criteria, task-specific recommendations, and common data formats. All parameters that should be included in data sheets for a complete specification are specified. The parameters are selected based on the ability to be measured with commonly available test equipment, and corresponding measurement procedures are suggested. While much of this is directly applicable for spectrometers, some adjustments are required, which leaves room for additional standardisation work relating to spectroscopy. In addition, a separate spectroscopy standard will be useful, as the full standard may be overwhelming, and impose a challenge in selecting what relates to spectrometers, and what concerns the spatial imaging properties.

Some of the work leading up to the P4001 standard is available, and particularly the work by Skauli in establishing radiometric performance characteristics [14, 32, 26] is highly relevant and adapted in this thesis.

Part II

Spectrometer performance characterisation

Chapter 5

Performance characteristics

This chapter defines performance characteristics for spectrometers. The characterisation is inspired by the "black box"-approach presented in [32], which is applied in the upcoming P4001 standard [31]. In this approach, which considers the overall performance of the spectrometer, the characteristics make up a minimal number of parameters that are sufficient to capture the quantities of interest for performance evaluation. The chosen characteristics are directly measurable by observing the performance without knowledge of the internals, or by performing simple simulations, and can be interpreted directly without no further analysis. Ideally, when applying the "black box"-approach, the characterisation holds for any spectrometer design. However, as diffraction grating spectrometers are the main focus of this thesis, some assumptions for the spectral characteristics are made that only hold for this design.

The aim is to describe the spectrometer in a complete but non-redundant way. Hence, when faced with multiple parameters describing the same characteristic, only one is specified. A minimal set of performance characteristics that should be measured and stated for a complete specification is given. As the thesis mainly is concerned about absorbance spectroscopy, the characteristics describe the overall performance of the spectrometer for such applications. The focus is the performance in terms of SNR and resolution, which are important for absorbance spectroscopy, rather than absolute radiometric measurements. Due to the limited scope of the thesis, not all characteristics that may influence the performance are described.

The purpose of the performance characterisation is twofold. It should both characterise the operation of the spectrometer, for better understanding of the data, and allow for comparison between spectrometers. The comparison should be made based on the potential of the spectrometer design, rather than the current performance, as some properties are relatively easily adjusted. For example, the sensitivity and SNR of the spectrometer can be increased, at the expense of reduced resolution, by resampling the signal or increasing the slit size. As will be discussed, the ratio of sensitivity to resolution then better describes the potential of the spectrometer design, and is better for comparison. Hence, a set of performance characteristics describing the current operation is defined, and a different set of derived performance characteristics is suggested for spectrometer comparison.

The specified characteristics should describe the average performance, and give an upper bound on the imperfections. The characterisation requires only approximate quantification of the parameters, not precise values, as this is sufficient for an overall spectrometer comparison, and the

combined effect of multiple characteristics defines the data quality.

The performance characteristics describe the spectrometer performance and data quality, but their effect on the results of their application, the multivariate model quality, is out of scope of this thesis. This translation of the characteristics from instrument domain to application domain would be advantageous and useful for the users of spectrometers, allowing for even more direct comparison based on application requirements, and should be considered for future work.

5.1 Spectral characteristics

5.1.1 Scope

Spectral characteristics concern the performance related to the spectral analysis, and how the spectrometer performs in measuring the spectral content of the light.

The following definitions hold for diffraction grating spectrometers with detector arrays.

The treatment here considers a signal that is sampled by detector elements. For hardware binning, the detector element width is changed, and otherwise the analysis applies. Other resampling techniques, such as smoothing and software binning, involves convolutions of a signal originally sampled by the detector elements, which effectively is a change of the detector element function used for sampling of the light reaching the detector array. Hence, the analysis is assumed applicable with modifications of the SRF due to changes in the effective detector element also when resampling techniques are applied.

5.1.2 Definitions

The detector array consists of a row of individual *detector elements*, or spectral *pixels*, that measure the incoming light at different positions. The diffraction grating spreads the light into a spectrum of wavelengths over the detector elements, and hence the detector elements at different positions receive different wavelengths. Each detector element performs a spectral sampling by measuring the incoming light over its extent, which corresponds to the light from the interval, or *band*, of wavelengths that are diffracted towards the element. The wavelengths reaching a single detector element are not further separated, and collectively constitute the detector signal, which depends on the sum of generated photoelectrons from all wavelengths.

The *spectral range* is the range of wavelengths that are detected by the spectrometer. It is defined as the outermost wavelengths that give nonzero detector signal when illuminated by a broadband source.

Each detector position corresponds to a position in the wavelength scale. This depends on the spread of wavelengths, is determined by the diffraction angles, and may vary over the spectral range due to angle dependent dispersion of the grating. An expression for the wavelength as a function of position on the detector array must be obtained through calibration. The *wavelength accuracy* describes the error in the calibration of wavelength as a function of position on the detector array.

The *spectral response function* (SRF), also termed the *bandpass function* [19] and optical transfer function [21], describes the distribution of responsivity in the spectral dimension for a spectral line, i.e., the spread of one single wavelength over the detector elements. As explained in subsection 3.1.2, the SRF also describes the distribution of wavelengths within one detector element, i.e., the corresponding band.

The *centre wavelength* of a detector element is, as will be discussed in subsection 5.1.5, the centre position in wavelength units of the Gaussian fit of the SRF corresponding to the detector element.

The *spectral sampling interval* is the wavelength increment between the centres of adjacent detector elements. It is alternatively described by the *detector element width*, also known as the *light collection bandwidth*, in wavelength units. If the fill factor of the detector array is unity, i.e., there is no separation between adjacent detector elements, which usually is the case for spectrometers, the detector element width is the average of the two adjacent spectral sampling intervals. Whether the detector element width or spectral sampling interval is used depends on context. Both usually varies over the spectral range from dispersion variation, as the detector elements normally have a fixed physical width [19].

The *number of spectral samples*, i.e., the number of detector elements in use, is found from the ratio of spectral range to the spectral sampling interval. This does however not necessarily correspond to the number of detector elements in the detector array, as, depending on the spectrometer design, the whole detector array is not necessarily in use. The detector elements that are not in use may be useful for measuring the dark current.

The SRF is generally wider than the detector element width and spectral sampling interval, causing each wavelength to be spread over multiple detector elements, and the SRFs to overlap. Hence, the *detector element resolution*, defined as the spectral sampling interval, does not sufficiently describe the ability to measure individual wavelengths. This is contained in the *optical resolution*, or simply resolution, which also includes the effect from the slit and the optics. This is described by the SRF peak width, commonly termed the *bandwidth*. The SRF generally has rounded edges, and its peak width is then not uniquely defined. As will be discussed in subsection 5.1.4, the SRF width and resolution is in this thesis defined as the *full width at half maximum* (FWHM) of the Gaussian fit of the SRF in wavelength units.

The overlapping of SRFs due to smaller sampling intervals than the SRF widths causes each wavelength to be detected by multiple detector elements. This is termed *oversampling* of the spectrum, as the same amount of information could be obtained by a larger spectral sampling interval and lower number of spectral samples, e.g., through resampling techniques such as binning and smoothing. The *number of independently resolved wavelengths* corresponds to the ratio of the spectral range to the mean resolution. This is however not a measure of the number of spectral samples conserving all information in the spectrum, which, as will be briefly mentioned in subsubsection 5.1.4.6, is higher.

5.1.3 Specifications

The following specifications are inspired by those currently included in the P4001 standard draft [31].

Performance characteristics that should be stated

The *spectral range* can be specified as the wavelengths of the outermost detector elements that give nonzero detector signal, using the centre wavelength plus/minus half the resolution, in units of nm.

The *wavelength accuracy* can be specified as the mean deviation from the measured wavelength to the actual wavelength, in units of nm, or further described if it varies considerably throughout the spectrum, or shows a variation trend.

For a non-redundant specification, only one of the *spectral sampling interval* and *number of spectral samples* should be specified, as they are related through the spectral range. The *spectral sampling interval* is considered the most useful, as it also describes the *detector element width*. It can be specified by the mean over the spectral range, in wavelength units (nm). If it varies considerably over the spectral range, by more than 10%, it can be further specified, as the range from the smallest to the largest.

The *resolution* can be specified in units of wavelength (nm), which gives a measure of its spectrum resolving capabilities, and is useful for understanding the data. In addition, it can be specified in units of detector elements, i.e., the number of detector elements the spectral line is spread over, as this is more useful for comparing spectrometers. However, this is also easily calculated using the spectral sampling interval. As the resolution may vary throughout the spectrum, it should be specified both by the mean and the minimum resolution, corresponding to the maximum SRF peak width, of the whole spectral range. If it varies considerably, it can be further specified for each detector element, as a function of wavelength over the spectral range.

Performance characteristics that can be derived from the stated values

The *number of spectral samples* can be calculated by dividing the given spectral range by the spectral sampling interval.

The *number of independently resolved wavelengths* can be calculated as the ratio of the given spectral range to the resolution.

5.1.4 Resolution

The *spectral resolution* of a spectrometer, referred to as the *resolution*, is a measure of the ability to detect and resolve rapidly varying spectral features. It can mean the difference between detecting a narrow spectral feature, and making the correct identification of e.g. a molecular fingerprint, or not. Different applications have different widths of their spectral features, and thus different resolution requirements. For example, Raman spectroscopy interprets narrow Raman shifts, and requires very high resolution, while NIR absorbance spectroscopy of liquids and solids typically involves overlapping bands and broader spectral features, and has lower resolution requirements. This can be seen in Figure 5.1, borrowed from a study on measurements of fatty acids in salmon [5], where typical spectra from Raman and absorption spectroscopy are shown over wavelength ranges of approximately **a)** 100 nm and **b)** 800 nm. The Raman spectrum displays many narrow peaks over the wavelength range of 100 nm, while the absorption

spectrum has much broader features over a wavelength range of 800 nm.

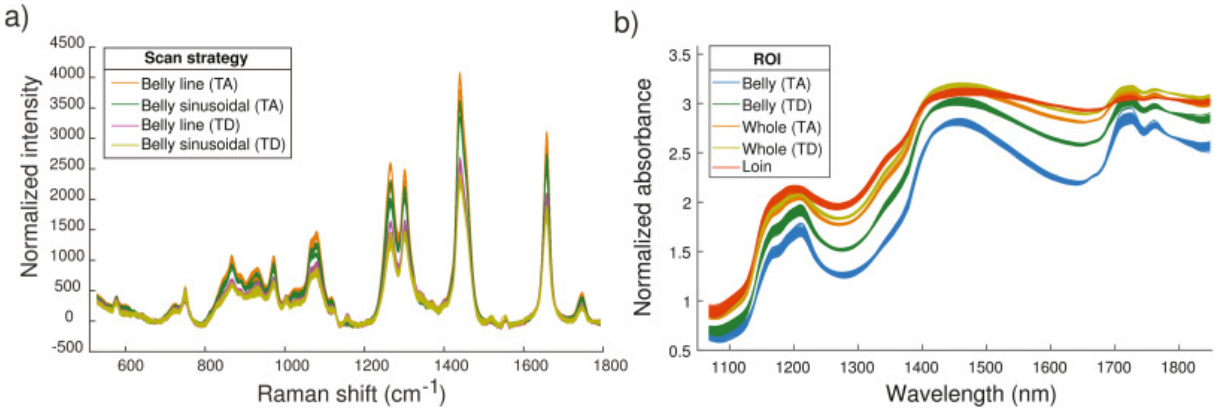

Figure 5.1: Typical spectra from **a)** Raman and **b)** absorption spectroscopy of solids and liquids, borrowed from a study on measurements of fatty acids in salmon [5]. Note that the x-axis in **a)**, which ranges from approximately 500 cm^{-1} to 1800 cm^{-1}, corresponds to Raman shifts from using a laser of wavelength 785 nm over a narrow wavelength interval from 817 nm to 914 nm. The x-axis in **b)** is approximately 8 times broader.

The resolution of a spectrometer is generally defined as the spectral separation between the two closest monochromatic components that the instrument can separate from one another, i.e., resolve [19]. The definition is not particularly descriptive for NIR absorbance spectroscopy of solids and liquids, with spectral features that generally are broader, may overlap and still give valuable information to the analysis. Their analysis methods, such as multivariate analysis, are able to separate their contributions. However, the spectral separation between the closest resolved monochromatic components is a measure of the ability to resolve the spectral features even in absorption spectra. The definition is thus considered suitable also for absorbance spectroscopy.

As explained in subsection 3.1.2, the SRF describes both the distribution of responsivity in the spectral dimension for a spectral line, and the distribution of wavelengths within one detector element. For *oversampled* spectra, the SRF is generally wider than the detector element width, causing the wavelengths to be spread over multiple detector elements, and the SRFs to overlap. Hence, the wavelength difference between adjacent detector elements, the *detector element resolution*, also known as the *pixel resolution* [19], does not sufficiently describe the ability to measure individual wavelengths. On the other hand, the width of the SRF peak, commonly termed the *bandwidth*, describes how monochromatic light is spread out, which limits the ability to resolve closely spaced peaks. This is thus a good measure of the actual resolution of the spectrometer, sometimes denoted as the *optical resolution* to separate it from the detector element resolution. For simplicity, the term *resolution* refers to this optical resolution.The resolution of the spectrometer is then defined as the SRF peak width.

For a diffraction grating spectrometer, the resolution in absence of blurring from the optics is well defined, and can be termed the *geometrical resolution*, corresponding to the resolution that is found from geometrical optics considerations. This resolution depends only on the slit function and detector element widths, and the corresponding SRF is the trapezoidal convolution of the rectangular slit and detector functions. For an infinitely narrow slit function, this geometrical resolution would correspond to the detector element resolution.

There is no straightforward definition of the width of the SRF, which is required for an unam-

biguous and standardised definition of the resolution. Only a perfect rectangular function has a clear and uniquely defined width, the FWHM. As discussed in subsection 3.1.2, the SRF of diffraction grating spectrometers is a convolution of the rectangular functions describing the slit function and detector width, i.e., a trapezoid, with rounded edges due to aberrations and blurring from the optics. Other spectrometer designs may have other shapes of the SRF. Rectangular SRFs are rarely encountered, and hence, the general SRF has no uniquely defined width. This challenge in defining the resolution is a recurring issue in many fields [26].

Due to the absence of a unique and unambiguous definition of the resolution, we are free to choose a definition based on what is considered the most suitable for the given context. The definition should yield resolutions that characterise the spectrometer performance, and are directly comparable. It should ideally be applicable also for other spectrometer designs than the diffraction grating spectrometers with Gaussian-like SRFs, such as Fabry Perot spectrometers with Lorentzian-shaped SRFs, and designs that may even produce irregular peak shapes of the SRF. The resolution should be measurable using spectral data, e.g. by a reference source with gas producing spectral emission lines, that, depending on the resolution, may partly overlap, and contaminate the detected peaks. The definition should be insensitive to such impurities. Another important aspect is that the definition should not deviate considerably from what is commonly used in data sheets and literature, as this may cause confusion and misconceptions.

5.1.4.1 Commonly used definitions of resolution

Spectrometer data sheets specify the resolution, usually in wavelength units (nm). This usually corresponds to the FWHM of the SRF, but the applied definition is not always specified, and it would be possible to envisage specifications where other resolution definitions are applied. In addition, as stated by [19], some manufacturers' specifications fail to distinguish whether the detector element resolution, i.e., the wavelength difference between adjacent detector elements, or the optical resolution is given. Hence, care should be taken when comparing instruments, as the given resolutions are not necessarily comparable.

In literature, the resolution is very commonly defined as the FWHM of the SRF in wavelength units, e.g., by [21, 22, 19]. As the FWHM of the SRF is a very common definition of resolution, both in literature and in spectrometer data sheets, the chosen definition should give values in the same order of magnitude. This is important for comparison purposes, and to avoid confusion and misconceptions.

[26] and [19] suggests a definition based on the parameters of a fit of the SRF to a given functional form, such as a Gaussian, or another function that is known from first principles, or more generally, assumed from the shape of the data.

The enclosed energy, i.e., the fraction of energy in the SRF that is contained within the detector element at its peak, has been suggested used by [14] and [15] as a measure of the resolution. It is not considered here, as it is not comparable with the conventional FWHM values, however it would work well as a supplement to the chosen resolution definition.

The SRF peak width is by the CIE 233:2019 standard [19] defined as the width of a rectangular function with the amplitude of the SRF at the centre wavelength, with the same area as as the SRF peak. It equals the FWHM for rectangular, triangular, and trapezoidal SRFs. However, as stated by [26], this resolution is dependent on the amplitude of a single point on the SRF, and

thus less robust against irregular SRF shapes, and impurities and noise on the spectral data. In addition, it depends on the area of the SRF, which is more important for absolute radiometric considerations than for absorbance applications, which are the primary concern of this thesis.

5.1.4.2 The FWHM definition

The FWHM of the SRF width in wavelength units (nm) is the most common method for specifying resolution. It is well defined by any SRF shape, simply interpreted, and easily and unambiguously measured on spectral data.

However, as is pointed out in the current draft of the P4001 standard [31], the FWHM is defined by the two single points with intensity corresponding to half of the maximum, which makes it sensitive to irregular peak shapes. It is thus not necessarily suited for describing all spectrometers with unknown SRF shapes. Its measurement routine is also highly sensitive to noise and other impurities.

The FWHM is the natural definition of peak width for rectangular functions, however, it may not give a fair representation of the resolution for other function shapes. Consider the SRF of an ideal diffraction grating spectrometer, with no blurring optics. Then the SRF is described by the convolution of the rectangular slit and detector functions, each with a given width, as shown in Figure 5.2. The resulting FWHM is the maximum of the widths of the two convoluted functions. For a detector function that is much more narrow than the slit function, as in Figure 5.2a, the resulting SRF is approximately rectangular, and the FWHM is a nearly unambiguous description of the SRF width. However, if the slit function and detector elements are of equal widths, as in Figure 5.2b, the resulting SRF is triangular. As the triangular function has no unambiguously defined width, it may be described by any definition. Convolutions are generally considered to broaden functions, and should thus also broaden the SRF. This is however not accounted for by the FWHM, which has the same width as both the slit and detector functions. The same problem is encountered when performing resampling such as binning and smoothing, described by convolutions. Hence, the FWHM definition may not necessarily give a fair characterisation of the resolution of all SRF shapes, and does not adequately describe the resolution of convoluted signals. This is a clear disadvantage of the definition.

5.1.4.3 The standard deviation definition

The standard deviation of the SRF distribution can also be used as a measure of the SRF peak width. This standard deviation describes the broadening of the SRF in wavelength units, and equals the root mean square (RMS) along the spectral dimension. It is not widely used to specify the width of the SRF and define the resolution. However, it has many desirable properties, and solves the discussed problems related to the FWHM definition. The standard deviation evaluates the whole SRF peak, unlike the FWHM, where only the two single points with intensity corresponding to half of the maximum are considered. It is thus less sensitive to irregularly shaped SRFs, measurement noise, and other impurities. It is considered a fair representation of the resolution of any function shape, as it favours collection around the centre, and thus properly penalises irregular, uneven, and asymmetric shapes.

The total standard deviation σ from convolution of two functions is given by the simple relation

of a quadrature sum,

$$\sigma = \sqrt{\sigma_1^2 + \sigma_2^2}. \tag{5.1}$$

By defining the resolution as the standard deviation of the SRF, this simple formula describes the total resolution when multiple known and independent factors with given standard deviations affect it, such as slit size, detector size, blurring from the optics, or a smoothing filter. In addition, the formula describes the effect on the resolution from resampling, such as binning and smoothing, which involves convolution with a given function. Such operations are thus well-defined and easily calculated.

Unlike the FWHM, and as desired, the standard deviation definition will always increase the width of a function that is broadened through convolution, such as in the case of convoluting the rectangular slit and detector functions shown in Figure 5.2, and similarly when binning and smoothing signal. The broadening from convolutions is then accounted for. Defining the SRF width using standard deviation is considered giving a more fair characterisation of the resolution of all SRF shapes, and suitable for comparing different spectrometers.

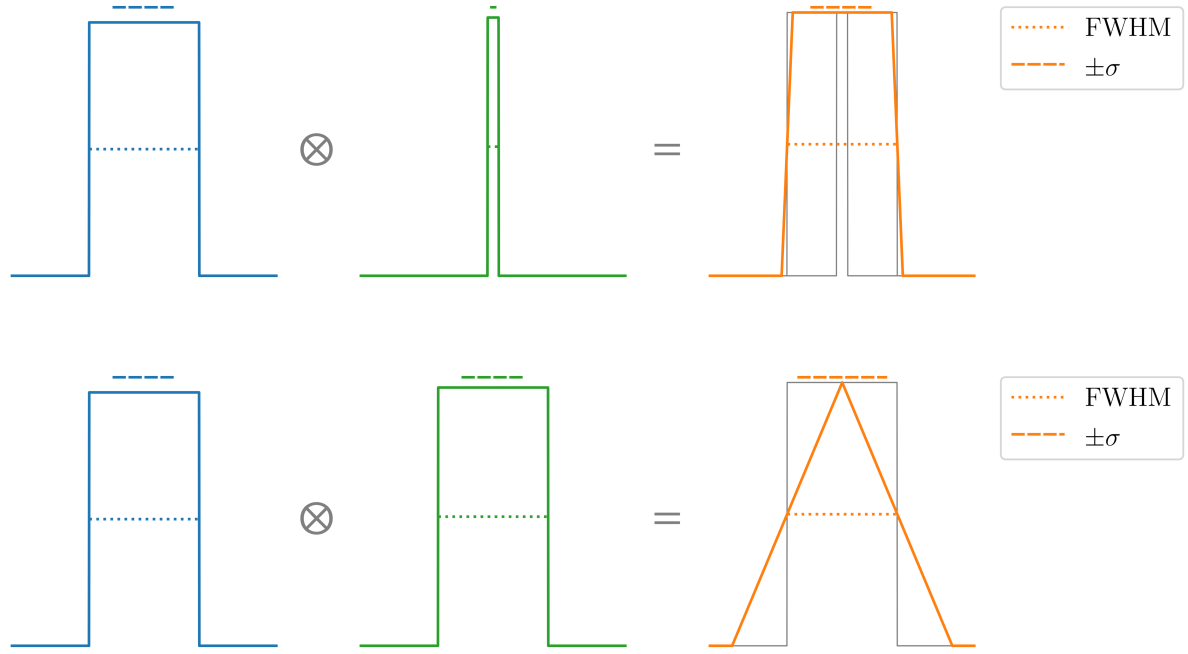

Figure 5.2: Comparison of FWHM and standard deviation for defining the SRF peak width for the convolution of the rectangular slit and detector functions, for **a)** detector elements that are much more narrow than the slit function, giving an approximately rectangular convolution, and **b)** slit function and detector elements of equal widths, giving a triangular convolution. The FWHM is equal in both cases, while the standard deviation is broader for **b)** than **a)**.

As shown in Figure 5.2, the standard deviation definition does not give a well suited physical interpretation of the width of the rectangular function, which is unambiguously defined by the FWHM. In an ideal world, with ideal optics and absence of any blurring effects, combined with a narrow slit function, the encountered SRFs could for diffraction grating spectrometers resemble rectangular functions. Then, based on this physical interpretation, it would be wise to reconsider the suitability of the standard deviation definition. However, its measure of the resolution is considered sufficient relative to the values obtained for other functions, as e.g.

a triangular function is considered having lower resolution than the rectangular function with the same FWHM. Also, in practice, the optics will always to some extent cause aberrations and blurring of the SRF, and rectangular SRFs are in principle never encountered. Then, the advantage of a physical interpretation is lost.

However, a considerable downside related to the standard deviation definition of resolution is that it is not defined for functions with long tails, such as Lorentzian functions, given by

$$f(x) = \frac{1}{1 + x^2} \tag{5.2}$$

and encountered in e.g. Fabry Perot spectrometers. In addition, as it considers the whole SRF, the measurement routines requires that the whole function is properly defined. This is not always possible, e.g., when measuring the SRF using a reference source with gas producing spectral emission lines that may partly overlap. Both cases can be solved by defining a cut-off value, either based on where it drops to a given percentage of the maximum level, or by specifying an amount of energy that must be included. The cut-off can be partly compensated for by scaling the standard deviation to that of the full function of a given shape, e.g., a Gaussian, that has the same standard deviation within the not-cut-off region. However, as seen in Figure 5.6 and Table 5.1, the cut-off still largely affect the estimated resolution for Lorentzian functions.

Adaptation of the standard deviation to FWHM: Gaussian standard deviation fit

As discussed, standard deviation is clearly favourable compared to FWHM for defining the width of the SRF, and correspondingly the resolution. As the standard deviation definition is both less sensitive to irregularly shaped SRFs, measurement noise, and other impurities, and more suitable for comparing different SRF shapes, it is considered better for the current task of standardising and comparing spectrometers. The effect on the resolution from convolutions, such as binning and smoothing, is well defined through Equation 5.1. By defining a cut-off for the standard deviation calculation, the resolution is defined for all function shapes, though sensitive to the cut-off level, and can be found from spectral measurements. However, it gives values with a different order of magnitude than those obtained from the conventional FWHM definition. This is problematic, as the standard deviation values thus deviate considerably from those stated in data sheets, and the results may be mistakenly conceived by people that are used to the FWHM definition.

A solution for making the standard deviation definition of resolution less deviating from the conventionally used FWHM definition, is to adapt it to a FWHM value in a way that conserves the advantages of using the standard deviation. A Gaussian function is well suited for such scaling of the standard deviation σ to a FWHM value, as they are linearly related as

$$\mathrm{FWHM}_{\mathrm{Gaussian}} = 2\sqrt{2\ln 2}\sigma \approx 2.355\sigma. \tag{5.3}$$

A simple solution for adapting the standard deviation definition of resolution to a FWHM value is through a rescaling using Equation 5.3. Essentially, the resolution is then defined as the FWHM of the Gaussian function having the same standard deviation as the SRF. For simplicity, this is denoted the *Gaussian std fit*, where *std* is an abbreviation of standard deviation. The definition has the same advantages as the standard deviation definition compared to the regular

FWHM definition, and is made more comparable with the common FWHM values. Only Gaussian functions obtain the same FWHM, while rectangular functions are defined as having higher resolution than given by the FWHM. The method makes no assumption of the SRF shape, and is robust for all SRF shapes, including irregular, uneven, and asymmetric peaks. The change in resolution from using binning and smoothing filters is thus well-defined and easily calculated. This way of defining the resolution is currently included in the P4001 draft [31].

5.1.4.4 Gaussian fit definition

The SRF of a diffraction grating spectrometer is, as discussed in subsection 3.1.2, a blurred trapezoid that in most cases is well approximated by a Gaussian function. As stated by [25], the Gaussian function is widely accepted for many array detector instruments. Other functions can also be used, such as trapezoids, which are more accurate in the case of optics with little blurring. However, the Gaussian has higher resemblance with also other function shapes, such as the central part of the Lorentzians found e.g. in Fabry Perot spectrometers. As this thesis mostly considers diffraction grating spectrometers, and is not concerned about asymmetric and unusually irregularly shaped SRFs, the SRFs are considered well approximated by the Gaussian.

Another possible solution for defining the resolution is to perform a Gaussian fit of the SRF, and use the corresponding FWHM as a measure of the SRF width. The Gaussian fit takes the whole peak into account, and finds the closest adaptation to a Gaussian function. The resolution is then evaluated based on an adaptation to the same shape, reducing the potential bias from the peak shape. It gives a slightly different weighting of different function shapes than the standard deviation, as seen in Figure 5.5, which may be considered equally as adequate for representing the resolution of different SRF shapes. The Gaussian fit method for defining resolution is applied e.g. by [24].

This method does not conserve all the advantages of the standard deviation definition. For example, the effect on the resolution from applying smoothing filters is not well defined in the same way as the standard deviation definition, only approximated by the relation in Equation 5.1. In addition, it requires that the SRF shape is even and symmetric. For oddly shaped and asymmetric peaks, the irregularities may not properly be included in the Gaussian fit, despite their possible influence on the resolution.

In return, for even and symmetric functions, this filtering of irregularities is beneficial for reducing the contribution from measurement noise, impurities, and partly overlapping peaks on real data. This can be seen in Figure 5.3, which shows typical diffraction grating spectrometer responses from measurements of spectral lines. While most peaks are well separated, the identified peak centred around 810 nm consists of three overlapping peaks. While the standard deviation takes the whole peak into account, and is largely affected, the Gaussian fit is clearly not considerably affected. Hence, in the case of SRFs that are even and symmetric, the Gaussian fit method is even more robust against measurement noise and impurities, than using the standard deviation directly.

While the Gaussian fit requires a cut-off level for separating peaks in real spectral data, e.g., with multiple spectral lines present, no such cut-off is required for functions with long tails. It is additionally less affected by the cut-off level than the standard deviation, as seen in Figure 5.6 and Table 5.1.

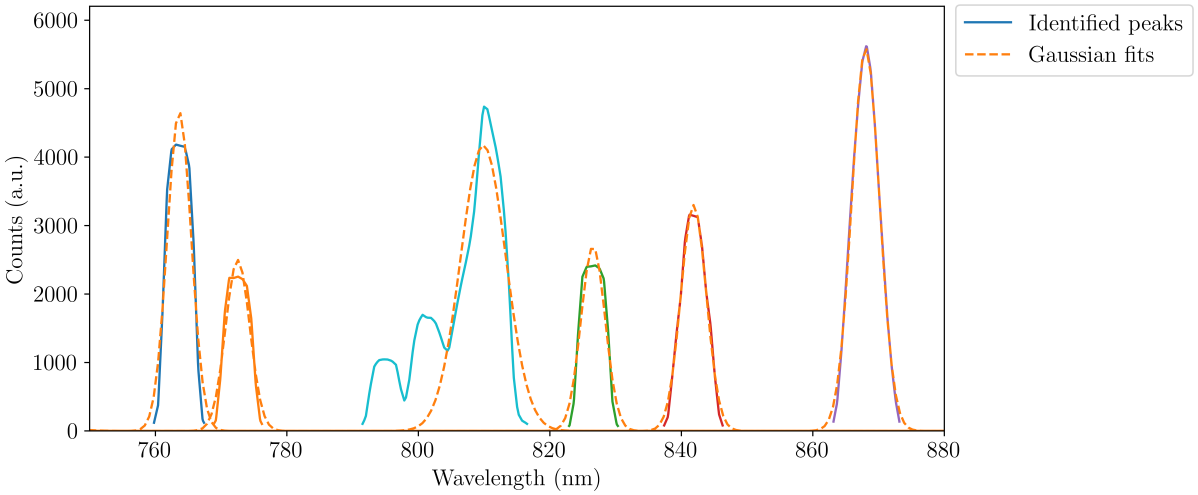

Figure 5.3: Responses to measurements of spectral lines by a diffraction grating spectrometer, and their Gaussian curve fits. The identified separate peaks are marked with different colours.

5.1.4.5 Discussion

As presented, this thesis considers three methods for defining the width of the SRF, and correspondingly the resolution: the FWHM of the SRF, its Gaussian std fit, and its Gaussian fit, all in wavelength units. The resulting functions for different ideal SRF shapes is shown in Figure 5.4.

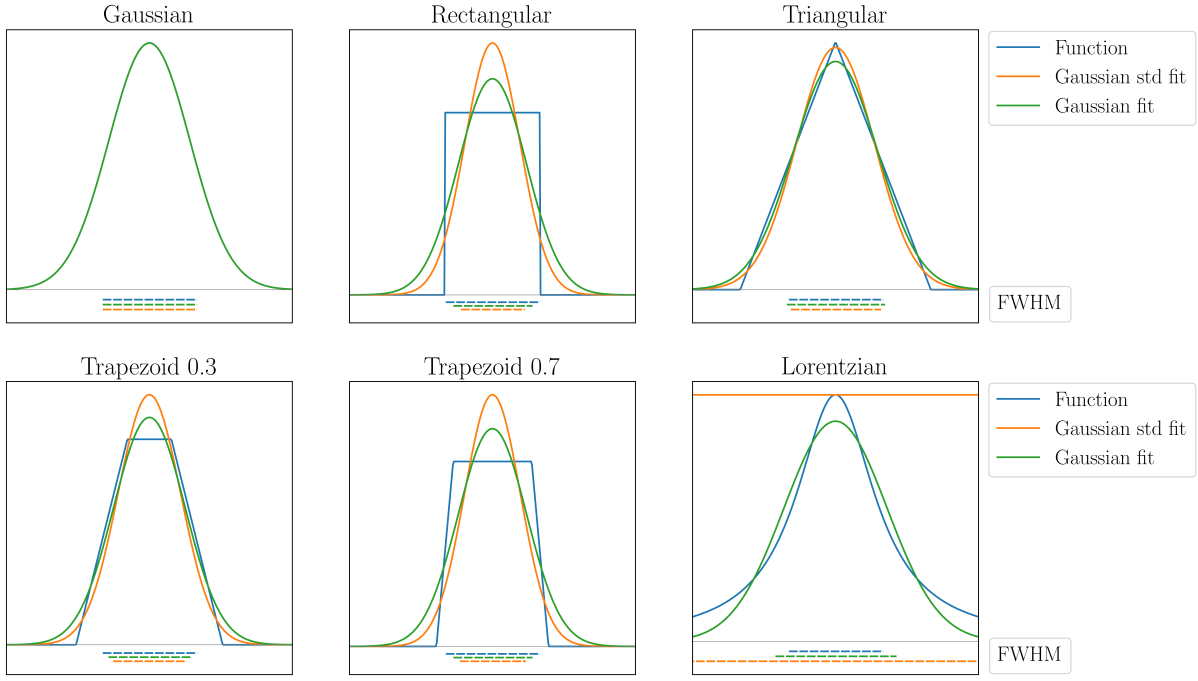

Figure 5.4: Comparison of different methods for defining the resolution of different peak shapes. The Gaussian fit amplitude is found from the curve fit, while the Gaussian std fit amplitude is chosen so that the Gaussian std fit area corresponds to the function area. The trapezoid number indicate the ratio of the top width to the bottom width.

Figure 5.5 compares how the relative resolutions of different ideal SRF shapes are defined for the three different definitions. Corresponding values are given in Table 5.1. The Gaussian std fit and Gaussian fit methods are considered more adequate than the FWHM method, as the rectangular function is defined as having higher resolution than triangular and Gaussian functions of the same FWHM. Which of the two methods the most optimal is not obvious, and depends on the application. The Lorentzian function has long tails, and no defined standard deviation, and subsequently no defined resolution when using the Gaussian std fit, while it is well defined using the Gaussian fit. In this case, the Gaussian fit is considered the most adequate

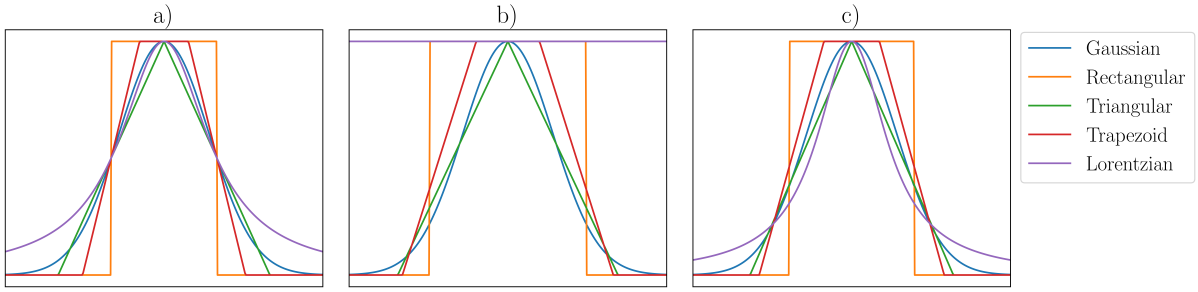

Figure 5.5: Different SRF shapes that are defined as having the same resolution when defining the resolution as the FWHM of **a)** the function, **b)** the Gaussian std fit, and **c)** the Gaussian fit. In **b)**, the Lorentzian function resolution is not defined.

Figure 5.6 shows the effect by using a cut-off value for delimiting the SRF peak, for trapezoidal and Lorentzian functions. The corresponding values are given in Table 5.1. The Gaussian std fit is scaled when using a cut-off, so that the measured standard deviation corresponds to the standard deviation within the non-cut-off region of the Gaussian. Hence, the cut-off has no effect on Gaussian functions.

Only well-defined, even, and symmetric function shapes were considered in Figure 5.5 and Table 5.1. As was seen in Figure 5.3, unless the peaks are unusually irregular, which is out of scope of this discussion, the Gaussian fit is assumed to be even more robust against measurement noise, impurities, and partly overlapping peaks than the standard deviation definition.

Figure 5.7 shows measurements of the SRF, and the resulting resolutions of the three definitions, for the three different diffraction grating spectrometers that are characterised and compared in chapter 6. These are obtained through measurements of the spectral gas emission lines produced by the HG-1 Mercury Argon calibration source from Ocean Optics [33]. The differences in the observed spectra show that the spectrometers clearly have different slit sizes and degree of blurring, as the SRF of spectrometer i) is more Gaussian, and it is more trapezoidal for spectrometers ii) and iii). Spectrometer iii) even have some peak irregularities, probably due to measurement noise. The relative differences between the methods are largest for spectrometers ii) and iii), where the peaks are more trapezoidal. As can be seen, all three methods give resolutions that are approximately even for the spectral line peaks throughout the spectral range. Some deviations of the estimated resolution are present around 800 nm, which is assumed to be caused by overlapping from adjacent peaks, due to the high density of peaks in this region. As expected, the Gaussian std fit is more sensitive to such overlapping peaks, and gives larger deviations than the Gaussian fit. The peak FWHM looks even more robust than the Gaussian fit, but as discussed, it depends on only the peak value and corresponding two points at half

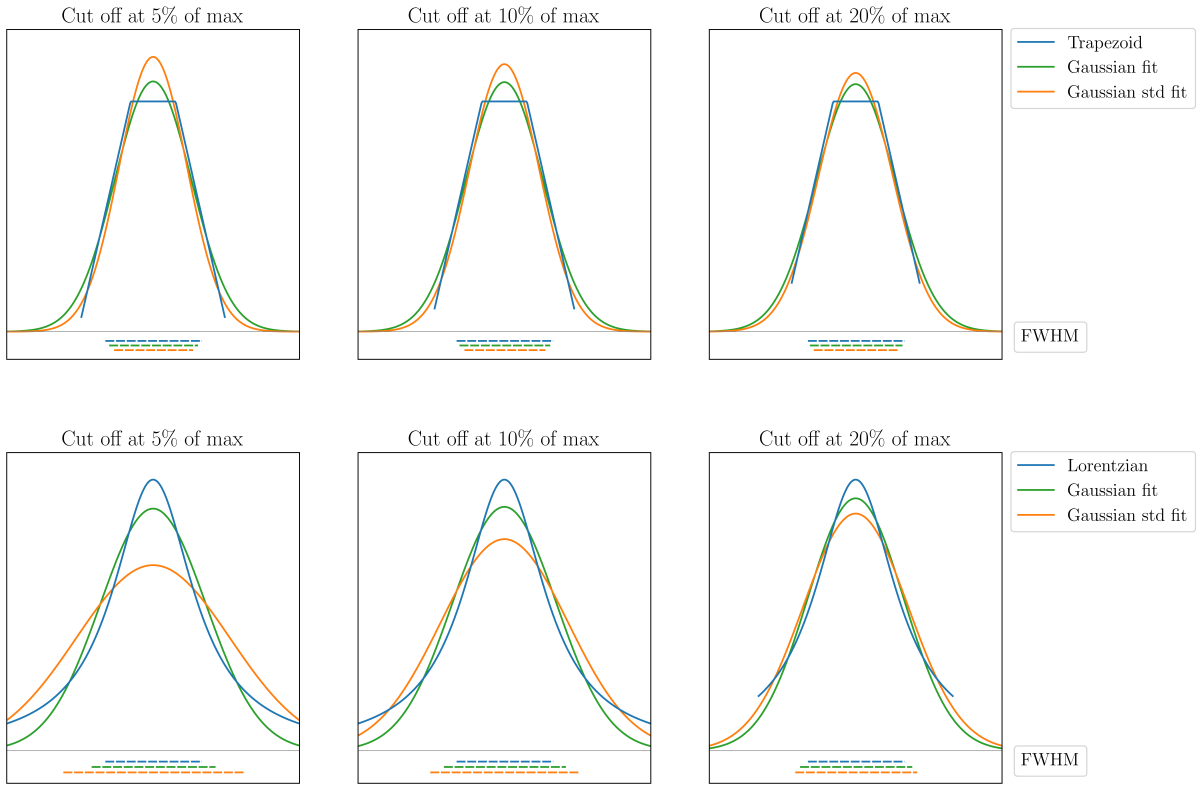

Figure 5.6: Comparison of the sensitivity of different resolution definitions to a cut-off value for delimiting the peak. The Gaussian with the same standard deviation is scaled so that the measured standard deviation corresponds to the standard deviation within the non-cut-off region of the Gaussian.

maximum, and the displayed robustness is a result of the data being very well behaved. In total, and as expected, the Gaussian fit is considered the most robust method against overlapping peaks. The corresponding data sheet values of resolution for spectrometer i) and ii) are 3 nm and 5 nm, and the estimations are in the same order of magnitude.

As discussed, there is no unique and unambiguous definition of the resolution, and we are free to choose a definition based on what is considered the most suitable for our application. The use of FWHM for defining SRF peak width seem to be convention, and is rarely discussed or explained. During the work with this thesis, no literature is found that comprehensively review its use, other than the current draft of the P4001 standard [31]. There seem to be no outstanding argument suggesting for the use of FWHM, other than its simple definition and ease of measurement, and to our knowledge, the clear disadvantage related to convolutions of rectangular functions, giving an inadequate representation of different function shapes, has not been pointed out. Combined with the sensitivity to irregular peak shapes, these are strong arguments for why the FWHM of the SRF should be avoided as a definition of the resolution.

The methods of Gaussian std fit and Gaussian fit are generally considered better than the FWHM definition, as they are less sensitive to measurement noise and impurities, and give a more adequate representation of the resolution of different function shapes. Unlike the Gaussian std fit, the Gaussian fit is not suited for irregularly shaped SRF peaks, as their irregularities are filtered out. In return, for even and symmetric functions, the contribution of overlapping peaks, measurement noise, and impurities is reduced even more than for the Gaussian std fit. The

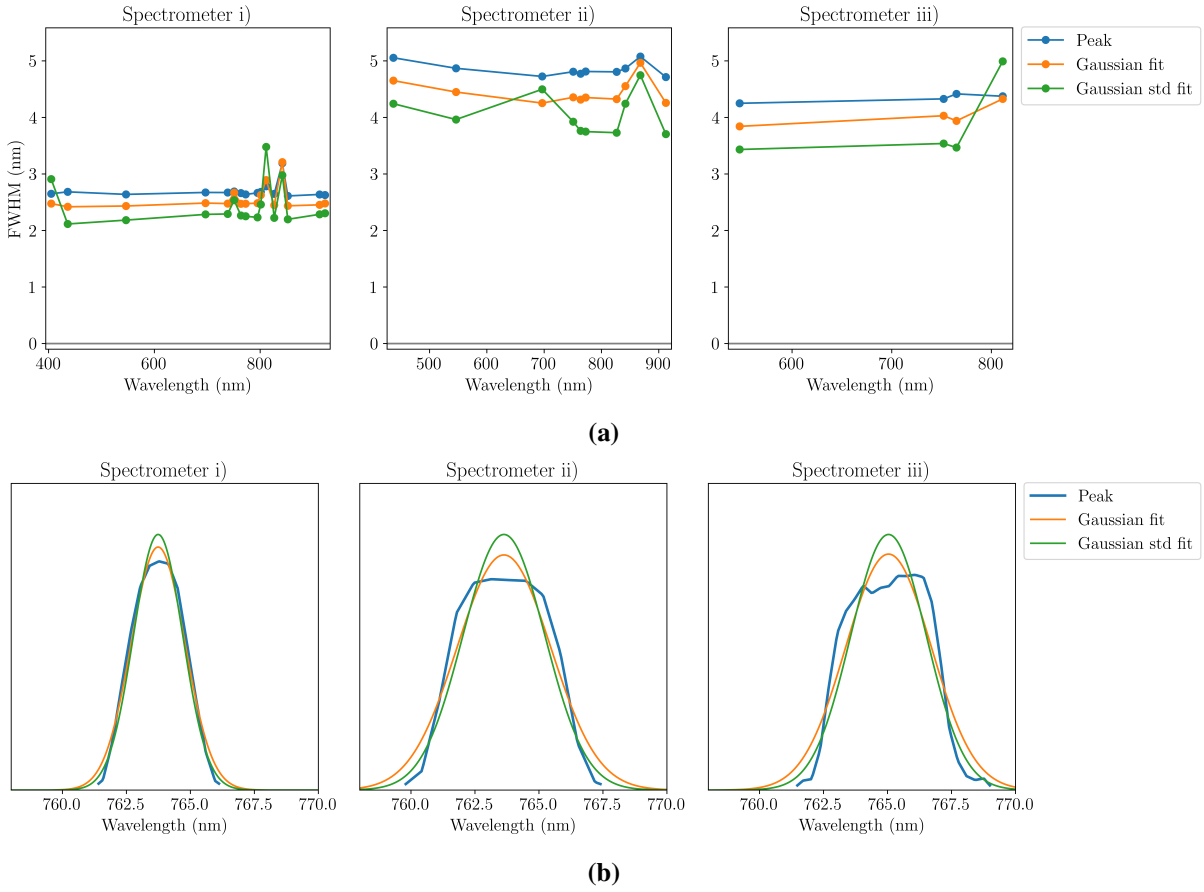

Figure 5.7: Comparison of the different methods for defining the resolution of measurements of spectral lines by three different diffraction grating spectrometers i), ii), and iii). **a)** shows the different estimated resolutions over the spectral range for the FWHMs of the peak, the Gaussian std fit, and the Gaussian fit, for the spectrometers with SRF shapes as shown in **b)**. The Gaussian std fit is scaled so that the measured standard deviation corresponds to the standard deviation within the non-cut-off region of the Gaussian. Due to low SNR for spectrometer iii), fewer peaks were properly detected than for spectrometer i) and ii).

Table 5.1: Comparison of different methods for defining the resolution of different SRF peak shapes. The values are given for functions with FWHM = 1, as this illustrates the discussed scaling of different function shapes. The Gaussian std fit is scaled so that the measured standard deviation corresponds to the standard deviation within the non-cut-off region of the Gaussian.

	FWHM	FWHM of Gaussian std fit	FWHM of Gaussian fit
Gaussian	1	1	1
Rectangle	1	0.67	0.83
Triangle	1	0.95	1.03
Trapezoid			
Top/bottom width ratio = 0.7	1	0.69	0.83
Top/bottom width ratio = 0.3	1	0.77	0.87
Cut off: 5%	1	0.81	0.91
Cut off: 10%	1	0.83	0.93
Cut off: 20%	1	0.87	0.95
Lorentzian	1	Undefined	1.27
Cut off: 5%	1	1.85	1.27
Cut off: 10%	1	1.53	1.25
Cut off: 20%	1	1.25	1.15

Gaussian fit is also less sensitive for the required cut-off criterion when separating peaks in real spectral data, and well suited for describing SRFs with long tails, in which the Gaussian std fit is undefined. This property and disadvantage of the Gaussian std fit is rarely discussed. For the Gaussian std fit, when the standard deviation is defined, the effect on the resolution from resampling, such as smoothing and binning, is well defined and easily calculated. It is not as well defined for the Gaussian fit, however, it is applicable also for functions with long tails, and without a defined standard deviation. What definition is optimal thus depends on the context. When measuring real data, the reduction in contribution of overlapping peaks and other impurities is valuable, and a cut-off is required. Then the Gaussian fit is optimal. However, having ideal data with well defined standard deviations, the Gaussian std fit may be optimal, as then the well-defined effect of resampling may be important.

In this thesis, the Gaussian fit method is chosen for defining the resolution. It is the most optimal based on our requirements, concerning measurements of real data in the case of even and symmetric SRF shapes from diffraction grating spectrometers, for characterising the spectrometer

performance for the purpose of comparison. The definition is not applicable for spectrometer designs giving asymmetric and irregularly shaped SRFs, for which the Gaussian std fit is assumed more robust. However, such designs are considered out of scope of this thesis.

For finding the resolution using spectral data with multiple peaks present, such as for a reference source with spectral emission lines, a defined cut-off of the peak is required. While more advanced methods for defining the cut-off are possible, such as requiring a given part of the energy to be within the peak, simply choosing a level at a given fraction of the maximum peak value is considered adequate. As shown in Figure 5.6 and Table 5.1, the resulting FWHMs of the Gaussian fit of both trapezoidal and Lorentzian functions are nearly unaffected by a cut-off level beneath 10%, and to ensure that this holds, 5% is suggested as a suitable cut-off.

5.1.4.6 Physical interpretation of the resolution definition

The resolution defines the spectral separation between the two closest monochromatic components that the instrument can resolve. When defining resolution as the width of the SRF, two wavelengths are considered resolved if their peaks are separated by the SRF width. For the chosen width definition, the FWHM of the Gaussian fit of the SRF, this corresponds to the spectra shown in Figure 5.8, where the separation ability of the two resolved wavelengths is indicated by the dip in their sum. This is similar to the description of spatial resolution by Abbe's diffraction limit, which defines the fundamentally highest achievable spatial resolution, adapted to the spectral dimension.

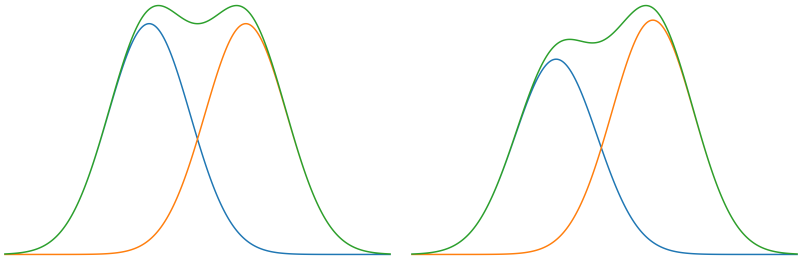

Figure 5.8: Physical interpretation of the resolution definition. The two Gaussian peaks illustrate spectral responses to two spectral lines of equal and different amplitudes. The dip in their sum indicates that they are resolved.

The amount of spectral information depends on the resolution. The spectra are commonly oversampled, meaning that the SRFs of adjacent detector elements overlap, and the same amount of spectral information could be obtained by reducing the number of spectral samples. The number of independently resolved wavelengths corresponds to the ratio of the spectral range to the mean resolution, i.e., the number of spectral samples when using the resolution as spectral sampling interval. In the P4001 draft [31], this is currently termed the *FWHM-equivalent band count*, but due to different terminology use in this thesis, it is rather termed the *number of independently resolved wavelengths*. This does not however correspond to the number of spectral samples that are required to conserve all information in the spectrum, which requires also sampling of the dip between the two resolved peaks, in analogy with the Nyquist sampling theorem. Further discussion of the relation of resolution and information content in the spectrum would be interesting, but is out of scope of this thesis.

5.1.5 SRF centre wavelength

The wavelength centre of a SRF, i.e., the *band centre*, must be defined. It defines the *centre wavelength* of the detector elements, which in turn defines the spectral sampling interval. It is also required for performing wavelength calibrations, or measuring the *wavelength accuracy* of the calibration, as it defines what wavelength corresponds to the measurement of a spectral line. As it is linked to the shape of the SRF, the following considerations are similar to those discussed for SRF peak width and resolution in subsection 5.1.4.

The simplest definition of centre wavelength is the centre position of the SRF. Similarly as for the FWHM definition of the resolution, this is based on a single point on the SRF, and thus very sensitive to irregular peak shapes. A more robust definition is the centroid, or the weighted average, of the SRF. This definition is used both in the CIE 233:2019 standard [19] and in the current draft of the P4001 standard [31]. For a symmetric SRF, it corresponds to the centre point of the SRF. It is well defined also for asymmetric and irregularly shaped SRFs, as it takes the whole peak shape into account. However, similarly as for the standard deviation definition of resolution, it may be affected by measurement noise and other impurities, such as overlapping peaks, when applied to spectral data. In the case of even and symmetric SRFs, performing a

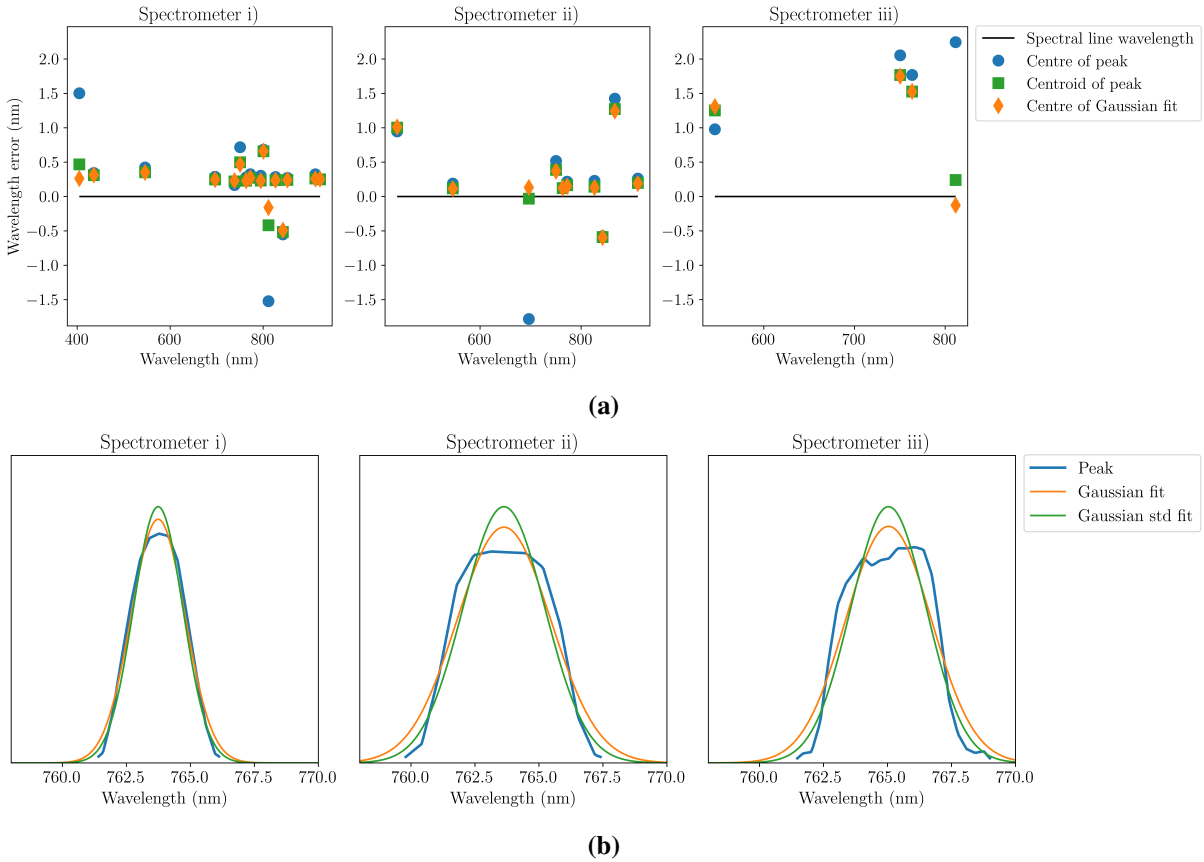

Figure 5.9: Comparison of different methods for defining the SRF centre wavelength, using spectral line measurements by three different diffraction grating spectrometers. **a)** shows the deviation between the estimated centre wavelength of a spectral line response, and the corresponding spectral line wavelength, when using the centre of the peak, the centroid of the peak, and the centre of the Gaussian fit, for the spectrometers with SRF shapes as shown in **b)**. Due to low SNR for spectrometer iii), fewer peaks were properly detected than for spectrometer i) and ii).

Gaussian fit of the SRF, and using its peak position, i.e., the centroid, is considered more robust against such impurities. As the diffraction grating spectrometers under consideration in this thesis have even and symmetric SRFs, the centre wavelength is defined as the peak position in wavelength units of the Gaussian fit of the SRF.

Figure 5.9 shows the errors in the wavelength calibration of the three definitions on measurements of spectral lines by different diffraction grating spectrometers. The error is the deviation between the estimated centre wavelength of a spectral line response and the corresponding spectral line wavelength. The peak centre is, as expected, less robust than the other methods, causing considerable deviations for peaks that are assumed influenced by noise or other impurities. It sometimes gives similar results, or even smaller deviations, but this is only the case for well behaved data. The Gaussian fit centre is in most cases equally good, or better, than the centroid, and, as expected, considered the most robust method against overlapping peaks.

5.2 Radiometric characteristics

5.2.1 Scope

Radiometric characteristics concern the performance related to measurement and quantification of the intensity property of light, and how the spectrometer performs in terms of detecting intensity variations of the incoming light.

The following definitions generally hold for any type of spectrometer.

The characteristics are specified in terms of photoelectrons rather than the digital numbers (DN) of the raw signal. The signal in photoelectron units can be obtained from the raw signal through photon transfer analysis, as discussed in subsection 3.3.4. The photoelectron unit is considered more intuitive, and convenient for describing noise characteristics, as these generally follow photoelectron statistics.

The characterisation assumes that the spectrometer noise follows the noise model discussed in subsubsection 3.2.2.2. Other noise sources are considered unknown errors, and may affect the total estimation of noise and SNR, similarly as other errors. Such errors are not characterised, and considered out of scope.

5.2.2 Definitions

The spectrometer collects light and converts it to a signal based on the number of generated photoelectrons. The ratio of generated photoelectrons to incoming light is described by the quantity A^*, which denotes the net light collection, or effective throughput, and thus the responsivity and sensitivity of the spectrometer. This is the combined effect from both étendue, optics losses, and detector quantum efficiency. It describes the combined system of spectrometer and any fibre used for light collection.

The *dark current* i_d is the number of generated photoelectrons per second in each detector element due to internal processes in the detector, independent of incoming light. It is temperature dependent, and may vary slightly between the detector elements, but is generally considered of approximately equal magnitude. For an integration time t_{int}, it contributes with the total number of photoelectrons $n_d = i_d \cdot t_{\text{int}}$ in each detector element. The dark current is generally removed through dark correction, but gives dark current noise, and reduces the saturation level and dynamic range of the measurement.

The *readout noise* n_r is the RMS fluctuation of the electron signal due to noise in the photodetector and readout electronics. It is independent of signal and integration time, temperature dependent, and generally considered of equal magnitude, and independent between the detector elements.

The *noise floor* of a given integration time is the sum of dark current noise and readout noise, and thus the total signal-independent noise.

The *total noise* is the sum of the noise floor, including dark current noise and readout noise, and the signal-dependent *shot noise*.

The *signal-to-noise ratio* (SNR) is the relative amount of noise with respect to signal. It describes the ability to discern the measured value from the noise, and thus the ability to access the information that is contained in the spectrum. Different applications have different SNR requirements, depending on the relative strength of the spectral features to be detected. The SNR is thus an important quality factor of the spectrometer, limiting whether it can be used for a given application.

Saturation occurs at some upper limit where the measured signal, and its noise, no longer follow the input light level. The saturation level thus sets the upper bound on the signal values that can be used for estimating the light level. Signal saturation may be caused by saturation of the photodetector, by reaching the *full well capacity*. For some spectrometers, the signal is abruptly non-linear when reaching a given photoelectron count close to, but lower than, the full-well capacity, as was seen in the PTC in Figure 3.5. This is caused by non-linearities in the ADC, and the signal is considered saturated at this level, even when the detector is not fully saturated. Saturation is thus defined as the lowest of the full-well capacity of the detector and the maximum level of linear response of the ADC, and denoted n_{sat}. While the dark current is removed through dark correction in the data analysis, it contributes to the detected signal, and thus lowers the effective saturation level of the proper signal. This *effective saturation level* describes the saturation level for the incoming light, and is found by subtracting the contribution n_d of the dark current i_d, given in units of photoelectrons per second, over the integration time t, from n_{sat}, as $n_{sat,eff} = n_{sat} - i_d \cdot t_{\text{int}}$.

The *dynamic range* is the ratio between the highest and lowest achievable signals in the spectrometer. It is defined as the ratio between the saturation level and noise floor, $n_{sat} / \sqrt{n_r^2 + i_d \cdot t_{\text{int}}}$. It is thus dependent of the integration time and temperature. The dynamic range can have a strong impact on the quality and integrity of the collected spectra. It is desirable to have a wide dynamic range, in order to accommodate signal variations across the spectrum.

The spectrometer is ideally linear over the dynamic range, up to the saturation level, which, as discussed, takes any emergence of abrupt non-linearity at a given signal level into account. However, the response may not be perfectly linear, and any deviation from proportionality between the signal and light level is denoted as a *linearity error*. This may e.g. be due to non-linearities in the ADC.

5.2.3 Use of A* for performance characterisation and comparison

As discussed in subsection 3.1.3 and [26], only the combined effect from all individual effects affecting the net light collection A^* is observed externally. Compared to separately giving characteristics for the internals, such as the étendue and detector quantum efficiency, which is the common method of current data sheets, A^* gives a direct and complete specification of the performance. In addition, it is independent of spectrometer internals, and thus directly comparable between spectrometers of different design. This makes A^* well suited as a performance characteristic describing the sensitivity of spectrometers.

A^* can be used for obtaining absolute radiometric measurements, such as measuring radiance spectra. However, it is also useful for spectrometer applications such as absorbance spectroscopy, which do not involve such absolute radiometric measurements, but rather relative intensity differences. As it characterises the spectrometer sensitivity, it is useful for estimating

the signal level, and correspondingly, and most importantly, the SNR for a given input light level and integration time.

The per-detector-element A_j^* represents the response of each detector element, and estimates the signal in each detector element as a function of incoming light. It is thus useful for a direct characterisation of the spectrometer. As the given levels of noise relates to each detector element, A_j^* is useful for estimating the total noise, including the signal-dependent shot noise, and correspondingly the SNR of the signal. It also defines the amount of incoming light that causes saturation of each detector element.

A^* is also useful for aiding comparison of the performance of different spectrometers. Noise is only important in relation to the total signal, i.e., through the SNR. As was shown in [26], A_j^* and the SNR scales with the same factor through resampling, and the normalised SNR per A_j^* is thus constant and independent on resampling interval. As the signal per A_j^* is constant for the spectrometer, the normalised noise per A_j^* thus indicates the noise performance independent of sensitivity or detector element width. This is useful for comparison of spectrometers, for indicating what spectrometer performs best in terms of SNR when measuring the same light level. Similarly, the saturation level is only comparable between different spectrometers when related to the amount of incoming light, through normalising by A^*.

A_j^* can easily be changed through resampling, such as binning, which simply impose a rescale dependent on the change of the sampling interval. On the other hand, the per-nm $A^*(\lambda)$ is independent of sampling or resampling interval. It measures the rate of generated photoelectrons to incoming photons as a function of wavelength, and thus gives a proper characterisation of the sensitivity that is useful for comparing spectrometers with different detector element widths. $A^*(\lambda)$ is simply obtained through dividing the per-detector-element A_j^* by the detector element width.

A^* is proportional to the slit size, and a spectrometer with larger slit size will thus appear to perform better. However, the resolution is also largely affected by the slit size. As we often are free to choose slit size when buying a new spectrometer, the spectrometer can be adjusted to having the required resolution depending on the application. The best performing spectrometer then has the largest A^* for the given resolution. Thus, in the case of comparing the theoretical performance of different spectrometer designs, A^* normalised for resolution is a suitable figure of merit. It can be obtained from the per-nm $A^*(\lambda)$, by dividing by the resolution, and is denoted the $A^*(\lambda)$ per nm resolution.

5.2.4 Specifications

The following specifications are inspired by those currently included in the P4001 standard draft [31].

The specification of performance characteristics should both be useful for characterising the operation of the spectrometer, and aid comparison between different spectrometers. A non-redundant specification states only a minimal set of parameters describing the operation of a spectrometer. Methods are given for generating additional information suited for more intuitive understanding of the parameters, for relating the parameters to applied integration times and signal levels, and for comparing spectrometers with different sensitivity and resolution.

Performance characteristics that should be stated

The sensitivity of the spectrometer should be given both as the per-detector-element A_j^*, for characterising the spectrometer operation, and as the per-nm $A^*(\lambda)$, for the purpose of spectrometer comparison. It generally varies considerably over the spectral range, and may have regions of no signal. The full A^* curves as a function of wavelength should thus be given. It can also be given as an average over the spectral range, i.e., within the region of non-zero signal, which is useful if the spectrometers have similar response curve shapes. Alternatively, the maximum value, or the value at a wavelength of interest, can be given. For NIR spectroscopy applications with CCDs, it is recommended to give the full A^* curves, and additionally the values at 800 nm.

The *dark current* i_d of the spectrometer can be specified as the mean value over all detector elements, in units of photoelectrons per second. If it varies considerably, also the maximum value should be given, such as if this is more than double of the mean value. As the dark current is highly temperature dependent, it should be given at the regular operation temperature, such as room temperature. If the spectrometer is designed to be used in other operating conditions, the value at the maximum expected temperature should be given.

The *readout noise* n_r of the spectrometer can be specified as the mean and max values over all detector elements, in units of photoelectrons.

The *saturation level* where non-linearities or full-well first occurs can be specified by n_{sat} in units of photoelectrons.

Any deviations from linearity that is not included in the saturation level should be additionally specified as the *linearity error*, as relative deviation from linearity over the dynamic range as a function of wavelength. The linearity error can be given as an percentage of the full-scale value. While the maximum can be given, the mean is considered the best specification. If the dynamic range have separated regions with different linearity errors, these should be specified separately. The linearity error specification is important for characterising the current operation of the spectrometer, but should not be considered too relevant when comparing spectrometers, as is can be corrected for through linearity corrections.

Specifying the *noise floor* in addition to the dark current and readout noise is considered redundant. It is dependent on integration time, and cannot be given by a single value, while it is fully described at any integration time by the dark current and readout noise.

The *total noise* and SNR could additionally be specified. However, they are signal dependent, and would require multiple specifications at different signal levels. It would also make the specification redundant, as they can be calculated for a given signal level using the specified dark current and readout noise.

The *dynamic range* can be specified, but it is dependent on integration time, and considered redundant, as it can be calculated from the specified saturation level, readout noise, and dark current.

Performance characteristics that can be derived from the stated values

The total signal $n_{e,j}$ in detector element j with width $\Delta\lambda_j$, can be calculated for a given input light level $L_{q\lambda,j}$ and integration time t_{int}, using $n_{e,j} = A_j^* L_{q\lambda,j} t_{int} \Delta\lambda_j$.

The *noise floor* for a given integration time t_{int} is found by calculating $\sqrt{n_r^2 + i_d \cdot t_{\text{int}}}$, where n_r is the readout noise, and i_d the dark current.

For a given signal level n_e, the *total noise* can be calculated using the specified dark current i_d and readout noise n_r, as $\sigma_{tot} = \sqrt{n_e + n_r^2 + i_d \cdot t_{\text{int}}}$. The corresponding SNR is the ratio between the signal level and the total noise, n_e/σ.

For relating the saturation level n_{sat} to the performance of the spectrometer, the SNR at saturation, $SNR_{max} \approx \sqrt{n_{sat}}$, which is the maximum achievable SNR, can be calculated.

For a more intuitive indication, the dark current can be specified in terms of the integration times where the dark current noise equals the readout noise, and thus considerably affect the signal, and where it gives saturation, to indicate the reduction in saturation level from the dark current. They are easily calculated based on the given specifications of dark current i_d, readout noise n_r, and saturation level n_{sat}, as $t = n_r/i_d$ and $t = n_{\text{sat}}/i_d$, respectively.

The *effective saturation level* can be calculated for a given integration time t_{int} by subtracting the contribution from dark current i_d, as $n_{\text{sat,eff}} = n_{\text{sat}} - i_d \cdot t_{\text{int}}$

The *dynamic range* for a given integration time t_{int} is the ratio of the saturation level to the noise floor, $n_{\text{sat}} / \sqrt{n_r^2 + i_d \cdot t_{\text{int}}}$, where n_{sat} is the saturation level, n_r is the readout noise, and i_d the dark current. The used saturation level can either be the regular or effective saturation level.

Performance characteristics for spectrometer comparison

For comparing the theoretical performance of different spectrometer designs, and with different slit widths, the $A^*(\lambda)$ per nm resolution is useful. It is found from dividing the per-nm $A^*(\lambda)$ by the specified resolution.

As discussed, normalising the noise and saturation levels by A^* is useful for comparing spectrometers with different sensitivities.

The readout noise can be normalised by A_j^*, in units of photons. This can be denoted as noise equivalent radiance dose, $NERD_{ph,j} = n_r \,/\, A_j^*$, as it describes the radiance dose, or number of incoming photons per area and solid angle, that gives a signal equal to the readout noise [32]. Similarly as A^*, this can be specified by giving the full curve, however, for comparison purposes, it may be equally descriptive when given only for a single wavelength of interest. For NIR spectroscopy applications, it is recommended to give the $NERD_{ph,j}$ of the detector element at 800 nm.

The *saturation level* can be normalised by A_j^*, in units of photons. This is the saturation spectral photon radiance dose $SSRD_{ph,j} = n_{\text{sat}} \,/\, A_j^*$, i.e., the radiance dose, or number of incoming photons per area and solid angle, that causes saturation. As the signal is considered saturated when at least one detector element is saturated, the *SSRD* should be given as the minimal value, describing the photon radiance dose that causes at least one detector element to be saturated,

$SSRD_{ph,min} = n_{\text{sat}} \,/\, A^*_{max}$. Alternatively, it can be given for the detector element at a wavelength of interest, such as 800 nm for NIR spectroscopy.

Using the quantities A^*_j, $NERD_{ph,j}$, and $SSRD_{ph,j}$ at a representative wavelength, such as 800 nm for NIR spectroscopy, thus gives a quick and simple overview comparison of the performance at a relevant wavelength for spectrometers with similar shapes of the A^*_j.

5.3 Other characteristics

The *range of integration times* that are supported by the spectrometer software should be specified, as it may determine whether the spectrometer is applicable for a given application.

The *operating temperature* of the spectrometer should be specified, as it determines whether the spectrometer is applicable for a given application with certain temperature conditions.

Some spectrometers may have installed *temperature control* of the detector, which ensures constant temperature conditions for the measurements. As the noise levels generally increase with higher temperature, this is beneficial for reducing the noise of the spectrometer, and making the dark current more stable. If the spectrometer has such temperature control, this should be stated.

The *measurement speed* of the spectrometer should be specified, as this may be a limiting factor for high-speed applications, or reduce the number of measurements that are performed within a given time for signal averaging and noise reduction. The current speed of the spectrometer software may be larger than the actual detector *readout time*, which gives the theoretically lowest measurement time than can be obtained through software optimisation. Both should be specified.

The *power consumption* of the spectrometer should be specified, as it may be a limiting factor for e.g. battery driven applications.

The *dimensions* of the spectrometer, such as size and weight, are critical for certain applications, and should be specified.

Finally, *price* should be specified, as it is a highly important factor when comparing spectrometers.

5.3.1 Characteristics that are not included

Due to the limited scope of this thesis, not all characteristics that may influence the performance are described and included in the specification. Given here are a few examples of characteristics that are omitted, but may be of importance when comparing spectrometers and investigating their suitability for different applications.

The specification does not include stray light characterisation. Stray light is unwanted light in the system, both from internal processes, such as other diffraction orders, or background light from the surroundings. It cause additional noise and distort the signal, and the stray light levels in a spectrometer is thus of relevance for a proper characterisation. For example, the signal

in different diffraction orders can be characterised, specified, and corrected for. Stray light characterisation is thoroughly specified in [19].

Similarly as for background light, also the sensitivity to other external influences of the surroundings, such as temperature, humidity, and spectrometer movement could have been characterised. This may be highly relevant for the suitability of a spectrometer for realistic measurement conditions, such as for inline spectroscopy [10].

The spectrometer may have bad detector elements with particularly high noise or other irregularities. What detector elements are considered bad, or their number, could have been specified.

The repeatability and stability of the spectrometer is not characterised. Information about signal drift could be useful for e.g. obtaining the optimal integration time that optimises the SNR, while omitting errors due to drift. Repeatability characterisation is useful for assessing the accuracy of the data and estimations from multivariate models, when carrying out measurements at different times.

Only the performance related to measurements of homogeneous samples and reference objects are considered. When also considering heterogeneous samples, effects such as point spread and spatial coregistration errors, which describes errors in the collection of light from the sample in the spatial dimension, should be considered. This is treated in e.g. [34].

5.4 Total specification

The recommended performance characteristics for a non-redundant specification are summarised in Table 5.2. The corresponding derived performance characteristics that can be obtained from the non-redundant specification are summarised in Table 5.3.

Table 5.2: Performance characteristics that should be given for a non-redundant specification. See subsection 5.1.3, subsection 5.2.4, and section 5.3 for more detailed description.

Quantity	Specification	Unit	Note
Spectral range	Wavelengths of the outermost detector elements that give nonzero signal	nm	
Spectral sampling interval	Distance between adjacent detector elements	nm	Mean
Wavelength accuracy	Deviation from measured wavelength to actual wavelength	nm	Mean
Resolution	FWHM of the Gaussian fit of the SRF	nm	Mean and minimum
Per-detector-element A_j^*	Response curve	μm^2	Graph and at e.g. 800 nm
Per-nm $A^*(\lambda)$	Sensitivity	μm^2	Graph and at e.g. 800 nm
Dark current i_d		e^-/s	Mean
Readout noise n_r		e^-_{rms}	Mean
Saturation level n_{sat}		e^-	
Linearity errors	Any deviation from linear response	%	Mean
Integration time range		ms	
Operating temperature		$°C$	
Temperature control options			
Readout time		ms	
Power consumption		W	
Price			
Size and weight			

Table 5.3: Derived performance characteristics that can be obtained from the non-redundant specification. See subsection 5.1.3 and subsection 5.2.4 for more detailed description.

Quantity	Specification	Calculation	Unit
Number of spectral samples		Spectral range / spectral sampling interval	Integer
Number of independently resolved wavelengths		Spectral range / resolution	Integer
Total signal $n_{e,j}$ in detector element j	For a given input light level $L_{q\lambda,j}$ and integration time t_{int}, for detector element j with width $\Delta\lambda_j$	$A^*_j L_{q\lambda,j} t_{int} \Delta\lambda_j$	e^-
Total noise σ_{tot}	For a given signal level n_e and integration time t_{int}	$\sqrt{n_e + n_r^2 + i_d \cdot t_{\text{int}}}$	e^-_{rms}
SNR	For a given signal level n_e and integration time t_{int}	n_e/σ_{tot}	Ratio
Effective saturation level $n_{\text{sat,eff}}$	For a given integration time t_{int}	$n_{\text{sat}} - i_d \cdot t_{\text{int}}$	e^-
Dynamic range	For a given integration time t_{int}	$n_{\text{sat}} \,/\, \sqrt{n_r^2 + i_d \cdot t_{\text{int}}}$	Ratio
Integration times where the dark current equals the readout noise and gives saturation		n_r/i_d and n_{sat}/i_d	ms
Maximum achievable SNR		$\sqrt{n_{\text{sat}}}$	Ratio
$A^*(\lambda)$ per nm resolution		$A^*(\lambda)$ / resolution	μm^2 per nm
$\text{NERD}_{\text{ph,j}}$	At a given representative wavelength, e.g., 800 nm	$n_r \,/\, A^*_j$	Photons per m^2 and sr
$\text{SSRD}_{\text{ph,j}}$	At a given representative wavelength, e.g., 800 nm	$n_{\text{sat}} \,/\, A^*_j$	Photons per m^2 and sr

5.5 How to use the performance characterisation

The different performance characteristics given in Table 5.2 and Table 5.3 are useful for characterising spectrometers in different ways, both for estimating the data quality, evaluating whether it is suited for a given application, and for comparing different spectrometers.

5.5.1 Data quality estimation

Some of the performance characteristics are useful for characterising the performance of a spectrometer, and the corresponding data quality.

The important quality factor of a measurement is the SNR. It describes the ability to access the information that is contained in the spectrum, and sufficient SNR is required for the data to be any useful. Higher SNR gives higher accuracy, and thus higher quality of the measurements, and we should always strive to increase the SNR within the given bounds of the measurement, such as requirements for speed and resolution. Additionally, the dynamic range is important for understanding the signal limitations. The specifications of noise and saturation are very important, but their use boils down to specifying the SNR and effective dynamic range.

The relative signal variations over the spectral range can be found using the per-detector-element A_j^*. This is useful for understanding the relative SNR and data quality of different spectral regions.

The signal at different wavelengths for a given light level can be estimated using the per-detector-element A_j^*. Together with the specified noise at the given integration time, this estimates the total noise and SNR for the different wavelengths, which is useful for assessing the quality of the signal in different spectral regions.

For absolute radiometric measurements, A_j^* can also be used to obtain the radiance spectrum of a measured light source. This is however not of relevance for absorption spectroscopy.

The saturation level n_{sat} indicates the maximum obtainable signal level, and the normalised saturation level $\text{SSRD}_{\text{ph,j}}$ is useful for selecting an optimal integration time for a given application and light level.

The resolution indicates what spectral features are resolved in the raw spectrum.

Through signal binning or smoothing, a higher SNR can be obtained at the expense of reduced resolution. If the resolution of the spectrometer is higher than what is required for the application, the SNR can be increased as much as possible, while retaining sufficient resolution.

When planning measurements, it can be useful to simulate the effect of different light levels and integration times, for estimating the noise levels, SNR, and saturation conditions. Signals corresponding to different light levels and integration times can be simulated, which is useful for e.g. studying the effect on the results and estimations from multivariate models. The optimal measurement conditions can then be determined, with sufficient integration time for obtaining sufficient data quality and avoiding saturation, while reducing the measurement time as much as possible. While this is commonly performed manually through many measurements, such simulations are simple and fast.

The wavelength accuracy characterises the mean deviation of the estimated wavelength to the real wavelength. Large deviations indicate that the spectrometer should be re-calibrated.

Non-negligible linearity errors indicate that the spectrometer should be linearity corrected.

It should be noted that also other performance characteristics that are out of scope of this thesis, discussed in subsection 5.3.1, are useful for characterising the data quality.

5.5.2 Evaluation of the suitability of a spectrometer for a given application

The suitability of a spectrometer for an application must be evaluated based on the performance characteristics.

For a spectrometer to be suited for an application, a few specific requirements must be fulfilled. They thus act as selection criteria.

The spectrometer must have a spectral range suited for the application, as different applications concern different wavelength regions that contain different spectral information. For example, to detect the NIR water absorption line at 970 nm, this wavelength must be contained within the spectral range.

An application may have specific speed requirements, e.g., when being used inline for measuring samples at a conveyor belt. The spectrometer must then have sufficiently short detector readout time, and allow for sufficiently short integration time, to stay within the given time limit of each measurement. Additionally, the measurement within this integration time limit, or the average of multiple measurements obtained within the time limit, must give sufficient SNR. Similarly, when measuring weak signals, the spectrometer must allow for sufficiently long integration time for obtaining sufficient signal strength.

Different applications require different resolution, and the spectrometer must have the required, or better, resolution to be able to detect the relevant spectral features. For example, Raman spectroscopy requires much higher resolution than NIR absorption spectroscopy of liquids and solids. If the resolution is better than required, it may be reduced through binning or smoothing for obtaining higher SNR and optical throughput, and allowing greater measurement speed. The resolution can be improved by reducing the slit size, however, this is generally only possible when purchasing a new spectrometer.

The spectrometer must also be suited for the application temperature conditions, such as in cold storage rooms, or in the direct sun on a field.

If the spectrometer is used in e.g. a battery driven application, the power consumption may be a limiting factor.

Some applications may have upper limits on the size and weight of the spectrometer, e.g., for handheld instruments.

Finally, the application may follow a budget, and price may also be a limiting factor of whether the spectrometer is applicable or not.

5.5.3 Spectrometer comparison

When comparing spectrometers in relation to a given application, the first step is to evaluate whether the spectrometers fulfil the application requirements, as described in subsection 5.5.2.

There is no immediately clear way to balance the remaining characteristics that describe the performance of the spectrometer. The comparison of spectrometers is highly application dependent, as the various performance characteristics may be valued and weighted differently for different applications. There exists no overall perfect spectrometer that suits all applications. For example, some applications require both high resolution and SNR, such as Raman spectroscopy, while others rather require sufficient SNR for high speed measurements, without the need of high resolution, such as for inline NIR absorbance spectroscopy of liquids and solids. Based on the requirements of the application, the performance characteristics must be traded off against each other. The exact performance requirements for a given application may not be clear, which complicates the comparison and selection of a suitable spectrometer. The user must perform a subjective assessment comparing the different performance characteristics to select the proper spectrometer for the application.

The per-nm $A^*(\lambda)$ compares their sensitivity normalised for the detector element width, and thus independent of smoothing and binning. When normalising $A^*(\lambda)$ for the resolution, the theoretical performance of the spectrometer designs are compared, adjusted to the same resolution and thus independent of slit size. This is useful when purchasing a new spectrometer, and being able to choose slit size.

For a proper comparison of the performance of spectrometers, the derived characteristics that are normalised for A^* are the most useful. As discussed, these indicate the performance independent of the sensitivity. $\mathrm{NERD}_{\mathrm{ph,j}}$ indicate what spectrometer performs best in terms of SNR when measuring the same light level, while $\mathrm{SSRD}_{\mathrm{ph,j}}$ indicate how much light can be measured before reaching saturation. The dynamic range also indicate the signal quality limitations.

Also factors such as price, size, power consumption, ease of use, and maintenance requirements may be taken into account in the spectrometer comparison.

Chapter 6

Experimental characterisation

This chapter presents methods for measuring the performance characteristics that were defined in chapter 5. The performance characteristics were defined using a "black box"-approach, and are thus measurable by observing the performance without knowledge about the internal structures and design of the spectrometer. The resolution is defined for diffraction grating spectrometers, while the remaining characteristics generally hold for any spectrometer design.

The measurement setup is designed to be reproducible, user-friendly, and reasonably priced, without requiring considerable experience and knowledge of optics. Together with the relatively simple suggested measurement routines, it is intended to have the potential of being reproduced, and used as a tool for generating information about spectrometers also by others.

The primary intent of the characterisation methods is not to fully characterise the performance characteristics, but rather to give an indication of the magnitude. This is considered sufficient to understand the data quality, to indicate whether a spectrometer is suited for a given application, and to aid the comparison of different spectrometers. Hence, the focus is rather on making the method user-friendly, and relatively simple and fast, without the need of expensive equipment, than to ensure particularly high accuracy and precision. Measurement uncertainties are not assessed in detail, but the order of magnitudes of the measured values are verified by simple estimations, and through comparison with data sheet values.

Lastly, results from applying the methods to three diffraction grating spectrometers are presented, and their performance is compared. The spectrometers are denoted as spectrometer i), ii), and iii), rather than revealing their identities, to protect potential collaboration relations with the manufacturers, and because the spectrometer identities are not considered of relevance for the demonstration of the methods. For spectrometer i) and ii), information about internals such as slit size and type of detector is known, together with data sheet values for resolution and noise. No such information is known for spectrometer iii), which is included for demonstrating that no such information is required for a proper characterisation.

The presented methods are summarised in the instructions manual given in Appendix A.

6.1 Measurement setup

The measurements of the performance characteristics are made using the light setup shown in Figure 6.1. This combination of a light source and an integrating sphere is described as

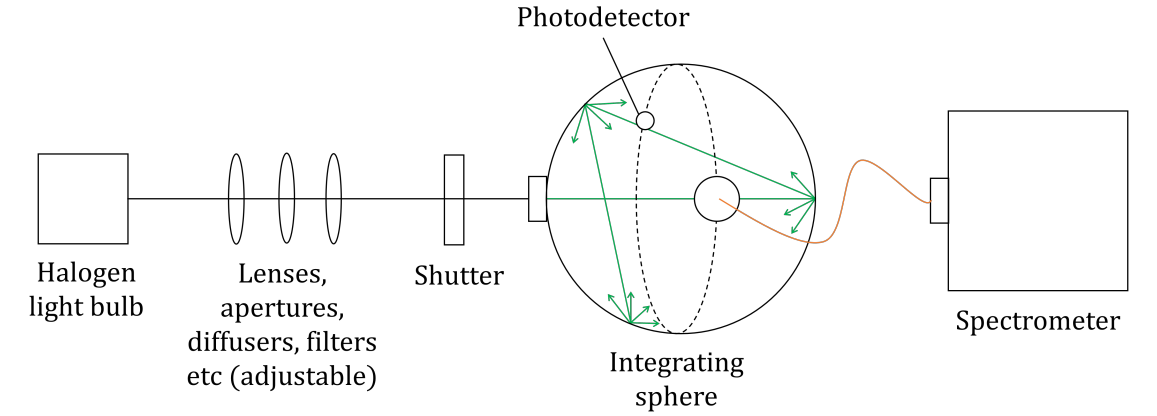

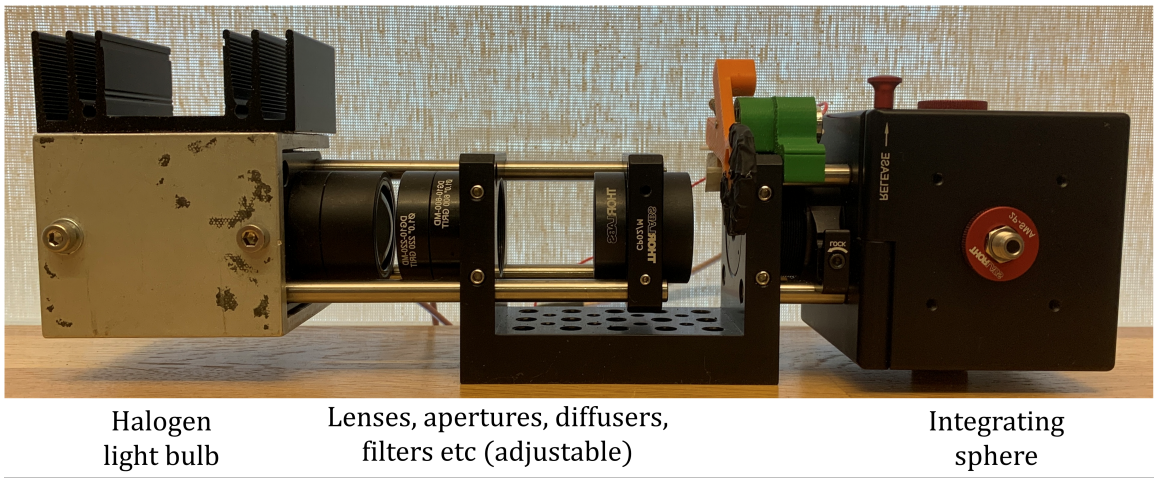

Figure 6.1: The measurement setup that is used for characterisation of spectrometers. The spectrometer is not included in the photograph.

a spectral radiance reference standard, and termed a *luminance gauge* by the CIE 233:2019 standard [19]. It is designed to provide a spatially uniform field with constant light level across both the input slit and the field of view of the spectrometer. The system is mounted using the ThorLabs optical cage system, and cage system covers, which are not shown in the figure, are used to protect the system from any background light. The light source is a 20 W halogen light bulb with a tungsten filament, which provides broadband illumination that approximates a blackbody spectrum of approximately 2500 K. The light directed into the system is focused by a lens, and made more homogeneous and uniformly distributed by two diffusers of 220 and 600 grit polishes. This is required as apertures of different sizes may be applied, and the transmitted intensity should be proportional to the aperture area, which only is the case for uniform distribution over the whole aperture. The light is then sent through a series of optional components, such as apertures and filters, which easily are replaced for different measurements. The light is then sent into an integrating sphere of diameter 5 cm, or blocked by a shutter,

which is used for performing subsequent dark measurement throughout a measurement series, and programmed to block the beam once every 1.5 s. The integrating sphere is coupled to a reference photodetector, which measures the light power in the sphere, and indicates any fluctuations in the light intensities. It has an output port with a fibre coupler, where an optical fibre that couples the light into the spectrometer is connected. For most measurements, an optical fibre with diameter 550 µm and numerical aperture $NA = 0.22$ is used.

In radiometric measurements, a 550 nm longpass filter is applied for removing the contribution from lower diffraction orders from wavelengths below 550 nm that are within the spectral range up to 1100 nm, and present on the detector array. Different filters can be applied for e.g. studying stray light. This is out of scope of this thesis, but reference is made to the CIE 233:2019 standard [19] for a thorough description of this method. For limiting and controlling the illumination level, an aperture of optional size is usually applied. This is particularly useful for varying the light level in a controlled manner for radiometric measurements, without changing the source spectrum. For this, precision pinholes of diameters 1 mm and 3 mm are used.

The setup is directly applicable for spectrometers with fibre coupling input, which is common for most portable diffraction grating spectrometers. It can also be used by other spectrometers by removing the fibre coupler from the integrating sphere, and placing the output port in the field of view of the spectrometer, and thus, similarly as when using the fibre coupler, providing uniform illumination over the field of view of the spectrometer. This reduces the quality of the integrating sphere output, as the light that would be reflected on the surface of the fibre coupler, which is covered in the same diffuse reflecting material as the interior of the integrating sphere, is lost. Through measurements using a diffraction grating spectrometer, it was found that opening one of the output ports of the integrating sphere yields an intensity reduction of approximately 30%, as seen in Figure 6.2. The measured spectra also had slightly different spec-

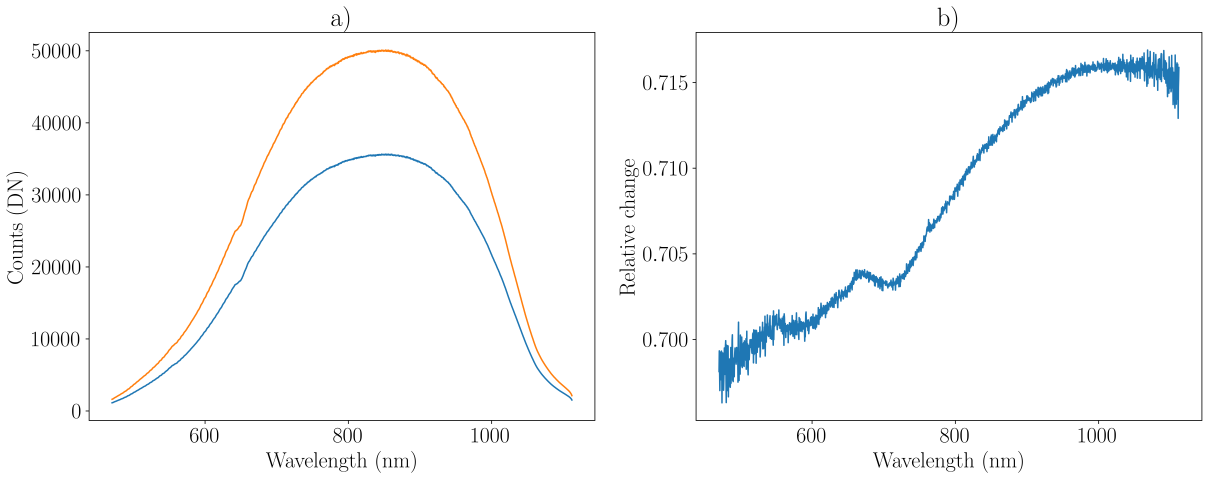

Figure 6.2: a) Measured spectra of the integrating sphere, fully closed (orange) and with a fully open output port (blue), and **b)** their ratio. The open output port was blocked using black plastic, which is considered fully opaque and absorbing for the considered wavelengths. The opening of an output port reduces the intensity with approximately 30%. It also yields a slightly different spectrum shape, however, this may be an effect of the spectrometer rather than the integrating sphere.

trum shapes, which may be an effect of the shorter wavelengths leaking out of the integrating sphere at a higher rate, or some unknown spectrometer effect. The setup may still be sufficient for measurement of the performance characteristics, but the effect by the reduced quality from the integrating sphere, and the possibly different spectrum shape, should be further investigated.

Table 6.1: Part list for the measurement setup. The part numbers of the halogen light bulb and focusing lens are unknown, and the components can be replaced with similar components when reproducing the setup. The shutter is custom made, and can be replaced by any design using a black material to block the beam.

Component	Part number	Manufacturer
Halogen light bulb, 20 W		
Focusing lens		
Diffuser, 220 GRIT	DG10-220-MD	ThorLabs
Diffuser, 600 GRIT	DG10-600-MD	ThorLabs
Longpass filter, 550 nm (optional)	FGL550M	ThorLabs
Precision pinhole, diameter 1 mm	P1000D	ThorLabs
Precision pinhole, diameter 3 mm	P3000K	ThorLabs
Shutter		Custom made
Integrating sphere, diameter 5 cm	2P3/M	ThorLabs
Fibre adapter for integrating sphere	2P-SMA	ThorLabs
Reference photodetector for integrating sphere	SM05PD1A	ThorLabs
Optical fibre, diameter 550 μm and numerical aperture 0.22	M37L01	ThorLabs
HG-1 Mercury Argon Calibration Light source		Ocean Optics
Blackbody source (optional)	ES1000-100	Electro Optical Industries Inc.

In addition to the described light source setup, a calibration source with gas producing spectral emission lines is recommended for characterising the resolution and wavelength accuracy. In this thesis, the HG-1 Mercury Argon calibration source from Ocean Optics [33] is used.

Additionally, the ES1000-100 blackbody source from Electro Optical Industries Inc. is applied for obtaining the light source spectrum at the output of the integrating sphere. When using the same measurement setup as presented here, or another setup with known source spectrum, this is not required.

The part numbers of all used components are given in Table 6.1.

6.1.1 Light source spectrum for the measurement setup

Absolute measurement of the response curve and net light collection of a spectrometer requires knowledge of the light source spectrum. This was obtained for the output of the integrating sphere setup through a two-step calibration process, similar to the source-based substitution procedure described in [19], by comparison with the measurement of a source with a known spectrum. The response curve of a spectrometer was obtained through measurements of a true blackbody source and comparison with Planck's law, Equation 2.11. The light source spectrum for the measurement setup, including all optical components, was then obtained using this response curve. The spectrum can then be used for further obtaining response curves also of other spectrometers, without the need of making an absolute calibration using the blackbody source. A python script for this method of obtaining the light source spectrum is given in section B.1.

The ES1000-100 blackbody source from Electro Optical Industries Inc. was measured using spectrometer i) and a fibre with diameter 550 µm. $650°C$ was found to be a suitable temperature giving a sufficiently high signal without reaching saturation of the detector for the lowest possible integration time of 10 ms. The response curve of the spectrometer was obtained for the wavelength range of 600 nm to 1100 nm, where the measured signal was sufficiently strong, through dividing the measurement by the blackbody spectrum at $650°C$, given by Planck's law in Equation 2.11. The light source spectrum for the measurement setup was then obtained through dividing the measured spectrum with the response curve. The results, obtained using the python script given in section B.1, are shown in Figure 6.3. It is worth noting that the response curve looks remarkably accurate at 600 nm, where both the measured signal and blackbody spectrum is very close to 0. Any stray light would largely distort the signal, and the results indicate negligible stray light levels.

As seen in Figure 6.4, the resulting light source setup shape resembles that of a blackbody spectrum at 2520 K, however, some deviations occur below 650 nm, and the spectrum drops rapidly off from the expected blackbody spectrum shape above 1000 nm. The cause of these deviations is unknown, but not considered of importance as they occur at the edges of the spectral range, where the responsivity is weak.

The intensity of the measurement setup illumination was, as shown in Figure 6.4, found to be only $3.6 \cdot 10^{-4}$ percent of the true 2520 K blackbody spectrum. This is due to only a small part of the light from the halogen lamp passing into the system, where it is further attenuated by diffusers, lenses, and other components in the light path. A 3 mm pinhole further reduces the intensity before it reaches the integrating sphere, where it is additionally attenuated. The intensity varies based on what optical components are used, and for absolute radiometric mea-

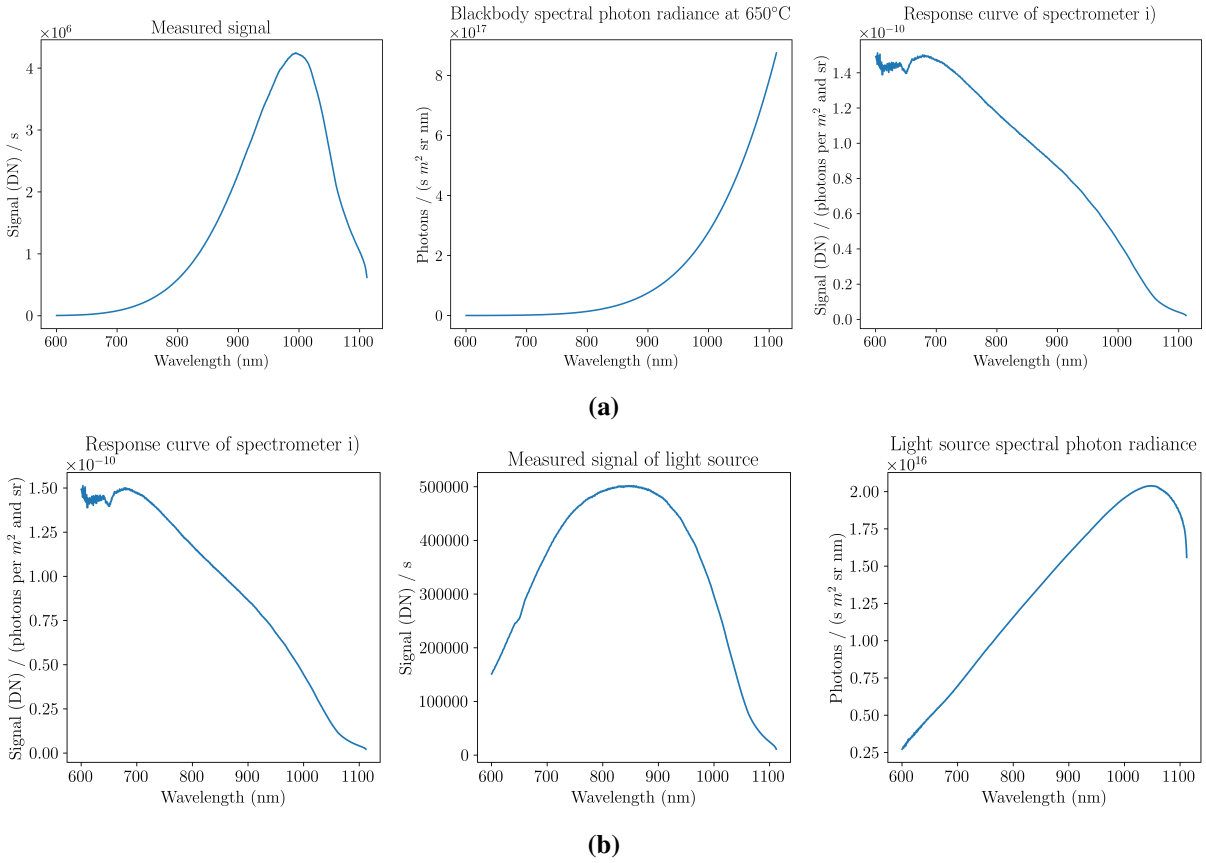

Figure 6.3: Calibration of the measurement setup illumination. **a)** The response curve of spectrometer i) was obtained from measuring the blackbody source at 650°C, and dividing by the blackbody spectral radiance spectrum. **b)** The illumination spectrum of the light source setup was obtained by dividing the measured signal by the calibrated response curve.

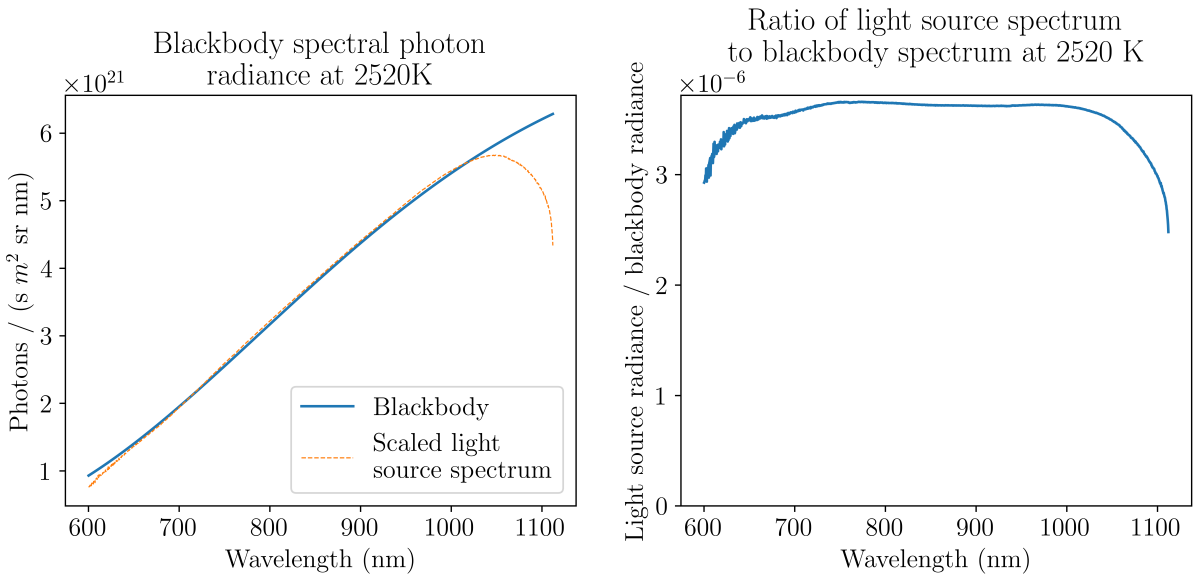

Figure 6.4: The estimated setup spectrum shape is well approximated by the blackbody spectrum at 2520 K for the wavelength range of approximately 650 nm to 1000 nm, with intensity corresponding to only $3.6 \cdot 10^{-4}$ percent of the true 2520 K blackbody spectrum.

surements, each combination of components should be calibrated separately. However, this thesis considers comparative measurements between instruments, and no absolute radiometric measurements are required.

The calibration method of the light source setup is not sufficient for obtaining high accuracy. It may introduce errors from e.g. varying measurement conditions of the blackbody and measurement setup measurements. The method is not optimised for reducing noise. However, it is considered sufficient for the purpose of approximate characterisation, as considered in this thesis.

6.2 Measurements of performance characteristics

6.2.1 Spectral characteristics

The treatment here assumes that the wavelength calibration of the spectrometer is given, either as a polynomial, relating the detector element number to a wavelength, or simply included in the spectrometer software by giving a wavelength vector with wavelengths corresponding to each detector element. This is usually the case, and re-calibration is out of scope, while the calibration accuracy will be measured.

The spectral sampling interval can be found using the wavelength calibration of the spectrometer, as the distance between adjacent detector elements in wavelength units, i.e., the difference between two adjacent elements in the wavelength vector.

The spectral range is easily obtained from measuring a broadband source, such as the light source setup presented in section 6.1, and using the wavelength vector elements corresponding to the two outermost detector elements where the signal is nonzero.

Spectrometers i), ii), and iii) have spectral ranges from 536 nm to 1112 nm, from 532 nm to 1154 nm, and from 536 nm to 1021 nm, respectively. Spectrometer i) has average sampling interval 0.36 nm, with 14% variation over the spectral range, from 0.32 nm to 0.37 nm. For spectrometer ii), the average sampling interval is 0.64 nm, with 39% variation over the spectral range, from 0.54 nm to 0.79 nm. Spectrometer iii) has average sampling interval 0.33 nm, with 18% variation over the spectral range, from 0.30 nm to 0.37 nm.

6.2.1.1 Resolution and wavelength accuracy

The resolution of a diffraction grating spectrometer was in subsection 5.1.4 defined as the full width at half maximum (FWHM) of the Gaussian fit of spectral response function (SRF) in wavelength units, while the centre wavelength of the SRF, which defines the wavelength of a spectral line measurement, in subsection 5.1.5 was defined as the centre position of the Gaussian fit of the SRF. Hence, measurement of the SRF at known wavelengths will both yield information about the resolution and the wavelength accuracy of the spectrometer.

As discussed in subsection 3.1.2, a simple and quick method for measuring the SRF at selected positions over the spectral range, using small and relatively inexpensive equipment, is by using

calibration sources with gas producing spectral emission lines. One single measurement then measures the SRFs over the whole wavelength range. The SRF is not found for all wavelengths, but in most cases, the SRFs corresponding to the spectral lines are adequate to estimate the SRF and its variation also for the wavelengths that are not measured. This is sufficient for the purpose of comparing spectrometers, as high accuracy measurements are not required. However, the peaks are overlapping in the spectrum, and the method requires data analysis, and a defined cut-off criterion, for delimiting the individual peaks.

As discussed in section 3.1, the wavelength accuracy can be measured using the same calibration source and measurements as used for the resolution.

As discussed in subsection 5.1.4, when using a calibration source with spectral emission lines, the peaks in the spectrum must be separated from each other through defining a cut-off criterion. From the effect on the cut-off on different function shapes, it was found that 5% was a suitable cut-off level. Gaussian curve fits are performed on all the identified peaks. The resolution is found by measuring its FWHM, alternatively scaling its standard deviation according to Equation 5.3, and the centre wavelength corresponds to the centre of the Gaussian fit.

A python script for the analysis of a spectrum with multiple emission lines is given in section B.2. Peaks considered corresponding to second diffraction orders, or having overlap from other peaks, are removed. The results may still not be perfectly accurate, as also other impurities in the spectra may cause deviation, but they are considered adequate for indicating the performance. The resulting resolutions and wavelength errors are plotted as a function of wavelength.

Measurement example

The HG-1 Mercury Argon calibration source from Ocean Optics [33] was measured using the three different diffraction grating spectrometers, and analysed using the script given in section B.2. The source has a fibre coupler output, but direct coupling via a fibre into the spectrometer was found to give too strong signal and cause saturation. Instead, it was coupled into the integrating sphere using a fibre, and the spectrometer was coupled to the integrating sphere using another fibre. For reducing the noise, 400 spectra were averaged. The averaged spectra, identified peaks, and Gaussian fits are shown in Figure 6.5, while the resulting resolutions and wavelength accuracies are shown in Figure 6.6. The plots indicate that the resolution is approximately constant over the spectral range. Some deviations from the approximately constant resolution are present around 800 nm, which, due to the high density of peaks in this region, is assumed to be caused by overlapping from adjacent peaks that is not corrected for. They are sufficiently small to be neglected. The wavelength errors are mostly small and constant over the spectral range, and may be explained by some offset in the wavelength calibration.

The estimated resolution of spectrometers i), ii), and iii) are, as shown in Figure 6.6a, approximately 2.5 nm, 4.5 nm, and 4 nm, respectively. The corresponding resolutions from the data sheets of spectrometer i) and ii) are 3 nm and 5 nm. The estimations are in the same order of magnitude as the data sheet values. The deviations may be due to inaccuracies from rounding, or the data sheet values may state the lower limit of the resolution performance.

As shown in Figure 6.6b, the estimated wavelength accuracy for spectrometer i) is approximately 0.3 nm. It varies more for spectrometer ii), with average of approximately 0.4 nm. For

spectrometer iii), three points deviates with approximately 1.5 nm, and the single point being close is considered an outlier for finding the wavelength accuracy.

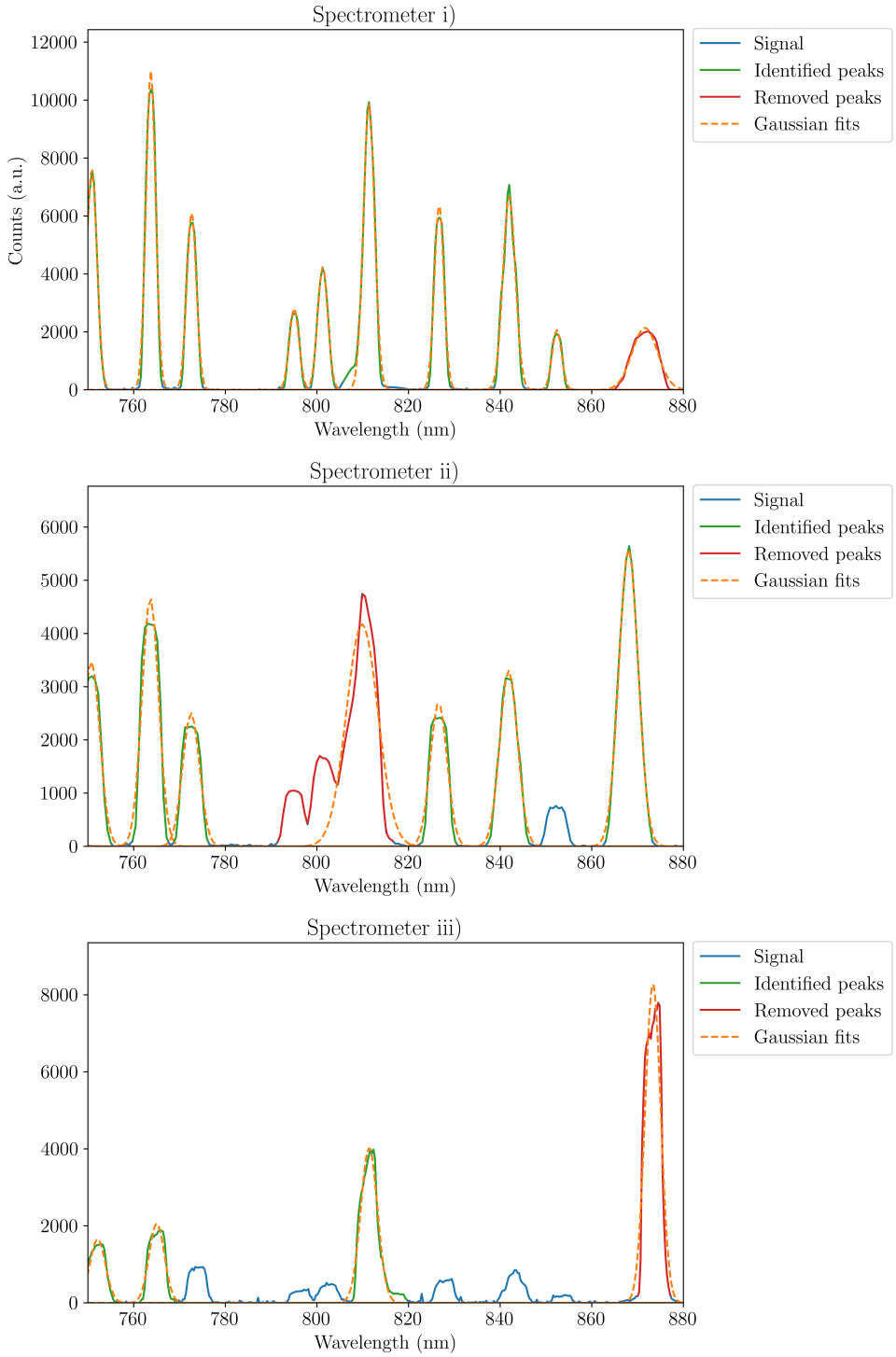

Figure 6.5: Measured spectra of the HG-1 Mercury Argon calibration source with spectral emission lines, and the identified peaks and Gaussian fits, for the three diffraction grating spectrometers. The removed peaks are either considered corresponding to second diffraction orders, or having overlapping peaks that are not resolved. Due to low SNR for spectrometer iii), fewer peaks are considered than for spectrometer i) and ii), as their relative intensity is below the chosen peak prominence level.

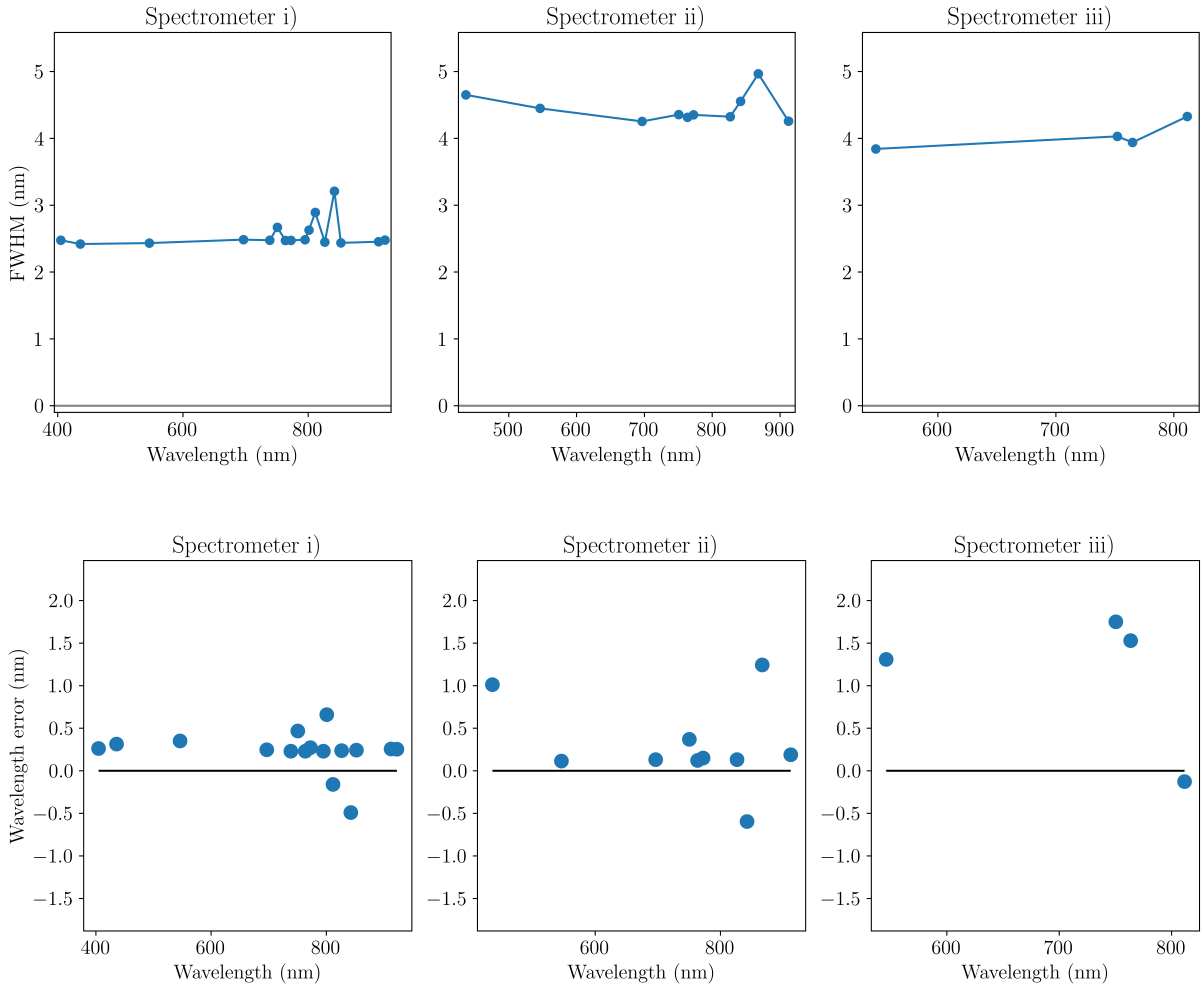

Figure 6.6: Estimated **a)** resolutions and **b)** wavelength accuracies of three different diffraction grating spectrometers from using the script in section B.2. Due to low SNR for spectrometer iii), fewer peaks were properly detected than for spectrometer i) and ii).

6.2.2 Radiometric characteristics

All measurements of the radiometric characteristics are based on measurements of a uniform light source with a slowly varying spectrum, such as the integrating sphere setup described in section 6.1. For minimising noise contribution, as described in subsection 3.3.1, 400 spectra are obtained and averaged to a single spectrum. The shutter in the integrating sphere setup blocks the beam every 1.5 s, and the signal spectrum is dark corrected by subtracting the average of the corresponding dark measurements.

6.2.2.1 Photon transfer analysis

As described in subsection 3.3.4, the photon transfer analysis finds the gain factor G_S of the spectrometer, which relates the signal in DN units to the photoelectron count, $S\ (DN) = G_S n_e$. It also determines properties such as the readout noise, dark current, linearity, saturation level, and dynamic range of the signal.

The photon transfer curve (PTC) can be generated by a single spectrum, as the measured values of the individual detector elements can be used as data points in the plot. This ensures a high density of data points constituting the PTC, which is desirable for statistical reasons. The spectrometers generally do not use all detector elements, leaving some for dark measurements, generating noise floor signals for the PTC. When the measurement is partly in saturation, the full dynamic range is then spanned within the single spectrum, and all features can be obtained from the PTC. This method requires that the readout noise and dark current are of equal magnitudes in all individual detector elements, which generally is assumed valid. Random small variations over the detector array does not affect the result considerably, and the overall average readout noise and dark current, which are of interest, are found. However, different values in different parts of the detector array, which correspond to different signal levels, will distort the estimations.

The PTC could also have been generated for the same detector element, or the average spectrum, by measuring different signal levels. As suggested in [32], this can be performed by varying the integration time. However, varying integration time cause variations in the dark current, and thus variations in the noise floor. Alternatively, the light level can be varied. However, many different data points are required for a good statistical estimation, making this a tedious task. Also the measurement conditions, especially temperature, needs to be constant over the whole measurement series, as both the dark current and readout noise are temperature dependent. Using a single spectrum measurement for the PTC generation requires only a single measurement, which is mush faster and ensures constant temperature conditions.

As described in subsection 3.3.2, the dark correction introduces more noise to the spectrum. However, when the same dark spectrum is subtracted from all signal spectra, the variance of the signal is left unchanged, and the effect of the dark signal noise is a constant distortion of the measured value without affecting the noise statistics. The noise statistics of the dark corrected spectrum then still describes the proper noise of a single non-dark-corrected measurement.

Photon transfer analysis is performed by generating the PTC, either the standard deviation PTC, which is the logarithmic plot of noise as a function of signal in DN units, or the variance PTC, the squared noise as a function of signal. The gain factor G_S and noise floor $\sigma_{\text{read+dark}}$ of a given integration time are found through a curve fit of the noise as a function of signal to the relation given by Equation 3.34, i.e.,

$$\sigma_{\text{total}}(DN) = \sqrt{\sigma^2_{\text{read+dark}}(DN) + G_S S(DN)}. \tag{6.1}$$

The saturation of the detector, either due to full-well, or occurrence non-linearities, is defined as the signal level where the noise starts decreasing. The dynamic range is then obtained from the ratio of the effective saturation to the noise floor.

Any linearity errors of the non-saturated signal is characterised by deviations from a perfectly linear slope of the shot noise.

A python script for photon transfer analysis of a single spectrum is given in section B.3.

Measurement example

The PTCs shown in Figure 6.7 were generated for the three diffraction grating spectrometers, by measuring the light source setup with an integration time causing the spectrum to be partly

saturated. The estimated gain factors, noise floor levels, saturation levels, and dynamic ranges are given in Table 6.2.

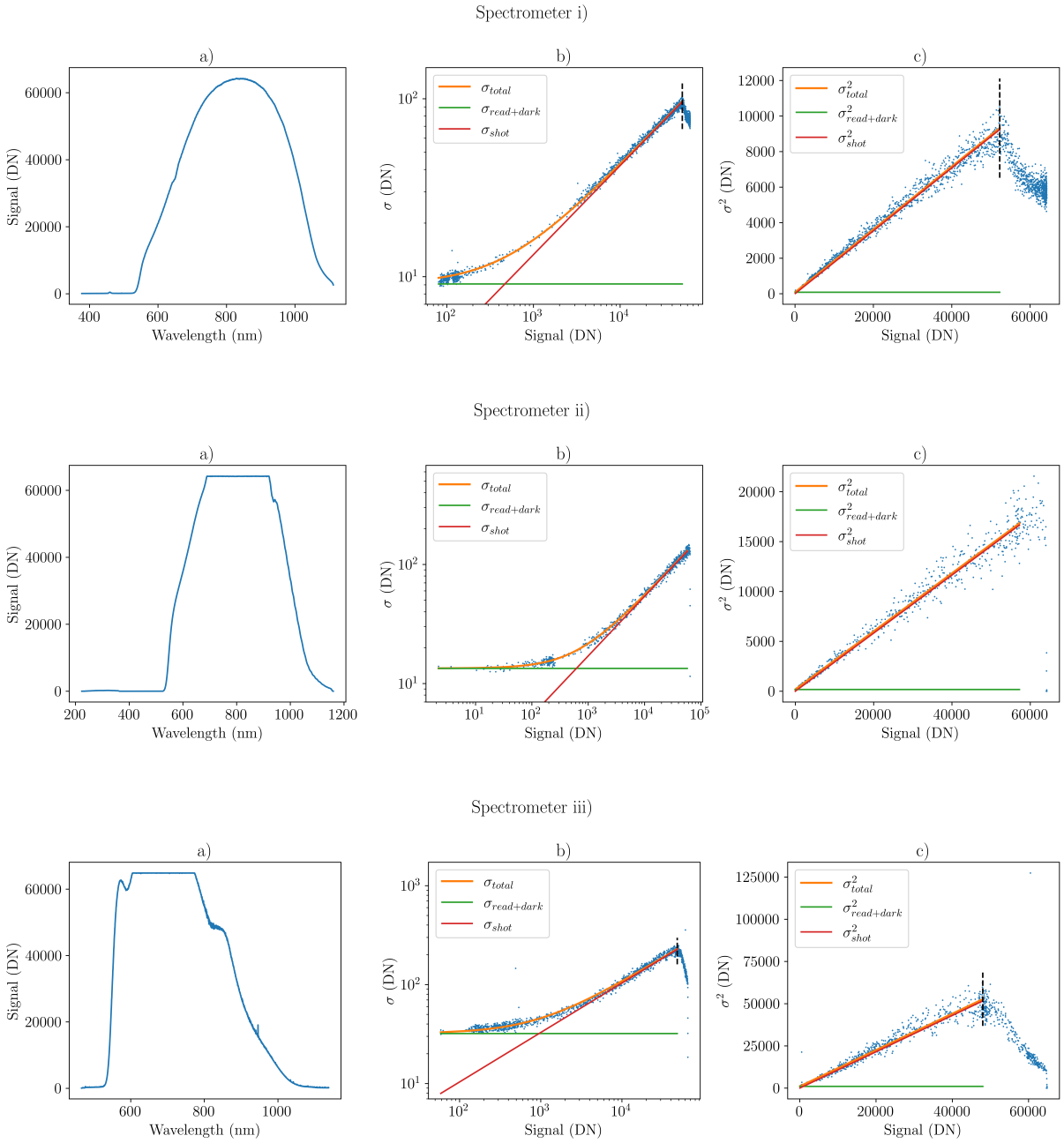

Figure 6.7: Generated photon transfer curves (PTCs) for the three diffraction grating spectrometers from using the script in section B.3. **a)** Measured spectrum. **b)** Standard deviation PTC. **c)** Variance PTC.

As can be seen from the PTCs, all three spectrometers have similar full well capacity in DN units. Spectrometer i) and iii) are nonlinear above a given signal level, while spectrometer ii) is linear up to the full-well capacity. All three spectrometers have negligible linearity errors within the non-saturated region. Spectrometer i) and ii) have comparable dynamic ranges, approximately 4 times higher than that of spectrometer ii).

The data sheet for the detector used in spectrometer i) states that it has a typical readout noise of 6 e^-_{rms}, and dark current 50 e^-/s per detector element, giving a dark current noise of 2.7 e^-_{rms}

Table 6.2: The estimated values from photon transfer analysis. The noise floor and dynamic range is given for one single integration time, as the dark current noise will increase slightly with longer integration time.

Spectrometer	i)	ii)	iii)
Gain factor G_S (DN/e^-)	0.18	0.28	1.08
Integration time t_{int} (ms)	150	25	1000
Noise floor $\sigma_{\text{read+dark}}$	9.10 DN 50.56 e^-	10.65 DN 38.03 e^-	32.03 DN 29.66 e^-
Saturation level	52 250 DN 290 278 e^-	64 183 DN 229 225 e^- (Full well)	47 998 DN 44 443 e^-
Dynamic range	5742	6027	1499

at 150 ms integration time. The sum is much lower than the corresponding measured sum of 50.56 e^-_{rms}. The cause of this deviation is unknown. Its full well capacity is given as 300 000 e^-, which corresponds well with the measured saturation level of 290 278 e^-. The estimated dynamic range, i.e., the ratio between the saturation and noise floor, is thus also much lower than that stated in the data sheet.

For spectrometer ii), the detector data sheet states the typical readout noise of 30 e^-_{rms}, and dark current 10 000 e^-/s per detector element, giving a dark current noise of 16 e^-_{rms} at 25 ms integration time. This is of the same order of magnitude as the measured sum of 38.03 e^-_{rms}. Also the stated full well capacity, given as 200 000 e^-, corresponds well with the measured saturation level of 229 225 e^-, meaning that also the estimated dynamic range is in the same order of magnitude.

As the estimations for spectrometer ii) are accurate, the deviations for the noise floor level in spectrometer i) are not assumed to be due to errors in the measurement method. They are rather assumed to be due to some unknown constant noise source in the spectrometer. The estimations are also assumed to be sufficiently accurate for spectrometer iii), for which no information of the noise levels is available from the vendor.

Only spectrometer i) is temperature controlled, and was set to 20°C during the measurements. Spectrometer ii) and iii) has no such temperature control, and the measurements were obtained with detector temperature of approximately 25°C. The given noise floor is thus affected by this temperature difference. While the given values are not completely comparable for the spectrometer designs, they characterise the current performance, taking into account that the temperature differences are present also for other measurements.

Dark current measurement

To determine the dark current, and separate the dark current noise and readout noise, PTCs at different integration times can be generated to obtain the noise floor as a function of integration time. Alternatively, the dark current can be obtained from dark signal measurements at different integration times, and dark current noise and readout noise from the corresponding noise, as $S_{\text{dark}} = G_s \cdot i_d \cdot t + \text{offset}$ and $\sigma^2_{read+dark}(DN) = G_S^2 \left[i_d \cdot t + n_r^2 \right]$.

However, this method is very sensitive to temperature drift, as both the dark current and readout noise are temperature dependent. The method may be feasible for temperature controlled spectrometers, but is not considered sufficient otherwise. This is illustrated in Figure 6.8.

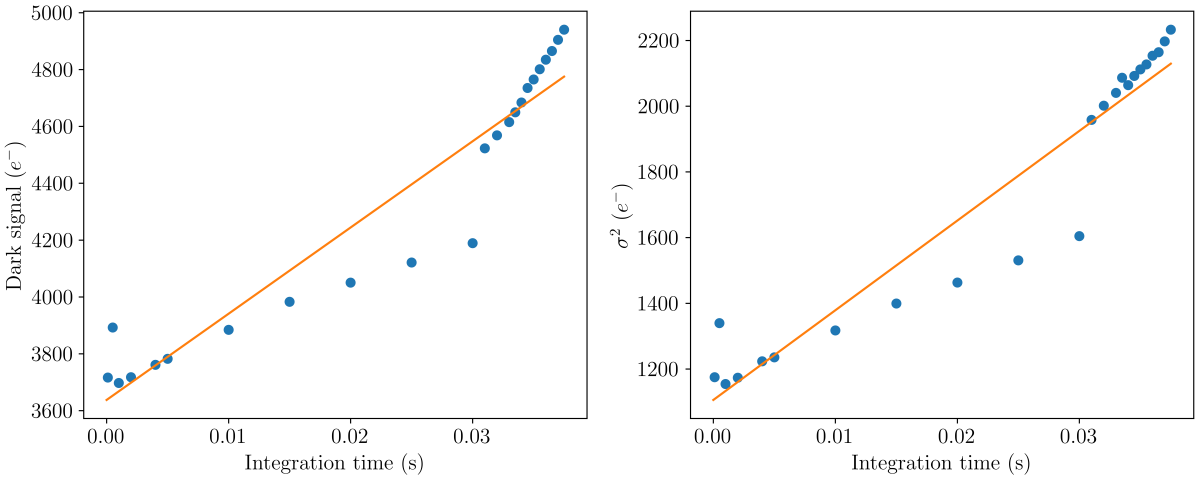

Figure 6.8: The effect by temperature change on the dark current for spectrometer ii). Two series of measurements were separated in time, and in the meanwhile, the detector had heated up from 29°C to 34°C. It seems reasonable that the increase within one of the separated measurement series is also subject to temperature drift, causing the slope to be too high.

In addition, it requires measurements at many different integration times to give accurate results, which is time demanding, and thus not suitable for the simple and fast characterisation. As seen in Figure 6.9, for spectrometer i), which is temperature controlled, the resulting estimations of the dark current by the three different methods varies considerably, 791.03e^-/s when using the estimated noise from photon transfer analysis, 1366.18e^-/s when using the slope of the dark current as a function of integration time, and 1822.94e^-/s when using the dark signal noise. This indicates that the number of measurements are not sufficient for a proper statistical assessment. The estimated readout noise from PTC and dark measurements agrees well, $\sqrt{2407.16} = 49.06$ photoelectrons and $\sqrt{2393.19} = 48.92$ photoelectrons, verifying that the measurements otherwise obtain similar results.

The dark current is thus not separated from the readout noise, and only the total noise floor for a given integration time is obtained. More measurements and an improved method is expected to succeed at such a characterisation, which is important for a full characterisation of the spectrometer. For a rough comparison between different spectrometers, their total effect at a representative integration time, as is obtained, is considered sufficient.

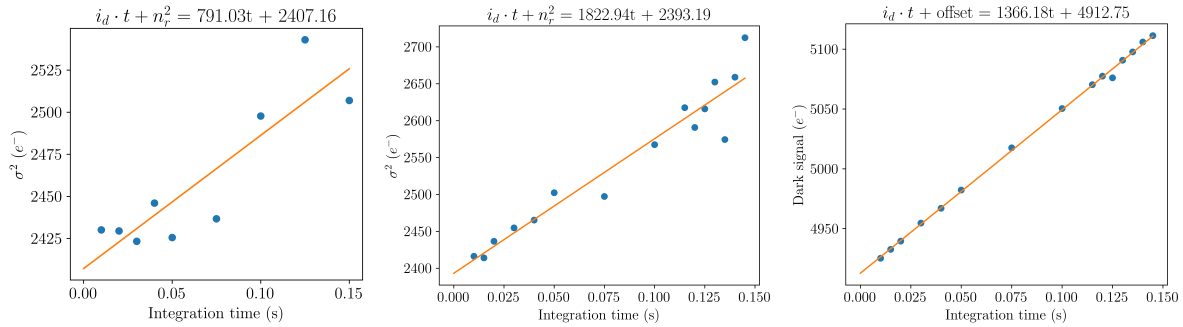

(a) **(b)** **(c)**

Figure 6.9: Three different methods for estimation of dark current and readout noise. **a)** The noise from photon transfer analysis as a function of integration time, **b)** the noise from dark measurements as a function of integration time and **c)** the dark signal as a function of integration time.

6.2.2.2 Sensitivity A^*

The sensitivity of the spectrometer is, as discussed in section 5.2, defined by the parameter $A^* = A\Omega\eta$ of net light collection, where $A\Omega$ is the étendue, and η is the combined effect of detector quantum efficiency, diffraction grating efficiency, and all losses in the optics. It can be given in units of μm^2. Using the measured signal of each detector element in photoelectron units, $n_{e,j}$, and Equation 3.7, the per-detector-element A_j^* in units of μm^2 can be calculated as

$$A_j^* = \frac{n_{e,j}}{t_{\text{int}} \Delta\lambda_j L_{q\lambda,j}} \cdot 10^{12}, \tag{6.2}$$

where t_{int} is the integration time in seconds, $\Delta\lambda_j$ is the detector element width in wavelength units (nm), and $L_{q\lambda,j}$ is the spectral photon radiance, in units of photons per second, m^2, sr, and nm, at the detector element centre wavelength λ_j. The per-nm $A^*(\lambda_j)$ can be found through dividing the per-detector-element A_j^* by the detector element width $\Delta\lambda_j$,

$$A^*(\lambda_j) = \frac{A_j^*}{\Delta\lambda_j} = \frac{n_{e,j}}{t_{\text{int}} \Delta\lambda_j^2 L_{q\lambda,j}} \cdot 10^{12}. \tag{6.3}$$

A^* can thus be found by measuring a broadband light source with known spectral photon radiance $L_{q\lambda,j}$, such as for the integrating sphere setup described in section 6.1. The spectral photon radiance of any setup can be obtained by measurements using a spectrometer with known response, e.g., from blackbody measurements, as outlined in subsection 6.1.1. A^* is found for the total system used for the measurement, including any optical fibres in addition to the spectrometer.

The measured signal can be converted from digital numbers (DN) to photoelectrons by using the gain factor obtained from photon transfer analysis, as described in subsubsection 6.2.2.1, either from previous characterisation of the spectrometer, or by generating a PTC of the measured spectrum.

A python script for finding A^* from a measurement of the setup is given in section B.4.

Measurement example

A^*, both per nm and per detector element, was found for the three different diffraction grating spectrometers, in combination with a fibre of diameter 550 µm and numerical aperture NA = 0.22. The integrating sphere setup, having spectral photon radiance as described in subsection 6.1.1, was measured. The integration times were chosen individually for each measurement, to give a strong signal but avoiding saturation. For each spectrometer, the gain factor, which is required for converting the measured A^* from DN to photoelectrons, was found through photon transfer analysis, as described in subsubsection 6.2.2.1. The resulting estimations of A^* from running the analysis script given in section B.4 are shown in Figure 6.10, with corresponding values for selected wavelengths given in Table 6.3.

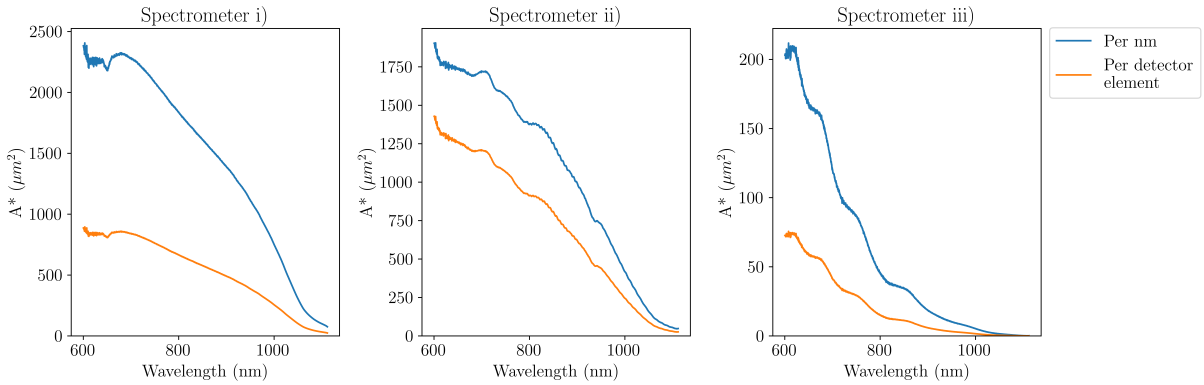

Figure 6.10: Estimated A^* curves of the three diffraction grating spectrometers from measuring the light source setup, and using the script in section B.4. Both the per-nm$A^*(\lambda)$ and per-detector-element A^*_j are given.

Table 6.3: Estimated per-nm $A^*(\lambda)$ at selected wavelengths, given in units of µm^2 for spectrometers i), ii), and iii), corresponding to the curves given in Figure 6.10.

	i)	ii)	iii)
750 nm	2077	1564	87
800 nm	1834	1380	46
850 nm	1612	1255	35
900 nm	1391	993	18
950 nm	1114	726	10
1000 nm	752	417	5.3
1050 nm	305	157	1.5

For a simple validation of the method, and estimation of the losses in the optics, the A^* of spectrometers i) and ii), for which the slit sizes, numerical apertures, and detector quantum efficiencies are known, are roughly estimated.

Spectrometer i) has slit area of approximately $50\,\mu m \times 550\,\mu m$, and numerical aperture NA = 0.25. In combination with the fibre, which covers the whole slit area and has lower NA = 0.22, this gives an acceptance area equal to the slit area, $A = 27\,500\,\mu m$, maximum projected solid angle defined by the fibre, $\Omega = \pi\, NA^2 = \pi\, 0.22^2$, and total étendue $A\Omega = 27\,500\,\mu m^2\, \pi\, 0.22^2 = 4180\,\mu m^2$. At 700 nm, the detector quantum efficiency is 85%. This results in an estimation $A^* \approx 4180\,\mu m^2 \cdot 0.85 \approx 3550\,\mu m^2$ at 700 nm, not taking into account the diffraction grating efficiency and losses in the optics, e.g., due to reflections at lens surfaces. The measured value, given in Figure 6.10, is approximately $2300\,\mu m^2$. Assuming that the diffraction grating efficiency is approximately 75%, the estimated total losses in the optics is approximately 14%, which seems reasonable. The measured A^* is thus considered reasonably accurate, and the method and calculations are assumed correct.

Spectrometer ii) has slit area of approximately $70\,\mu m \times 750\,\mu m$, and numerical aperture NA = 0.2. In combination with the fibre of diameter 550 µm, the whole slit area is not covered, giving an acceptance area $A = 70\,\mu m \times 550\,\mu m$, while the maximum projected solid angle is defined by the spectrometer, $\Omega = \pi\, NA^2 = \pi\, 0.2^2$. The total étendue is then $A\Omega = 38\,500\,\mu m^2\, \pi\, 0.2^2 = 4836\,\mu m^2$. At 700 nm, the detector quantum efficiency is approximately 75%, resulting in an estimation, not taking losses and diffraction grating efficiency into account, of $A^* \approx 4836\,\mu m^2 \cdot 0.75 \approx 3627\,\mu m^2$. The measured value, given in Figure 6.10, is approximately $1750\,\mu m^2$. Assuming a diffraction grating efficiency of 70%, the estimated losses are as large as 30% in the optics. This is much larger than for spectrometer i). The estimation is very rough, and is considerably affected by small deviations in e.g. the spectrometer slit size or numerical aperture. As the estimation is in the same order of magnitude as the measured value of A^*, the measurement is also in this case considered reasonably accurate, and based on correct methods and calculations.

6.2.3 Other

Information about the readout time of a spectrometer can be obtained from the software for acquiring measurements. The time used for making a single measurement represents the readout time for the applied software. However, this may be longer than the actual detector readout time, which sets an lower limit on the readout time for an application. This readout time can be found from the detector data sheet.

Information about cost, size, weight, and power requirement must be acquired from the manufacturer or data sheet. These characteristics may be critical when choosing a spectrometer for a given application, but they are out of scope for the spectrometer comparison in this thesis.

6.2.4 Derived performance characteristics

The remaining performance characteristics that are not included in the non-redundant specification, are derived from the specified parameters, as given in Table 5.3. They can be calculated using the measured values, as specified in subsection 5.1.3 and subsection 5.2.4.

6.3 Example: Comparison of three spectrometers

As discussed in section 5.5, there is no standardised method for spectrometer comparison. It is highly application dependent, and requires a subjective assessment, and trade off between the performance characteristics. This is illustrated here, as the overall performance of spectrometers i), ii), and iii) are compared, without relating it to a specific application.

The results from measurements of the performance characteristics of spectrometers i), ii), and iii) were presented in section 6.2, and are summarised in Table 6.4. The corresponding derived performance characteristics, calculated using the measured values, are given in Table 6.5. Note that the combined effect of the spectrometer and the applied fibre, with diameter 550 µm and numerical aperture NA = 0.22, is characterised. Spectrometer i) has higher numerical aperture than the fibre, and spectrometer ii) has larger area than what is covered by the fibre. The following comparison thus concerns a performance that is limited by the fibre, and other results would have been obtained when using a different fibre.

The integration times in the photon transfer analysis used for measuring the noise floor was different. This was required for the measurements to span the whole dynamic range. The specified noise floor and dynamic range thus correspond to different contributions from dark current noise. However, the dark current noise is assumed much smaller than the readout noise at the given integration times. The given noise floors are thus considered approximately comparable, which is sufficient for an overall spectrometer comparison.

The applied methods did not succeed in quantifying the dark noise, and separating the dark current noise from the readout noise. More measurements and an improved method is expected to succeed at such a characterisation, which is important for a full characterisation of the spectrometer. The parameters relating to dark current, such as the effective saturation level, are thus not considered in the comparison.

Properties such as readout time and measurement speed, operating temperature range, power consumption, price, size and weight, and ease of use are not discussed here. They may be highly relevant for spectrometer comparison in relation to an application, and when selecting what spectrometer to purchase, but this is out of scope of this discussion.

The spectrometers have similar spectral ranges and similar A^*-shapes, and are thus suited for the same applications in terms of spectral range requirements.

All spectrometers have negligible linearity errors. Spectrometer i) and ii) have better wavelength accuracy, indicating that spectrometer iii) needs a wavelength recalibration.

Using the specified $\mathrm{SSRD_{ph,j}}$, a suitable integration time for a given light level can be estimated. Spectrometer i) has $SSRD_{ph,j} = 4.4 \cdot 10^{14}$ photons/(m^2 sr) in the detector element at 800 nm, detector element width approximately equal to the average spectral sampling interval 0.36 nm, and reaches thus saturation at a photon radiance dose of $1.22 \cdot 10^{15}$ photons/(m^2 sr nm). When measuring the integrating sphere setup, which has spectral photon radiance spectrum given in Figure 6.3, equal to 10^{16} photons/(s m^2 sr nm) at 800 nm, the detector element is thus saturated when using an integration time of 122 ms. Similar calculations reveal that spectrometer ii) reach saturation at 39 ms and spectrometer iii) at 910 ms. Spectrometer ii) will thus obtain a strong signal faster, and is thus suited for higher speed, while spectrometer iii) is much slower. In addition, within a set measurement time, spectrometer ii) can then acquire more than 3.13 times

Table 6.4: The measured performance characteristics for the three different spectrometers i), ii), and iii).

Spectrometer	i)	ii)	iii)
Spectral range	536 nm – 1112 nm	532 nm – 1154 nm	536 nm – 1021 nm
Wavelength accuracy	0.3 nm	0.4 nm	1.5 nm
Spectral sampling interval	0.36 nm (0.43 nm–0.37 nm)	0.64 nm (0.54 nm–0.79 nm)	0.33 nm (0.30 nm–0.37 nm)
Resolution	2.5 nm	4.5 nm	4.0 nm
Per-detector-element A_j^* at 800 nm	665 µm^2	914 µm^2	15 µm^2
Per-nm $A^*(\lambda)$ at 800 nm	1835 µm^2	1380 µm^2	46 µm^2
Noise floor	50.56 e^- (at t_{int} = 150 ms)	38.03 e^- (at t_{int} = 25 ms)	29.66 e^- (at t_{int} = 1000 ms)
Saturation level	290 278 e^-	229 225 e^-	44 443 e^-
Linearity errors	0	0	0
Dimensions	Largest	Medium	Smallest

more high-signal measurements, which increases the SNR with a factor $\sqrt{3.1} = 1.8$ when used for averaging.

Spectrometer i) performs best in terms of resolution, with 2.5 nm, while spectrometer ii) and iii) have nearly half as good resolution, 4.5 nm and 4.0 nm, respectively. Hence, spectrometer i) is suited for applications requiring higher resolution. When lower resolution is sufficient, spectrometer i) can then obtain higher SNR through resampling than spectrometers ii) and iii). The exact increase is, as discussed in subsection 3.3.6, yet to be determined. When assuming that the SRF is approximately Gaussian, the increase from 2.5 nm to 4.5 nm can be obtained through convolution with a Gaussian function with $FWHM = 3.7$ nm, which yield an increase in the SNR of $\sqrt{FWHM/0.664} = 2.4$.

Spectrometer i) and ii) are comparable in terms of light collection, sensitivity, and noise, while spectrometer iii) overall has much lower performance. Its A^* is approximately 2% of that of spectrometer ii) and iii), and it has approximately 25 and 50 times higher noise. However, it

Table 6.5: Derived performance characteristics from the measured characterisation of spectrometer i), ii), and iii), using the values from Table 6.4.

Spectrometer	i)	ii)	iii)
$A^*(\lambda)$ at 800 nm, per nm resolution	734 μm^2	307 μm^2	12 μm^2
$NERD_{ph,j}$ at 800 nm	$7.6 \cdot 10^{10}$ photons per m^2 and sr (at $t_{\text{int}} = 150$ ms)	$4.2 \cdot 10^{10}$ photons per m^2 and sr (at $t_{\text{int}} = 25$ ms)	$2.0 \cdot 10^{12}$ photons per m^2 and sr (at $t_{\text{int}} = 1000$ ms)
$SSRD_{ph,j}$ at 800 nm	$4.4 \cdot 10^{14}$ photons per m^2 and sr	$2.5 \cdot 10^{14}$ photons per m^2 and sr	$3.0 \cdot 10^{15}$ photons per m^2 and sr
Dynamic range	5742	6027	1499
SNR_{max}	536	447	289

can measure approximately 10 times more light without reaching saturation, and its dynamic range is thus approximately 4 times lower. It can reach SNR of approximately 54% and 64% of the spectrometer i) and ii) SNRs. Overall, spectrometer iii) is considered less performing in all ways. It is however smaller and cheaper than the other spectrometers, and may be sufficient for some applications where price and size are important requirements, and the signal is sufficiently high to give adequate data quality even with the low spectrometer performance.

While spectrometer ii) has higher response per detector element A_j^* than spectrometer i), it also has approximately twice as big spectral sampling interval. The per-nm $A^*(\lambda)$ is largest for spectrometer i), approximately 33% larger than for spectrometer ii), and thus, spectrometer i) is considered performing better in terms of net light collection and sensitivity. As spectrometer i) additionally has better resolution, its theoretical performance, described by the $A^*(\lambda)$ normalised for resolution, is more than twice as big as for spectrometer ii). Note that in this last case, when normalised for resolution, the relative SNR improvement for smoothing is not relevant.

The noise floors and saturation levels are comparable for spectrometer i) and ii). Spectrometer ii) has higher response per detector element A_j^*, and performs approximately twice as well as spectrometer i) in terms of $NERD_{ph,j}$ and noise. However, spectrometer i) has approximately double $SSRD_{ph,j}$, and can thus measure more light without reaching saturation, which makes the dynamic ranges similar. Spectrometer i) can reach approximately 20% higher SNR than spectrometer ii).

Taking all the discussed properties into account, what spectrometer is considered best performing is dependent on the application. Considering the direct performance, spectrometer i) is considered better than spectrometer ii). It has higher light collection and sensitivity, and while spectrometer ii) has lower noise, spectrometer i) can still reach higher SNR. Its dimensions are larger than spectrometer ii), this is as expected, and illustrates the problem of spectrometer miniaturisation. Spectrometer i) also has better resolution, and the SNR can be scaled with

approximately 2.4 when resampling to obtain the same resolution as spectrometer ii). However, when given a set measurement time, spectrometer ii) can increase the SNR with a factor 1.8 through measurement averaging compared to spectrometer i). Thus, when time is a limiting factor, spectrometer ii) is considered better than spectrometer i).

Also other performance characteristics that are out of scope of this thesis, discussed in subsection 5.3.1, would be useful for the comparison. For example, significant differences in the amount of stray light could also be important when comparing the overall performances.

6.4 Discussion

The given methods for determining the performance characteristics were applied and demonstrated on diffraction grating spectrometers. Their performances were measured and evaluated experimentally, without use of information from the data sheets besides verification of the measurements. This illustrates the ability of the methods to generate information of spectrometers with unknown properties.

The presented integrating sphere measurement setup, and methods for data acquisition and analysis, are intended for a user friendly, and relatively simple and fast characterisation of spectrometers. The primary intent is to give a rough estimation of the characteristics, indicating their magnitude. This is considered useful for understanding the data quality, and evaluating whether the spectrometer is suited for a given application or not. The characterisation is not useful for applications requiring high accuracy, such as for performing data corrections, and thus the uncertainties of the measurements have not been treated. However, the measured characteristics were compared with data sheet values, which verified that the estimations were in the same order of magnitude, and thus seemed to give sufficient accuracy. This is considered sufficient also for an overall comparison of different spectrometers, as this involves evaluating many parameters whose detailed accuracy is not of importance in the big picture. For example, if A^* differs by 50%, neither a small error in the measured A^* nor in the resolution has any effect on the total comparison.

Due to the limited scope of this thesis, not all characteristics that may influence the performance are described and included in the performance specification, and correspondingly not measured. Examples of other characteristics that are required for a complete characterisation is given in subsection 5.3.1. The characterisation is thus not considered complete, and characteristics that are left out may have influenced the given results. For example, stray light is not concerned, and may be present, distorting the measurements, and causing errors in the specified values. The stability is not investigated, and large instabilities may also give instabilities in the specified results, which reduces their accuracy. These errors are however not expected to be of such extent to cause significant distortions of the rough estimation of the characteristics.

During the experimental work, some odd characteristics and features of the spectrometers under test were discovered. For example, one spectrometer had an offset that increased both with integration time and signal level. This is expected to be smear due to continued exposure of the detector array during readout, as described in [19]. While its effect was attempted corrected for in the measurements through a simple offset subtraction, it may have had some influence on the measurements, and caused some errors in the estimations. This influence is assumed negligible,

but the offset should be further studied for investigating its cause and effect on the data, and properly correcting for its influence.

The experimental characterisation did not succeed at quantifying the dark current, as three different methods gave large variations in the estimation. This is assumed being caused by insufficient number of measurements, and thus scarce statistical foundation for the estimations. While increasing the number of measurements may improve the suggested method, this is not compatible with the intent of the method being quick and easy. In addition, the method is highly temperature dependent, and only applicable for spectrometer with temperature control. Thus, work remains to obtain a proper method of dark current estimation.

The chosen method for defining resolution holds only for spectrometers with even, symmetric, and well behaved SRF. This holds for diffraction grating spectrometers, which is the focus of this thesis, and caution should be made when extending the method to other spectrometer types.

When considering the performance of a spectrometer, it is important that all characteristics are presented and taken into account, as only their combination give a proper specification of the overall performance. By selecting certain parts of the specifications, any spectrometer can be considered performing better than others, while the overall picture may be different. For example, spectrometer iii) was overall considered performing much below spectrometer i) and ii), but considering only the noise floor, or the saturation spectral radiance dose *SSRD*, it appears to be better. When not taking into account the spectral sampling interval differences between spectrometer i) and ii), spectrometer ii) appears to have larger sensitivity A^* (as given by A^*_j), while in reality, spectrometer i) is better (as given by $A^*(\lambda)$). As spectrometer data sheets may have insufficient description of the stated performance characteristics, and may be constructed in favour of the spectrometer, selecting specifications that paint the best picture of the spectrometer performance, caution should be made to make sure the proper and comparable performance is obtained.

The characterisation methods investigate the direct performance and data quality of the spectrometers. Their results are not connected to the application performance, such as the quality of multivariate models, which may be of higher value for the spectrometer users. While this is out of scope of this thesis, the translation of the work in the instrument domain to the application domain would be highly advantageous, and possibly increase the usefulness of the work. This would allow for better understanding of the multivariate model results, investigations of how different measurement parameters affect the results, and direct comparison of spectrometers based on the application requirements. This should be highly prioritised in future work within the project.

Part III

Final remarks

Chapter 7

Current status of the project

The thesis work revealed a field of spectrometer standardisation in relation to absorbance spectroscopy with significant lacks and shortcomings. The only full spectrometer standard that was found, the CIE 233:2019-standard [19], is mostly concerned about spectrometers for absolute radiometric measurements, and thus has a different scope. The upcoming P4001 standard is more relevant, but is not yet finished and available. It concerns hyperspectral cameras, and while many of the properties are directly applicable for spectrometers, the full standard may be overwhelming, and impose a challenge in selecting what relates to spectrometers, and what concerns the spatial imaging properties. Additionally, inconsistent use of various terms and definitions was discovered throughout the various literature, which may impose additional confusion for inexperienced users. This caused an unexpectedly large part of the thesis work to involve literature search for relevant standards, investigating the meaning of different terminology, adapting the descriptions for hyperspectral cameras to spectrometers, and developing own definitions of the performance characteristics.

As there is generally no full and complete text book giving a sufficient introduction to the working principles of spectrometers, a lot of work was spent reading various literature, collecting and combining various theory describing the operation of a diffraction grating spectrometer, and learning what was required to understand the full spectrometer and importance of various performance characteristics. The aim was to give an introduction to the working principles required for understanding the definitions and standardisation. As such a publication giving an overview of the relevant theory of spectrometers has not yet been found, this thesis will hopefully act as such a reference work. It may be the basis of a white paper intended for the spectrometer users, to aid the understanding of the meaning of the performance characteristics.

The work has resulted in the development of a rough standardisation of spectrometer performance, based on first principles and physics, with focus on absorbance spectroscopy and diffraction grating spectrometers. Much has been an adaptation of the work related to standardisation of hyperspectral imagers for the upcoming P4001 standard [31], particularly in relation to the definition of A^* as a performance characteristics for sensitivity [14, 32, 26]. Some modifications and adjustments are made, such as a slightly different definition of resolution.

The set of performance characteristics is not yet complete, as it does not treat all properties that may influence the performance of a spectrometer. Examples of properties that are yet to be included, and required for a complete specification, are stray light, point spread, and spatial

coregistration, which may cause errors when measuring heterogeneous samples, instabilities, robustness, and sensitivity to external influences such as temperature, humidity, and movement. However, the included characteristics are considered covering the most important properties, and giving a sufficient performance characterisation, and indication of what spectrometer is the best performing, despite being incomplete.

The performance characteristics may be used to modify what is currently given in data sheets, but this requires careful evaluation and thorough specifications to make sure the full performance is displayed in a fair way. Some characteristics are better suited for comparison than others, and when misused, the characterisation of different properties can be constructed to give the impression of too high performance. For example, when not properly specified, the per-detector-element A_j^*, which is not suited for comparison, can be used to falsely indicate higher relative sensitivity of a spectrometer with larger detector elements. The proper comparison is performed using the per-nm $A^*(\lambda)$, and it is important that the different scopes of these parameters are properly specified.

A standardisation is not useful if it cannot be related to real spectrometers and applied for generating useful information about the spectrometer. A set of methods for measuring the full set of suggested performance characteristics is suggested. The measurement routines are simple and fast, based on a simple measurement setup designed to be reproducible, user-friendly, and reasonably priced, and corresponding simple analysis code and calculations. Obtaining the simplicity of the method was of high priority, to make it attractive and useful as a simple and quick way of characterising a spectrometer. While measurement of dark current is not yet successful, due to large variations of the current estimations and requirements of temperature control, all other performance characteristics are determined with what is considered sufficient accuracy for a rough estimation of their magnitudes, suitable for understanding the data quality, evaluating what spectrometers are suited for a given application, and aid comparison.

The measurement of the performance characteristics was successfully demonstrated for three different diffraction grating spectrometers. The results were used for performance evaluation and comparison, which proved the usefulness and suitability of the defined characteristics for a proper overall performance assessment that is directly comparable for spectrometers with different internals.

The suggested performance characteristics, and corresponding measurement methods, will hopefully be useful and applied when in need of a quick and simple characterisation of a spectrometer.

Currently, the standardisation relates only to the spectrometer properties and their effect on the raw signals. It is not connected to application domain, and the importance of individual performance characteristics, such as SNR, on the overall result for a given application is not yet investigated. It does not say anything about the performance in applications, such as the quality of multivariate models based on the spectrometer data. While the described spectrometer performance can be useful for physicists and others with good instrumentation knowledge, it is the performance in application domain that is of relevance to the spectrometer users. Evaluating the performance of a spectrometer through its effect on the results in application domain gives the true spectrometer performance, and comparison allows for directly obtaining what spectrometer is the most suited for a given application.

The current work in instrument domain is a basic and required step along the way to this ul-

timate goal of application domain standardisation. Hopefully this will facilitate and improve multidisciplinary collaboration within spectroscopy, making us better equipped for successfully pushing the size limit and realising miniaturised interactance spectroscopy, which will be an important contribution to the modernised food industry.

7.1 Future work

The current project will be continued in an upcoming PhD, and based on the work with this thesis, multiple suggestions for continuation of the project are presented.

A first step towards the ultimate goal of an application domain standardisation is investigating the effect from the various performance characteristics on multivariate models. This can e.g. be performed by building multivariate models, such as partial least squares regression (PLS) and principal component analysis (PCA), on certain reference samples, and studying the effect of different properties such as resolution, through signal resampling, and SNR, through increasing the light sensitivity or signal averaging. This can also be useful for studying the robustness to external influences such as temperature, humidity, background light, and movement, and thus the suitability of the spectrometer to real conditions, such as in inline applications. The reference samples should have distinct spectral features that induce different spectral behaviour and are suited for building multivariate models, and plastic transmission reference samples of different colours are suggested.

The importance of SNR on the signal quality should be prioritised when translating to application domain. This is important for the spectrometer performance assessment, but not least for highlighting the importance of optimising the measurement methods for increasing the SNR. The effect of the SNR on a multivariate model should be thoroughly investigated and described. This could also result in a useful tool for simulating the SNR and multivariate model quality for different light levels and integration times for a given spectrometer. The SNR estimation requires only measurements of the noise levels of the spectrometer, which is readily obtained through the presented methods, and an "SNR calculator" can easily be made. Extending this to include the effect on multivariate models would simplify the planning of measurements, and has the potential of becoming a useful tool for the spectrometer users.

The translation to application domain also is useful for demonstrating the importance of obtaining good measurements, e.g., by indicating the effect by spectrometer movement on the estimations.

The continuation of the project should also focus on describing and standardising more performance characteristics, aiming at a complete description. Corresponding simple and quick measurement methods should be developed. This includes successfully measuring the dark current.

The measurement setup is designed with the feature of simple insertion of optical components such as filters, apertures, and reference samples into the light beam. It thus has the potential for being used for a variety of measurements, and for simplicity, the new measurement methods should be based on this setup, e.g., by measuring the effect of such components on the applied broadband light source. For example, the presence of internal stray light, and light in other diffraction orders, is easily revealed and quantified using various long pass or band pass filters.

It is also suited for the outlined measurements of reference samples for investigation of the effects on multivariate models.

The characterisation methods were designed for a rough estimation of the performance characteristics, indicating their magnitude. Simple verifications indicated sufficient accuracy of the estimations, but no comprehensive uncertainty analysis is performed. The results are thus currently not sufficient for applications requiring high accuracy of the estimations. Further development of the methods should thus include uncertainty assessment, for understanding the measurement accuracy and revealing error sources that can be removed or corrected for.

When characterisation methods for a full set of performance characteristics hopefully are completed, the setup, and corresponding measurement methods and analysis software, may have the potential of being distributed to the spectrometer users. The setup consists of off-the-shelf products, and is thus easily reproduced. Optimisation of the full product package of both hardware and software for this purpose can thus be looked into.

While diffraction grating spectrometers were the focus in this thesis, it would be interesting to study also other spectrometer designs with other principles of operation, such as scanning grating spectrometers, FT-IR spectrometers, or spectrometers with different detectors, such as amplifying and reading the photodetector current directly rather than using CCDs. This would possibly require adaptations and extending of the measurement methods. Additionally, as the resolution definition is based on symmetric and even SRFs, it may be required to extend the definition to be more general, or definition of more specific resolution definitions for designs with different SRFs. The performance characteristics and measurement methods were defined based on the "black box"-approach, ideally independent of spectrometer design and internals, so it would be interesting to study how well this is fulfilled, and the quality of the estimations.

Only errors related to the spectrometer itself are concerned, while also other factors in the measurement process, such as sample presentation, may cause errors and inaccuracies in the final measurement. It would be interesting to investigate such errors.

During the experimental work of this thesis, some odd characteristics and spectrometer artefacts were discovered, such as the signal-dependent offset discussed in section 6.4. This should be further investigated, both for better spectrometer understanding, and for optimising the correction methods, and thus improving the measurement accuracy.

Optical fibres are commonly applied for light collection and transportation to the spectrometers, and different diameters and numerical apertures may affect the performance of the measurement system. Particularly, the light collection properties are affected, but it was also discovered that some fibres were more leaky than others, which additionally caused background light to penetrate into the fibre, and contributing to the signal. Such effects would be interesting to study.

As was discussed in subsubsection 3.3.5.3, it would be interesting to investigate the relation between resolution decrease and SNR increase for different smoothing functions. Also investigating the effect of SRF shape for different applications would be useful for better understanding and optimisation of signal smoothing for different applications.

As was briefly mentioned in subsection 5.1.4, the information content in a spectrum depends on the resolution. However, this does not correspond to the number of samples that are required to conserve all information in the spectrum, which requires also sampling of the dip between the

two resolved peaks, in analogy with the Nyquist sampling theorem. Further investigation of the relation of resolution and information content in the spectrum would be interesting, and could be useful for optimising the SNR based on any resolution requirement.

More properties to study will surely be uncovered along the way, and it will be very interesting to see the future development of the project through the PhD work.

Chapter 8

Conclusion

The field of spectrometer standardisation in relation to absorbance spectroscopy has significant lacks and shortcomings. The various literature use different terminology, the data sheet specifications are insufficient for a proper assessment of the spectrometer performance, and there is no clear and easily applicable method for comparing spectrometers. These deficiencies are approached by this thesis, in which a rough standardisation of spectrometer performance is developed, intended both for direct characterisation, and for comparison of spectrometers. The treatment is rooted in first principles and physics, and focused on diffraction grating spectrometers, which are commonly applied for NIR absorbance and Raman spectroscopy. It is inspired by the upcoming IEEE P4001 standard for specification of hyperspectral cameras, and applies its "black box"-approach, concerning only externally observable properties.

For describing the spectral and radiometric spectrometer performance, with focus on resolution, sensitivity, and SNR, a set of performance characteristics is developed. It consists of a minimal set of parameters that can be measured from relatively simple measurement routines, and are suited for describing the current operation. A corresponding set of derived properties are easily calculated from the measured parameters, and suited for spectrometer comparison. While the performance characteristics set is not yet complete, and lacks properties such as stray light and sensitivity to external influences, the main characteristics are included, and considered useful for a rough initial standardisation revealing the most important properties.

Routines for simple and fast measurements of the performance characteristics are developed for a relatively simple, user-friendly, reproducible, and reasonably priced setup. The primary intent is to give an indication of the magnitude, sufficient to understand the data quality, to indicate whether a spectrometer is suited for a given application, and to aid the comparison of different spectrometers. Applied on three different diffraction grating spectrometers, the methods are successfully shown to determine all performance characteristics with sufficient accuracy, except for dark current, for which a method evading temperature drift remains to be developed.

The standardisation relates only to the spectrometer properties, and their effect on the raw signals. If translated to the application domain, through investigating the effect of the performance characteristics on multivariate models, the performance for a given application can be evaluated. This is an ultimate goal for further development of the project, as it simplifies the understanding of multivariate model quality, and comparison of spectrometers. It is useful for transferring knowledge to those concerning data analysis, such as chemometricians, and may be a crucial

step towards a common understanding of the physical limitations of spectrometers, allowing for multidisciplinary collaboration.

The thesis work is a first step towards a proper and fundamental method for performance characterisation, allowing for full understanding of the spectrometer properties and performance, and the physical limitations that govern the spectrometer operation. Such an understanding is required for investigating the relation between spectrometer size and performance. This is central in the successful implementation of miniaturised spectrometers in applications requiring particularly high performance, such as interactance spectroscopy, for which high SNR is crucial. Such realisation and use of miniaturised spectrometers is expected to lead to significant advancements, e.g., in the digitisation and modernisation of the food industry.

References

[1] Krzysztof B Beć et al. “Handheld near-infrared spectrometers: Where are we heading?” en. In: *NIR news* 31.3-4 (June 2020), pp. 28–35. DOI: 10.1177/0960336020916815. URL: http://journals.sagepub.com/doi/10.1177/0960336020916815 (visited on 01/29/2023).

[2] Regjeringen. *Hovedrapport 2020 - Bransjeavtalen om reduksjon av matsvinn*. Tech. rep. 2020. URL: https://www.regjeringen.no/no/tema/klima-og-miljo/forurensning/matsvinn/bransjeavtale-om-matsvinn-reduksjon/id2891198/ (visited on 05/30/2023).

[3] Centre for Research-Based Innovation in Digital Food Quality. *DigiFoods*. URL: https://digifoods.no/.

[4] Jens Petter Wold et al. “Optimization of Instrument Design for In-Line Monitoring of Dry Matter Content in Single Potatoes by NIR Interaction Spectroscopy”. en. In: *Foods* 10.828 (Apr. 2021). DOI: 10.3390/foods10040828. URL: https://www.mdpi.com/2304-8158/10/4/828 (visited on 05/30/2023).

[5] Tiril Aurora Lintvedt et al. “Raman spectroscopy and NIR hyperspectral imaging for in-line estimation of fatty acid features in salmon fillets”. en. In: *Talanta* 254.124113 (Mar. 2023). DOI: 10.1016/j.talanta.2022.124113. URL: https://linkinghub.elsevier.com/retrieve/pii/S0039914022009092 (visited on 05/12/2023).

[6] Marion O’Farrell and Jon Tschudi. *The juggling act of making compact and mobile sensors*. DigiFoods. Apr. 2023. URL: https://digifoods.no/2023/05/the-juggling-act-of-making-compact-and-mobile-sensors/ (visited on 05/30/2023).

[7] Nageshvar Patel, Hugo Toledo-Alvarado, and Giovanni Bittante. “Performance of different portable and hand-held near-infrared spectrometers for predicting beef composition and quality characteristics in the abattoir without meat sampling”. en. In: *Meat Science* 178.108518 (Aug. 2021). DOI: 10.1016/j.meatsci.2021.108518. URL: https://linkinghub.elsevier.com/retrieve/pii/S0309174021000942 (visited on 01/29/2023).

[8] Krzysztof B. Beć, Justyna Grabska, and Christian W. Huck. “Principles and Applications of Miniaturized Near-Infrared (NIR) Spectrometers”. en. In: *Chemistry – A European Journal* 27.5 (Jan. 2021), pp. 1514–1532. DOI: 10.1002/chem.202002838. URL: https://onlinelibrary.wiley.com/doi/10.1002/chem.202002838 (visited on 01/29/2023).

[9] Verena Wiedemair et al. “Investigations into the use of handheld near-infrared spectrometer and novel semi-automated data analysis for the determination of protein content in different cultivars of Panicum miliaceum L.” en. In: *Talanta* 205.120115 (Dec. 2019). DOI: 10.1016/j.talanta.2019.120115. URL: https://linkinghub.elsevier.com/retrieve/pii/S0039914019307416 (visited on 01/29/2023).

[10] Jon Tschudi, Marion O’Farrell, and Kari Anne Hestnes Bakke. “Inline Spectroscopy: From Concept to Function”. en. In: *Applied Spectroscopy* 72.9 (Sept. 2018), pp. 1298–1309. DOI: 10.1177/0003702818788374. URL: http://journals.sagepub.com/doi/10.1177/0003702818788374 (visited on 01/29/2023).

[11] Celio Pasquini. “Near infrared spectroscopy: A mature analytical technique with new perspectives – A review”. en. In: *Analytica Chimica Acta* 1026 (Oct. 2018), pp. 8–36. DOI: 10.1016/j.aca.2018.04.004. URL: https://linkinghub.elsevier.com/retrieve/pii/S0003267018304793 (visited on 02/20/2023).

[12] Bernard G. Barthès et al. “Performance comparison between a miniaturized and a conventional near infrared reflectance (NIR) spectrometer for characterizing soil carbon and nitrogen”. en. In: *Geoderma* 338 (Mar. 2019), pp. 422–429. DOI: 10.1016/j.geoderma.2018.12.031. URL: https://linkinghub.elsevier.com/retrieve/pii/S0016706118303719 (visited on 01/29/2023).

[13] Krzysztof B. Beć, Justyna Grabska, and Christian W. Huck. “Miniaturized NIR Spectroscopy in Food Analysis and Quality Control: Promises, Challenges, and Perspectives”. en. In: *Foods* 11.1465 (May 2022). DOI: 10.3390/foods11101465. URL: https://www.mdpi.com/2304-8158/11/10/1465 (visited on 01/29/2023).

[14] Torbjørn Skauli. “Feasibility of a standard for full specification of spectral imager performance”. en. In: ed. by David P. Bannon. Anaheim, California, United States, Apr. 2017, 102130H. DOI: 10.1117/12.2262785. URL: http://proceedings.spiedigitallibrary.org/proceeding.aspx?doi=10.1117/12.2262785 (visited on 01/29/2023).

[15] John R. Gilchrist, Torbjorn Skauli, and Christopher Durell. “Developing the IEEE P4001 standard for characterisation and calibration of hyperspectral imaging devices”. en. In: *Algorithms, Technologies, and Applications for Multispectral and Hyperspectral Imaging XXVIII*. Ed. by David W. Messinger and Miguel Velez-Reyes. 1209402. Orlando, United States: SPIE, May 2022. DOI: 10.1117/12.2623487. URL: https://www.spiedigitallibrary.org/conference-proceedings-of-spie/12094/2623487/Developing-the-IEEE-P4001-standard-for-characterisation-and-calibration-of/10.1117/12.2623487.full (visited on 03/22/2023).

[16] Vilde Vraalstad. “Analysis and further development of a multi-modal spectroscopic microscope for complete polarimetric imaging”. Project thesis. Trondheim: Norwegian University of Science and Technology, Dec. 2022.

[17] Frank L. Pedrotti, Leno Matthew Pedrotti, and Leno S. Pedrotti. *Introduction to optics*. eng. 3rd ed. Cambridge: Cambridge university press, 2018.

[18] Hamamatsu. *CCD linear image sensor S11156-2048-02*. URL: https://www.hamamatsu.com/eu/en/product/optical-sensors/image-sensor/ccd-cmos-nmos-image-sensor/line-sensor/for-spectrophotometry/S11156-2048-02.html (visited on 05/18/2023).

[19] Cie. *CIE 233:2019 Calibration, Characterization and Use of Array Spectroradiometers*. en. Tech. rep. International Commission on Illumination (CIE), June 2019. DOI: 10.25039/TR.233.2019. URL: https://cie.co.at/publications/calibration-characterization-and-use-array-spectroradiometers (visited on 03/31/2023).

[20] A.R. Robertson. "Standardization in transmission spectrophotometry in the visible and ultraviolet spectral regions". en. In: *Journal of Research of the National Bureau of Standards Section A: Physics and Chemistry* 80A.4 (July 1976), pp. 625–630. DOI: 10.6028/jres.080A.061. URL: https://nvlpubs.nist.gov/nistpubs/jres/80A/jresv80An4p625_A1b.pdf (visited on 01/29/2023).

[21] Wenjie Shi et al. "The Evaluation of Spectral Resolution in the Optical Design of a Czerny-Turner Spectrometer". en. In: *Photonics* 9.678 (Sept. 2022). DOI: 10.3390/photonics9100678. URL: https://www.mdpi.com/2304-6732/9/10/678 (visited on 03/28/2023).

[22] John F. Silny. "Resolution modeling of dispersive imaging spectrometers". en. In: *Optical Engineering* 56.08 (Aug. 2017), p. 081813. DOI: 10.1117/1.OE.56.8.081813. URL: https://spiedigitallibrary.org/journals/optical-engineering/volume-56/issue-08/081813/Resolution-modeling-of-dispersive-imaging-spectrometers/10.1117/1.OE.56.8.081813.full (visited on 05/01/2023).

[23] Kye-Sung Lee, Kevin P. Thompson, and Jannick P. Rolland. "Broadband astigmatism-corrected Czerny–Turner spectrometer". en. In: *Optics Express* 18.22 (Oct. 2010), pp. 23378–23383. DOI: 10.1364/OE.18.023378. URL: https://opg.optica.org/oe/abstract.cfm?uri=oe-18-22-23378 (visited on 05/01/2023).

[24] Karim Lenhard, Andreas Baumgartner, and Thomas Schwarzmaier. "Independent Laboratory Characterization of NEO HySpex Imaging Spectrometers VNIR-1600 and SWIR-320m-e". In: *IEEE Transactions on Geoscience and Remote Sensing* 53.4 (Apr. 2015). Conference Name: IEEE Transactions on Geoscience and Remote Sensing, pp. 1828–1841. DOI: 10.1109/TGRS.2014.2349737.

[25] Edward J. Milton and Kyu Young Choi. "Estimating the spectral response function of the CASI-2". In: Annual Conference of the Remote Sensing and Photogrammetry Society, 2004. URL: https://eprints.soton.ac.uk/9188/1/RSPS2004b.pdf (visited on 03/30/2023).

[26] Torbjørn Skauli. "A Performance Characteristic for Net Light Collection in Hyperspectral and Conventional Cameras: A*". In: *IEEE Transactions on Geoscience and Remote Sensing* 60.5635415 (2022). DOI: 10.1109/TGRS.2022.3228071. (Visited on 03/01/3023).

[27] Bernd Girod, Rudolf Rabenstein, and Alexander Stenger. "Describing Random Signals". eng. In: *Signals and systems*. 1st ed. Chichester ; New York: Wiley, 2001, pp. 403–435.

[28] Neil Storey. *Electronics: A Systems Approach*. 5th ed. Pearson, 2013.

[29] James R. Janesick. *Photon transfer*. en. Bellingham, Wash: SPIE, 2007.

[30] E13 Committee. *Guide for Establishing Spectrophotometer Performance Tests*. en. Tech. rep. ASTM International. DOI: 10.1520/E1866-97R21. URL: http://www.astm.org/cgi-bin/resolver.cgi?E1866-97R21 (visited on 02/20/2023).

[31] IEEE. *P4001 Standard for Characterization and Calibration of Ultraviolet through Shortwave Infrared (250 nm to 2500 nm) Hyperspectral Imaging Devices*. May 2023. URL: https://standards.ieee.org/ieee/4001/7314/.

[32] Torbjørn Skauli. “Specifying radiometric performance of hyperspectral and conventional cameras: a minimal set of independent characteristics”. en. In: *Algorithms, Technologies, and Applications for Multispectral and Hyperspectral Imagery XXVI*. Ed. by David W. Messinger and Miguel Velez-Reyes. Vol. 11392. 113920B-1. Online Only, United States: SPIE, Apr. 2020. DOI: 10.1117/12.2559670. URL: https://www.spiedigitallibrary.org/conference-proceedings-of-spie/11392/2559670/Specifying-radiometric-performance-of-hyperspectral-and-conventional-cameras--a/10.1117/12.2559670.full (visited on 01/29/2023).

[33] TaorLab. *HG-1 Mercury Argon Lamp Wavelength Calibration Fiber Light Source Spectrometer Calibration*. URL: https://www.taorlab.com/product/hg-1-mercury-argon-light.

[34] Torbjørn Skauli. “An upper-bound metric for characterizing spectral and spatial coregistration errors in spectral imaging”. en. In: *Optics Express* 20.2 (Jan. 2012), pp. 918–933. DOI: 10.1364/OE.20.000918. URL: https://opg.optica.org/oe/abstract.cfm?uri=oe-20-2-918 (visited on 04/17/2023).

Appendix A

Instructions manual

Here, a summary of the methods for generating information about a spectrometer is presented. The performance characteristics, presented in chapter 5 and summarised in Table 5.2 and Table 5.3, are measured using the methods presented in chapter 6. The reader is referred to these chapters for more detailed explanations.

The HG-1 Mercury Argon calibration source from Ocean Optics [33] is used for measuring the *resolution* and *wavelength accuracy*. For reducing the intensity, the light is coupled into an integrating sphere using a fibre, and the spectrometer is coupled to the integrating sphere using another fibre. For reducing the noise, 400 spectra are acquired and averaged. The resulting spectrum, with corresponding wavelength vector, is analysed using the script in section B.2 to obtain the resolution and wavelength accuracy of the spectrum.

The following measurements are made on the measurement set up presented in section 6.1, consisting of a halogen light bulb that provides broadband illumination that approximates a blackbody spectrum of approximately 2500 K, a set of lenses, apertures and diffusers, and an integrating sphere. This provides a spatially uniform field, which is useful for spectrometer characterisation. It spectrum, given in subsection 6.1.1, was obtained from measurements of a blackbody and the analysis script in section B.1. It is connected to the spectrometers using an optical fibre with diameter 550 µm and numerical aperture $NA = 0.22$. The setup also has a shutter for frequent dark measurements. For minimising the noise, 400 spectra are obtained and averaged to a single spectrum. This spectrum is dark corrected by subtracting the average of the dark measurements obtained when the light source was blocked by the shutter.

The *spectral sampling interval* is found using the difference between adjacent elements in the wavelength vector of the measurements. The *spectral range* is found as the wavelength vector elements corresponding to the two outermost indices where the signal spectrum from measurements of the light source setup is nonzero.

To obtain the *gain factor* of the spectrometer, relating the signal in digital numbers (DN) to photoelectrons, photon transfer analysis is performed. This also obtains the *noise floor* of the applied integration time, the *saturation level*, and correspondingly the *dynamic range*, and reveals any *non-linearities*. The light source set up is measured with an integration time causing the spectrum to be partly saturated, and the spectrum is analysed using the script in section B.3.

The net light collection A^* of the spectrometer is obtained by measuring the light source set up with an integration time giving a strong signal but avoiding saturation. The corresponding spectrum is analysed using the gain factor obtained from photon transfer analysis and the script in section B.4.

The derived performance characteristics are calculated using the measured values as stated in Table 5.3.

Appendix B

Code files for analysis

This section presents python-scripts for analysis using the methods described in subsection 6.1.1 and section 6.2.

B.1 Find light source spectrum

The following python-script finds the response curve of a spectrometer using a measurement of a blackbody source, and Planck's law, i.e., Equation 2.11. The obtained response curve is then used for finding the light source spectrum of a measurement setup.

Example results from using the script are shown in subsection 6.1.1.

```
import numpy as np
import matplotlib.pyplot as plt
from analysis_file import get_wavelength,get_spectra,get_dark_spectra

# Spectral photon flux in units of photons / s / m^2 / sr / m, photons per second per unit area, solid angle and wavelength interval
def Plancks_law(wl,T):
    c = 2.99729458E8
    h = 6.62608015E-34
    kB = 1.380649E-23
    L = 2*h*c**2/wl**5/(np.exp(h*c/(wl*kB*T)-1)) # In energy units
    return L/(h*c/wl) # In photon units

############ Find response curve using the blackbody measurement ################
blackbody_file = "Blackbody measurement at 650 degC"
T = 650+273.15
integrationtime = 10e-3

# Read spectra, dark spectra and wavelength arrays from datafile
wl = get_wavelength(blackbody_file)
bright_spectra = get_spectra(blackbody_file)
dark_spectra = get_dark_spectra(blackbody_file)

# Find dark corrected and averaged spectrum
```

```
spectrum = (np.average(bright_spectra,axis=0)-np.average(dark_spectra,axis
    =0))

# Choose a selected wavelength interval with sufficient signal
idx = np.where((wl > 600) & (wl < 1100))[0]

detector_element_width = wl[idx]-wl[idx-1]
response_wl = wl[idx]

# Perform a simple offset-correction, using the non-signal region below 500
    nm
BB_spectrum = (spectrum[idx]-np.average(spectrum[np.where(wl < 500)[0]]))

BB = Plancks_law(wl*1E-9,T)*1E-9 # Spectral photon flux per nm

# The response curve is the ratio of signal (DN) to the incoming number of
    photons per m^2 and sr
response = BB_spectrum/(integrationtime*BB*detector_element_width)

fig, (ax1,ax2,ax3) = plt.subplots(1,3,figsize=(15,5))
ax1.plot(response_wl, BB_spectrum)
ax1.set_title("Measured blackbody signal")
ax1.set_ylabel("Signal (DN) / s")
ax1.set_xlabel("Wavelength (nm)")
ax2.plot(wl, BB,label=degC)
ax2.set_title(r"Blackbody spectral photon radiance")
ax2.set_ylabel(r"Photons / (s $m^2$ sr nm)")
ax2.set_xlabel("Wavelength (nm)")
ax3.plot(wl,response,label=degC)
ax3.set_title("Response curve")
ax3.set_ylabel(r"Signal (DN) / (photons per $m^2$ and sr)")
ax3.set_xlabel("Wavelength (nm)")


############ Find measurement setup light source spectrum using the
    response curve #################

setup_lightsource_file = "Measurement setup light source measurement"
integrationtime = 75e-3

# Read spectra, dark spectra and wavelength arrays from datafile
wl = get_wavelength(setup_lightsource_file)
bright_spectra = get_spectra(setup_lightsource_file)
dark_spectra = get_dark_spectra(setup_lightsource_file)

# Find dark corrected and averaged spectrum
spectrum = (np.average(bright_spectra,axis=0)-np.average(dark_spectra,axis
    =0))

#Choose the wavelength interval corresponding to the blackbody measurement
idx = np.where((wl >= response_wl[0]) & (wl <= response_wl[-1]))[0]

detector_element_width = wl[idx]-wl[idx-1]
measurement_wl = wl[idx]

# Perform a simple offset-correction, using the non-signal region below 500
    nm
measured_spectrum = (spectrum[idx]-np.average(spectrum[np.where(wl < 500)
```

```
    [0]]))

#Find the light spectrum using the response curve
light_spectrum = spectrum/(integrationtime*response*detector_element_width)
    # Spectral photon flux per nm


fig, (ax1,ax2,ax3) = plt.subplots(1,3,figsize=(15,5))

ax1.plot(response_wl,response)
ax1.set_title("Response curve")
ax1.set_ylabel(r"Signal (DN) / (photons per $m^2$ and sr)") #Per detector
    element
ax1.set_xlabel("Wavelength (nm)")
ax2.plot(measurement_wl, measured_spectrum)
ax2.set_title("Measured signal of light source")
ax2.set_ylabel("Signal (DN) / s") #Per detector element
ax2.set_xlabel("Wavelength (nm)")
ax3.plot(measurement_wl,light_spectrum)
ax3.set_title(r"Light source spectral photon radiance")
ax3.set_ylabel(r"Photons / (s $m^2$ sr nm)") #Per nm
ax3.set_xlabel("Wavelength (nm)")
plt.show()
```

Light source calibration.py

B.2 Find resolution and wavelength accuracy from measurement of spectral lines

The following python-script finds the resolution and wavelength accuracy from the peaks corresponding to spectral lines in the measured spectrum of the HG-1 Mercury Argon calibration source [33], with spectral lines at the indicated wavelength positions. The peaks are found using `find_peaks` and `peak_widths` from `scipy.signal`, with a relative peak prominence of 5%, and delimited based on the given cut-off level of 5%. Each peak is fitted to a Gaussian using the function `curve_fit` from `scipy.optimize`. The peak centre is then defined as the peak of the Gaussian fit, while the resolution is defined as its FWHM, both in wavelength units.

The corresponding spectral line wavelength for each peak is defined as the closest laying peak from the given list of spectral lines in the calibration source spectrum. The peak is considered consisting of overlapping peaks that are not resolved, and removed, if the distance to the closest laying spectral line is lower than the resolution. It is considered corresponding to a second diffraction order, and removed, if it lays closer to twice the wavelength of another spectral line, than to the closest spectral line. Other possible impurities in the spectra, that may cause deviation, are not corrected for. Finally, the wavelength errors are defined as the deviations between the measured peak wavelengths, and corresponding spectral lines.

The resulting resolutions and wavelength errors are plotted as a function of wavelength.

Example results from using the script is shown in subsubsection 6.2.1.1.

```
import numpy as np
import matplotlib.pyplot as plt
from scipy.signal import find_peaks, peak_widths
from scipy.interpolate import interp1d
from scipy.optimize import curve_fit
from analysis_file import find_wavelength, find_spectrum

# Read spectrum (averaged and dark corrected) and wavelength arrays from datafile
datafile = "HG-1 calibration source spectrum"
spectrum = find_spectrum(datafile)
wavelength = find_wavelength(datafile)

relative_peak_prominence = 0.05
peak_cutoff = 0.05

# Spectral line wavelengths in the HG-1 Mercury Argon calibration source
spectral_line_wl = np.array
    ([184.95,253.652,296.728,302.150,313.155,334.148,365.015,404.656,
    407.783, 435.833, 546.074, 576.960, 579.066, 696.543, 706.722, 710.748,
    727.294, 738.393, 750.387, 763.511, 772.376, 794.818, 800.616, 811.531,
    826.452, 842.465, 852.144, 866.794, 912.297, 922.450])


# Inperpolate the given data to a higher sampling rate
def interpolate(data, indices):
    x = np.arange(len(data))
    f = interp1d(x, data)
    return f(indices)

def Gaussian(x,a,mu,std):
    return a*np.exp(-(x-mu)**2/(2*std**2))

# Identify the peaks in the spectrum more prominent than relative_peak_prominence, and using the cut-off level peak_cutoff
def identify_peaks(spectrum,wavelength,relative_peak_prominence,peak_cutoff):

    # Perform offset correction
    offset = np.median(spectrum)
    spectrum = spectrum-offset

    # Only consider the spectrum between 400 nm and 930 nm
    idx = np.where((wavelength < 930) & (wavelength > 400))[0]
    spectrum = spectrum[idx]
    wavelength = wavelength[idx]

    peaks, properties = find_peaks(spectrum,prominence=
    relative_peak_prominence*np.max(spectrum))
    widths_idx, width_heights, peak_left_idx, peak_right_idx = peak_widths(
    spectrum,peaks,rel_height=1-peak_cutoff)

    return peak_left_idx, peak_right_idx


def find_wavelengths_and_resolution(spectrum,wavelength,
    relative_peak_prominence,peak_cutoff):
```

```
    peak_left_idx, peak_right_idx = identify_peaks(spectrum,wavelength,
relative_peak_prominence,peak_cutoff)

    # Analyse each separate peak
    interpolated_wls = []
    interpolated_spectra = []
    peak_centra = []
    resolutions = []
    popts = []
    spectral_lines = []
    errors = []
    for i in range(len(peak_right_idx)):

        # Interpolate the given data to a higher sampling rate
        interpolated_wl = interpolate(wavelength,np.linspace(peak_left_idx[
i],peak_right_idx[i],100))
        interpolated_spectrum = interpolate(spectrum,np.linspace(
peak_left_idx[i],peak_right_idx[i],100))

        # Perform a Gaussian fit of the peak
        guess = (2000,np.mean(interpolated_wl),2) #a, mu, std
        popt, pcov = curve_fit(Gaussian,interpolated_wl,
interpolated_spectrum,p0=guess)
        peak_centre = popt[1]
        peak_std = popt[2]
        resolution = 2*np.sqrt(2*np.log(2))*peak_std #FWHM of the Gaussian
fit of the peak

        #Find the spectral line that is the closest to the measured
wavelength
        spectral_line = spectral_line_wl[np.argmin(np.abs(spectral_line_wl-
peak_centre))]
        error = peak_centre-spectral_line

        # A peak is considered having overlapping peaks, i.e. the adjacent
peaks are not resolved, if the closest spectral line lies closer than
the estimated resolution
        overlapping = False
        closest_peak = spectral_line_wl[np.argmin(np.abs(spectral_line_wl-
spectral_line))]
        if np.abs(closest_peak-spectral_line) < resolution:
            overlapping = True

        # A peak is considered corresponding to a second diffraction order
if it lies closer to this than to a spectral line
        second_diffraction_order_peak = False
        second_diffraction_order = spectral_line_wl[np.argmin(np.abs(
spectral_line_wl*2-peak_centre))]
        if np.abs(peak_centre-second_diffraction_order*2) < np.abs(error):
                second_diffraction_order_peak = True

        if (not overlapping) and (not second_diffraction_order_peak):

            interpolated_wls.append(interpolated_wl)
            interpolated_spectra.append(interpolated_spectrum)
            peak_centra.append(peak_centre)
            resolutions.append(resolution)
```

```
            popts.append(popt)
            spectral_lines.append(spectral_line)
            errors.append(error)

    return [interpolated_wls,interpolated_spectra,np.array(peak_centra),np.array(resolutions),np.array(popts),np.array(spectral_lines),np.array(errors)]

def plot_spectrum_and_peaks(spectrum,wavelength,returns,xlim=[]):
    interpolated_wls,interpolated_spectra,peak_centra,resolutions,popts,spectral_lines,errors = returns

    fig, ax = plt.subplots(1,1,figsize=(10,5))

    ax.plot(wavelength,spectrum,color="tab:blue",label="spectrum")

    for i in range(len(interpolated_wls)):
        ax.plot(interpolated_wls[i],interpolated_spectra[i],color="tab:green",label="Identified peaks")
        ax.plot(wavelength,Gaussian(wavelength, *popt[i]),linestyle="dashed",color="tab:orange",label="Gaussian fits")
        ax.legend(bbox_to_anchor=(1,1.03))

    ax.set_title("Measured peaks")
    ax.set_xlabel("Wavelength (nm)")
    ax.set_ylabel("Signal (DN)")
    if xlim != []:
        ax.set_xlim(xlim[0],xlim[1])
        ax.set_ylim(0,1.2*np.max(spectrum[np.where((wavelength > xlim[0]) & (wavelength<xlim[1]))[0]]))

    fig.show()


def plot_wavelength_accuracy(returns):
    interpolated_wls,interpolated_spectra,peak_centra,resolutions,popts,spectral_lines,errors = returns

    fig, ax = plt.subplots(1,1,figsize=(5,5))

    ax.hlines(0,spectral_lines[0],spectral_lines[-1],linestyles="solid",color="black",label="Spectral line wavelength")
    ax.plot(spectral_lines,peak_centra-spectral_lines,'o',markersize=10,color="tab:blue",label="SRF centre wavelength")

    ax.set_xlabel("Wavelength (nm)")
    ax.set_ylabel("Wavelength error (nm)")
    ax.set_title("Error in the measured peak position wavelengths")
    ax.legend(bbox_to_anchor=(1,1.03))

    fig.show()


def plot_resolution(returns):
    interpolated_wls,interpolated_spectra,peak_centra,resolutions,popts,spectral_lines,errors = returns

    fig, ax = plt.subplots(1,1,figsize=(5,5))
```

```
1142     ax.plot(peak_centra,resolutions,"-o",color="tab:blue")

1144     ax.set_xlabel("Wavelength (nm)")
         ax.set_ylabel("Resolution (nm)")
1146     ax.set_title("Resolution a function of wavelength")

1148     fig.show()

1150 def find_wavelengths_and_resolution_and_compare(spectrum,wavelength,
    relative_peak_prominence,peak_cutoff):
         returns = find_wavelengths_and_resolution(spectrum,wavelength,
    relative_peak_prominence,peak_cutoff)
1152
         plot_spectrum_and_peaks(spectrum,wavelength,returns)
1154     plot_spectrum_and_peaks(spectrum,wavelength,returns,xlim=[750,880])

1156     plot_wavelength_accuracy(returns)
         plot_resolution(returns)
1158

1160 find_wavelengths_and_resolution_and_compare(spectrum,wavelength,
    relative_peak_prominence,peak_cutoff)
```

Resolution and wavelength accuracy.py

B.3 Photon transfer analysis

The following python-script generates a photon transfer curve (PTC) from one single dark-corrected spectrum. The spectrum is the average of multiple dark corrected measurements, and the noise is the standard deviation of the measurements at each detector element. The noise of each detector element is plotted as a function of signal, and a curve fit using `curve_fit` from `scipy.optimize` is performed to Equation 6.1 for finding the gain factor, and the noise floor level.

The resulting standard deviation PTC is plotted, together with the corresponding curve fit, noise floor, and shot noise.

If saturation is reached, i.e., the noise starts decreasing with signal, the saturation level is indicated in the plot. This level is found by the maximum of the noise that is smoothed with a smoothing filter, to obtain the smooth and clean PTC, using a Gaussian kernel with standard deviation 20 through the function `gaussian_filter` from `scipy.ndimage`.

The resulting gain factor and noise floor level in both DN and photoelectron units is printed, together with their uncertainties, which quantify any linearity error. If the spectrum reaches saturation, also the saturation level and dynamic range is printed.

Example results from using the script is shown in subsubsection 6.2.2.1.

```
1000 import numpy as np
     import matplotlib.pyplot as plt
1002 from scipy.ndimage import gaussian_filter
     from scipy.optimize import curve_fit
```

```
from analysis_file import get_wavelength,get_spectra,get_dark_spectra

# Read spectra, dark spectra and wavelength arrays from datafile
datafile = "Measurement with some saturation"
bright_spectra = get_spectra(datafile)
dark_spectra = get_dark_spectra(datafile)
wavelength = get_wavelength(datafile)

# Define the function used for curve fitting of the noise as a function of signal
def total_noise(signal,gain_factor,constant_noise):
    return np.sqrt(gain_factor*signal+constant_noise**2) # photoelectrons = signal(DN) / gain_factor

# Generate the photon transfer curve and find the gain factor, constant noise, saturation level, and dynamic range of the spectrometer
# Inputs: wavelength, bright spectra to be averaged and dark_spectra to be averaged and used for dark correction.
def PTC(wavelength,bright_spectra, dark_spectra):

    # Find averaged and dark corrected signal and noise
    dark_spectrum = []
    for i in range(len(dark_spectra)):
        dark_spectrum.append(np.average(dark_spectra[i],axis=0))
    dark_spectrum = np.average(np.array(dark_spectrum),axis=0)
    signal = np.average(bright_spectra-dark_spectrum,axis=0)
    noise = np.sqrt(np.var(np.array(bright_spectra-dark_spectrum),axis=0))

    # Remove any signal below 0, which may be present after the dark correction
    idx = np.where(signal > 0)[0]
    wavelength = wavelength[idx]
    signal = signal[idx]
    noise = noise[idx]
    noise = noise[np.argsort(signal)]
    signal = signal[np.argsort(signal)]

    fig,ax1 = plt.subplots(1,1,figsize=(8,5))

    # Plot the noise as a function of signal, with logaritmic scales
    ax1.loglog(signal,noise,'o',markersize=0.5)

    # Find effective saturation level, due to full-well or occurence of non-linearities, defined as the signal level where the noise starts decreasing
    # Use a smoothing filter to obtain a smooth curve of the noise, and define the saturation level as the max of this smoothed noise
    saturation_idx = np.where(gaussian_filter(noise,20) == np.max(gaussian_filter(noise,20)))[0][0]
    saturation = False
    saturation_level = False
    if len(signal)-saturation_idx > 100:
        signal = signal[:saturation_idx]
        noise = noise[:saturation_idx]
        saturation_level = signal[-1]
        saturation = True

    # Curve fit of the noise
```

```
    noisefloor_guess = noise[0]
    gain_factor_guess = (np.max(noise)-noise[0])**2/signal[-1]
    popt, pcov = curve_fit(total_noise,signal,noise,p0=(gain_factor_guess,
    noisefloor_guess))
    gain_factor = popt[0]
    noisefloor = popt[1]

    # Standard deviations of the curve fit
    gain_factor_uncertainty = np.sqrt(np.diag(pcov))[0]
    noisefloor_uncertainty = np.sqrt(np.diag(pcov))[1]

    # Plot the photon transfer curve, and the contribution from the
    constant noise and shot noise
    ax1.loglog(signal,total_noise(signal,*popt),linewidth=2,label=r"$\
    sigma_{total}$")
    ax1.loglog(signal,noisefloor*np.ones(len(signal)),label=r"$\sigma_{
    constant}$")
    ax1.loglog(signal,np.sqrt(gain_factor*signal),label=r"$\sigma_{shot}$")
    ax1.legend(loc="upper left")
    ax1.set_ylim(ymin=7)
    ax1.set_xlabel("Signal (DN)")
    ax1.set_ylabel(r"$\sigma$ (DN)")

    if saturation:
        ax1.vlines(signal[-1],total_noise(signal[-1],*popt)*0.7,total_noise
    (signal[-1],*popt)*1.3,linestyle="dashed",color="black")

    plt.show()

    dynamic_range = saturation_level/noisefloor

    return gain_factor, noisefloor, saturation_level, dynamic_range,
    gain_factor_uncertainty, noisefloor_uncertainty


gain_factor, noisefloor, saturation_level, dynamic_range,
    gain_factor_uncertainty, noisefloor_uncertainty = PTC(wavelength,
    bright_spectra, dark_spectra)

if saturation_level != 0:
    print("Gain factor (signal(DN) per photoelectron): {:.2f} +- {:.5f}\
    nNoise floor in DN and photoelectron units: {:.2f} +- {:.5f} and {:.2f}
    +- {:.5f}\nSaturation level in DN and photoelectron units: {:.2f} and
    {:.2f}\nDynamic range in DN and photoelectron units: {:.2f} and {:.2f}".
    format(gain_factor,gain_factor_uncertainty,noisefloor_uncertainty,
    noisefloor/gain_factor,noisefloor_uncertainty/gain_factor,
    saturation_level,saturation_level/gain_factor,dynamic_range,
    dynamic_range/gain_factor))
else:
    print("Gain factor (signal(DN) per photoelectron): {:.2f}+- {:.5f}\
    nNoise floor in DN and photoelectron units: {:.2f} +- {:.5f} and {:.2f}
    +- {:.5f}".format(gain_factor,gain_factor_uncertainty,noisefloor,
    noisefloor_uncertainty,noisefloor/gain_factor,noisefloor_uncertainty/
    gain_factor))
```

Photon transfer analysis.py

B.4 Net light collection A*

The following script finds the A^* curve from a measurement of the light source setup described in section 6.1. The measured spectrum is the average of multiple dark corrected measurements. It is converted from DN units to photoelectron units using a gain factor obtained for the spectrometer through photon transfer analysis. The spectral photon radiance spectrum of the source, obtained as described in subsection 6.1.1, is loaded from file, and interpolated to the same wavelength vector as the measured spectrum. Finally, the per-detector-element A^*_j and per-nm $A^*(\lambda)$ are obtained using the relations given in Equation 3.7 and Equation 3.8, and plotted together as a function of wavelength.

Example results from using the script is shown in subsubsection 6.2.2.2.

```
import numpy as np
import matplotlib.pyplot as plt
from scipy.io import loadmat
from scipy.interpolate import interp1d
from analysis_file import get_wavelength,get_spectra,get_dark_spectra

def interpolate(data, indices):
    x = np.arange(len(data))
    f = interp1d(x, data) # data = f(x)
    return f(indices)

# A* = electron_count / (t_int * wavelength_increment * spectral photon
    radiance), in units of um^2

gain = 0.18 # Gain factor = DN per photoelectron for the spectrometer,
    obtained from photon transfer analysis.
integrationtime = 20*1e-3

# Read spectra, dark spectra and wavelength arrays from datafile. Find
    measured photoelectrons per detector element
datafile = "Measurement of integrating sphere setup"
bright_spectra = get_spectra(datafile)
dark_spectra = get_dark_spectra(datafile)
measurement_wl = get_wavelength(datafile)
measured_spectrum = (np.average(bright_spectra,axis=0)-np.average(
    dark_spectra,axis=0))
measured_spectrum = measured_spectrum/gain # From DN to photoelectron units

# Load calibrated spectrum of integrating sphere setup, given in spectral
    photon radiance per nm
light_source_calibration = loadmat("Integrating sphere light source
    calibration")
light_source_spectrum = light_source_calibration["light_spectrum"][0]
calibration_wl = light_source_calibration["wavelength"][0]


# Scale wl axis to be equal for light spectrum and measured signal
start_wl = np.max([measurement_wl[0],calibration_wl[0]])
stop_wl = np.min([measurement_wl[-1],calibration_wl[-1]])
wl = measurement_wl[np.where(measurement_wl>=start_wl)[0][0]:np.where(
    measurement_wl>=stop_wl)[0][0]]
measured_spectrum = measured_spectrum[np.where(measurement_wl>=start_wl)
    [0][0]:np.where(measurement_wl>=stop_wl)[0][0]]
```

```
light_source_spectrum = interpolate(light_source_spectrum,np.arange(len(wl)
    )*len(calibration_wl)/len(wl))

detector_element_width = wl-measurement_wl[np.where(measurement_wl>=
    start_wl)[0][0]-1:np.where(measurement_wl>=stop_wl)[0][0]-1]

Astar_per_detectorelement = measured_spectrum/(integrationtime*
    detector_element_width*light_source_spectrum)*1e12
Astar_per_nm = Astar_per_detectorelement/detector_element_width

plt.plot(wl,Astar_per_detectorelement,label="Per detector\nelement")
plt.plot(wl,Astar_per_nm,label="Per nm")
plt.ylabel(r"A* ($\mu m^2$)")
plt.xlabel("Wavelength (nm)")
plt.ylim(ymin=0)
plt.legend(loc="upper left",bbox_to_anchor=(1,1.03))
plt.show()
```

Astar.py

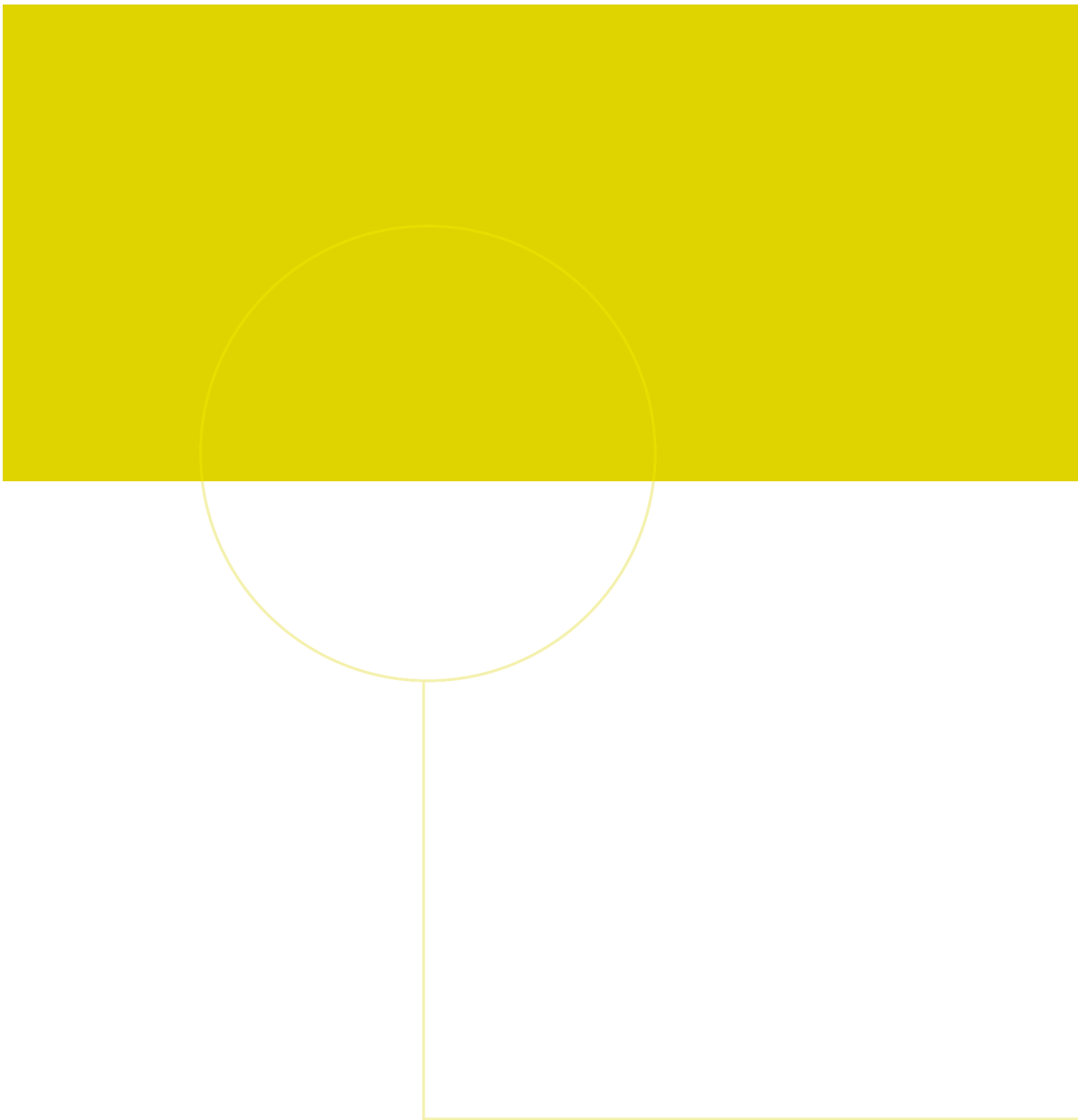

NTNU
Norwegian University of
Science and Technology

SINTEF